

KfK 2686
Oktober 1978

Annual Report

Teilinstitut Kernphysik
(July 1, 1977 - June 30, 1978)

Editors:
G. Haushahn, K. Wisshak
Institut für Angewandte Kernphysik

Kernforschungszentrum Karlsruhe

Als Manuskript vervielfältigt
Für diesen Bericht behalten wir uns alle Rechte vor

KERNFORSCHUNGSZENTRUM KARLSRUHE GMBH
ISSN 0303-4003

KERNFORSCHUNGSZENTRUM KARLSRUHE

KfK 2686

Institut für Angewandte Kernphysik

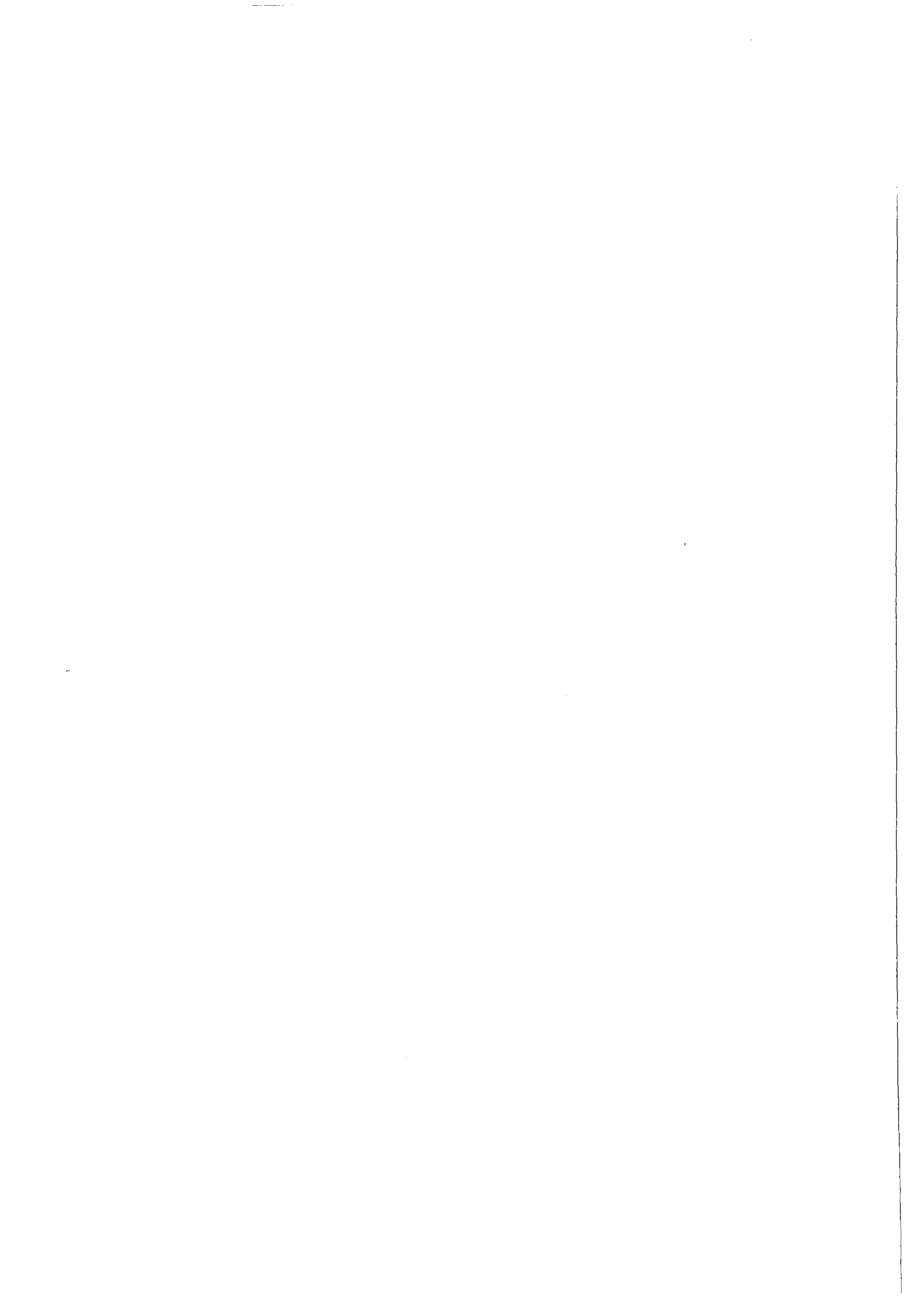
A N N U A L R E P O R T

Teilinstitut Kernphysik

(July 1, 1977 - June 30, 1978)

Editors: G. Haushahn and K. Wisshak

Kernforschungszentrum Karlsruhe GmbH, Karlsruhe

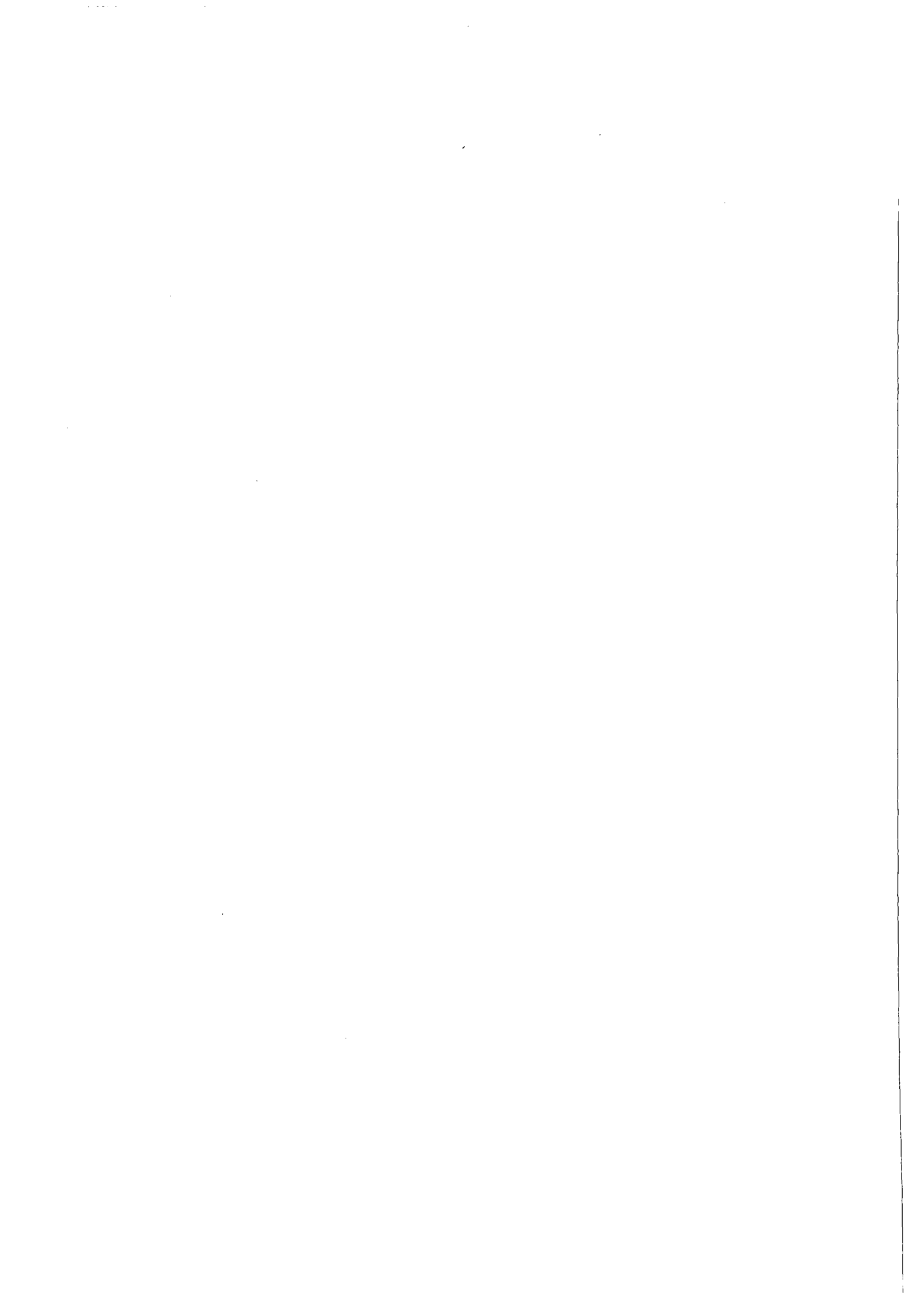


Abstract

The activities of the Nuclear Physics Section of the Institute of Applied Nuclear Physics from mid-1977 to mid-1978 are surveyed. The research program comprises both contributions to fundamental and applied nuclear research. The activities on the application of nuclear methods mainly concentrate on the measurements of cross sections of neutron-induced nuclear reactions for the fast breeder project, the application of gamma-ray spectrometry to nuclear fuel assay problems, the development of a proton microbeam for elemental analysis, and the production of ^{123}J for medical application. The study of nuclear reactions induced by α particles, ^6Li ions and fast neutrons, and the measurement of optical hyperfine structure using high-resolution laser spectroscopy form the major part of the fundamental research work. In addition, the operation of the two accelerators of the institute, an isochronous cyclotron and a 3 MV Van de Graaff accelerator, are briefly reviewed.

Zusammenfassung

Es wird über die Tätigkeit des Teilinstituts Kernphysik des Instituts für Angewandte Kernphysik von Mitte 1977 bis Mitte 1978 berichtet. Das Forschungsprogramm beinhaltet sowohl Anwendungen der Kernphysik auf Probleme der Kernenergie als auch grundlagenphysikalische Arbeiten. Schwerpunkte der angewandten Arbeiten bilden die Messungen von Neutronenwirkungsquerschnitten für das Projekt Schneller Brüter, die Anwendung gammaspektrometrischer Meßverfahren zur Spaltstoffbestimmung, die Entwicklung einer Protonenmikrosonde für die Elementanalyse sowie die Erzeugung von ^{123}J für medizinische Anwendungen. Zu den grundlagenphysikalischen Arbeiten gehören Untersuchungen von Kernreaktionen mit α -Teilchen, ^6Li -Ionen und schnellen Neutronen sowie die Messung der optischen Hyperfeinstruktur mittels hochauflösender Laserspektroskopie. Ferner wird der Betrieb der beiden Beschleuniger des Instituts, eines Isochronzyklotrons und eines 3 MV Van de Graaf Beschleunigers, kurz geschildert.



The Institute of Applied Nuclear Physics of the Karlsruhe Nuclear Research Centre is engaged in research work on the application of nuclear physics to problems of nuclear energy, solid state physics, medicine, and analysis. These investigations are supported by some fundamental research. This report, the fourth in a series of annual reports, gives a survey of the work of the Nuclear Physics Section from mid-1977 to mid-1978. Progress of the Nuclear Solid State Physics Section is reported separately.

Measurements of cross sections of neutron-induced nuclear reactions are among the main activities of the institute. Part of this work provides nuclear data required for the design of fast breeder reactors. In this field, a new detector for measuring fission cross sections of samples with high α activity has been developed. Other neutron cross section measurements aim at data relevant to the astrophysical s-process of nucleosynthesis. For such measurements, a technique for determining capture cross sections of noble gases has been established and applied to several krypton isotopes. The results should allow to determine the abundance of krypton in the solar system.

Methods of gamma-ray spectrometry are applied to problems of the nuclear fuel cycle such as the determination of plutonium in waste and of the isotopic composition of nuclear fuel. For similar applications a method for measuring the concentration of uranium and plutonium in solutions by X-ray absorption around the K-absorption edge has been successfully demonstrated.

The proton microbeam installation which was developed during the last three years has been completed and has achieved a beam diameter of 5 μm at an intensity up to several nA.

Further research in fundamental nuclear physics is carried out in two fields, the study of nuclear reactions at the Karlsruhe Isochronous Cyclotron and laser spectroscopy of small radioactive samples. The latter work has yielded results on five unstable isotopes and isomers of barium. Three new magnetic moments and two new quadrupole moments have been determined in addition to the measurements of the five isotopic shifts. The nuclear reaction work concentrated on reactions induced by ${}^6\text{Li}$ ions at 156 MeV and on a careful study of the neutron distributions in ${}^{40}\text{Ca}$ and ${}^{48}\text{Ca}$ by α particle scattering.

The institute operates two accelerators. A 3 MV single stage Van de Graaff accelerator is primarily used for neutron time-of-flight experiments and solid state physics. The Karlsruhe Isochronous Cyclotron, a fixed frequency machine, provides beams of 52 MeV deuterons, 104 MeV alpha particles, 26 MeV protons, and 156 MeV ${}^6\text{Li}$ ions. The cyclotron group has been able to increase intensity and reliability of the ${}^6\text{Li}$ beam considerably during the past year, and some exciting results have been obtained with this beam. The radionuclide ${}^{123}\text{J}$ is now being produced routinely and supplied to three hospitals for use in diagnosis. The contracts guarantee full recovery of production cost. For the major part of its beam time, the cyclotron is used by a large number of groups from other institutes of the research centre, from universities, and several other institutes for research in a variety of fields. This report covers only that part of the work at the cyclotron in which staff of the Institute of Applied Nuclear Physics has participated.



(G. Schatz)

Das Institut für Angewandte Kernphysik des Kernforschungszentrums Karlsruhe beschäftigt sich mit Anwendungen der Kernphysik auf Probleme der Kernenergie, Festkörperphysik, Medizin, und Analyse. Diese Untersuchungen werden durch grundlagenphysikalische Arbeiten begleitet. Der vorliegende Bericht, der vierte in der Reihe der Jahresberichte, gibt einen Überblick über die Arbeiten des Teilinstituts Kernphysik von Mitte 1977 bis Mitte 1978. Über die Tätigkeit des Teilinstitutes Nukleare Festkörperphysik wird getrennt berichtet.

Die Messung von Wirkungsquerschnitten neutroneninduzierter Kernreaktionen stellt eines der Hauptarbeitsgebiete des Teilinstituts dar. Ein Teil dieser Arbeiten dient der Bestimmung von Kerndaten, die für den Entwurf schneller Brutreaktoren benötigt werden. Dafür wurde ein neuer Detektor entwickelt, der die Messung von Spaltquerschnitten an stark α -aktiven Proben gestattet. Andere Messungen dienen der Bestimmung von Wirkungsquerschnitten, die für den astrophysikalischen s-Prozeß der Elementsynthese von Bedeutung sind. Hierfür wurde eine Technik zur Messung von Einfangquerschnitten an Edelgasen entwickelt und auf einige Kryptonisotope angewendet. Die Ergebnisse sollten es erlauben, die Häufigkeit von Krypton im Sonnensystem zu bestimmen.

Methoden der Gamma-Spektroskopie werden auf Probleme des Kernbrennstoff-Zyklus angewandt. Beispiele dafür sind die Bestimmung von Plutonium in radioaktivem Abfall und die Messung der Isotopenzusammensetzung in Kernbrennstoffen. In diesem Zusammenhang wurde eine Methode zur Konzentrationsmessung von Uran und Plutonium in Lösungen entwickelt. Sie nutzt die unterschiedliche Absorption von Röntgenstrahlen an beiden Seiten der K-Kante des betreffenden Elementes aus.

Die Protonenmikrosonde, die in den letzten drei Jahren entwickelt wurde, ist jetzt fertiggestellt und erreicht einen Strahldurchmesser von 5 μm bei einer Stromstärke von einigen nA.

Weitere Arbeiten zur Grundlagenkernphysik werden auf zwei Gebieten durchgeführt, der Untersuchung von Kernreaktionen am Karlsruher Isochronzyklotron und der Laserspektroskopie kleiner radioaktiver Substanzmengen. Auf dem letzten Gebiet wurden Ergebnisse an fünf instabilen Bariumisotopen bzw. -isomeren erzielt. Drei neue magnetische Momente, zwei neue Quadrupolmomente sowie alle fünf Isotopieverschiebungen konnten bestimmt

werden. Die anderen Arbeiten konzentrierten sich auf Kernreaktionen mit ${}^6\text{Li}$ -Ionen von 156 MeV und auf eine sorgfältige Studie der Neutronenverteilungen in ${}^{40}\text{Ca}$ und ${}^{48}\text{Ca}$ mit Hilfe der Streuung von α -Teilchen.

Das Institut betreibt zwei Beschleuniger. Ein einstufiger Van de Graaff Beschleuniger von 3 MV wird hauptsächlich für Neutronenflugzeitexperimente und für die Festkörperphysik benutzt. Das Isochronzyklotron Karlsruhe, ein Festfrequenz-Zyklotron, liefert Strahlen von 52 MeV-Deuteronen, 104 MeV-Alphaeilchen, 26 MeV-Protonen und 156 MeV- ${}^6\text{Li}$ -Ionen. Der Zyklotron-Betriebsgruppe gelang es im letzten Jahr, Intensität und Zuverlässigkeit des ${}^6\text{Li}$ -Strahls wesentlich zu verbessern. Mit diesen Teilchen wurden bereits einige sehr interessante Ergebnisse erzielt. Das Radionuklid ${}^{123}\text{J}$ wird jetzt routinemäßig hergestellt und an drei Krankenhäuser für diagnostische Anwendungen geliefert. Die entsprechenden Verträge sehen eine volle Erstattung der Herstellungskosten vor. Überwiegend wird das Zyklotron jedoch weiterhin von Gruppen aus anderen Instituten des Kernforschungszentrums und von Universitäten sowie anderen externen Forschungs-Instituten für Arbeiten auf den verschiedensten Forschungsgebieten genutzt. In diesen Bericht wurden nur diejenigen Arbeiten am Zyklotron aufgenommen, an denen Mitarbeiter des Instituts für Angewandte Kernphysik beteiligt waren.

Schatz

(G. Schatz)

CONTENTS

	Page
1. NEUTRON PHYSICS	1
1.1 FUNDAMENTAL RESEARCH: NUCLEAR PHYSICS	1
1.1.1 A Measurement of the Total Neutron Cross-Sections of ^3He and ^4He with High Resolution between 1 and 30 MeV H.O. Klages, W. Heeringa, B. Haesner, H. Dobiasch, B. Zeitnitz, G. Schmalz, B. Leugers, D. Erbe, F. Käppeler	1
1.1.2 Investigation of Isospin-Forbidden T=3/2 Resonances in ^{13}C and ^{17}O S. Cierjacks, D. Erbe, F. Hinterberger, B. Leugers, P. von Rossen, G. Schmalz	2
1.1.3 Isobaric Analog Impurity from Total and Differential Neutron Scattering Cross-Sections of Silicon S. Cierjacks, S.K. Gupta, I. Schouky	4
1.1.4 Investigation of the Validity of the Valence Model for Neutron Capture in the Mass Range $40 < A < 70$ H. Beer	4
1.1.5 Measurement of Partial Radiation Widths of High Energy Transitions from keV Capture Resonances in ^{56}Fe and $^{58,60}\text{Ni}$ H. Beer, R.R. Spencer, F. Käppeler	8
1.1.6 Intermediate Structure in the Capture-to-Fission Ratio of ^{235}U between 10 and 100 keV H. Beer, F. Käppeler	8
1.1.7 (E_{kin}, ν)-Measurements on Correlated Fragments in the Fission of ^{235}U and ^{237}Np at Neutron Energies of 550, 800 and 5500 keV R. Müller, A.A. Naqvi, F. Käppeler	11
1.2 FUNDAMENTAL RESEARCH: ASTROPHYSICS	13
1.2.1 A Capture Cross-Section Measurement of ^{58}Fe and its Implication for the s-Process Near the Iron Seed L.D. Hong, H. Beer, F. Käppeler	13

1.2.2	The Neutron Capture Cross-Section of Natural Krypton between 10 and 200 keV F. Hensley, F. Käppeler	14
1.2.3	Improvements in the Determination of Capture Cross-Sections for Neutron Energies from 5 to 200 keV B. Leugers	15
1.2.4	The Application of the Neutron Activation Method to Measure keV Neutron Capture Cross-Sections for Astrophysics H. Beer	18
1.3	NUCLEAR DATA FOR REACTORS	20
1.3.1	Resonance Analysis of the ^{10}B Total Cross-Section in the Energy Range from 90 to 420 keV H. Beer	20
1.3.2	Precision Measurements of Neutron Resonance Energies of Carbon and Oxygen between 3 and 15 MeV S. Cierjacks, D. Erbe, G. Schmalz, B. Leugers	21
1.3.3	Investigation of s-Wave Resonances and a Possible Doorway State in Fe below 850 keV S. Cierjacks, I. Schouky	23
1.3.4	A Possibility to Investigate the 27.7 keV Capture Resonance in ^{56}Fe Avoiding Effects of Detector Neutron Sensitivity F. Käppeler	24
1.3.5	A Measurement of the Total Neutron Cross-Section of Iron-58 in the Energy Range from 7 to 325 keV H. Beer, L.D. Hong, F. Käppeler	27
1.3.6	Neutron Total Cross-Sections for ^{240}Pu and ^{242}Pu in the Energy Range from 10 to 375 keV F. Käppeler, L.D. Hong, H. Beer	27
1.3.7	Recent Capture Cross-Section Measurements at Karlsruhe H. Beer, F. Hensley, L.D. Hong, F. Käppeler, B. Leugers, K. Wisshak	30

	Page
1.3.8 Neutron Capture Cross-Section Ratios of ^{240}Pu and ^{242}Pu versus ^{197}Au in the Energy Range from 50 to 250 keV K. Wisshak, F. Käppeler	30
1.3.9 Neutron Capture Cross-Section Measurement of ^{241}Am in the Energy Range from 10 to 250 keV K. Wisshak, F. Käppeler	31
1.3.10 A Measurement of the Subthreshold Neutron Fission Cross-Section of ^{240}Pu in the Energy Range from 10 to 250 keV K. Wisshak, F. Käppeler	33
1.3.11 Measurement of the ^{239}Pu and ^{240}Pu Fission Cross-Sections Relative to the ^{235}U Fission Cross-Section and the Scattering Cross-Section $\text{H}(n,p)$ in the Neutron Energy Range from 0.5 to 20 MeV K. Kari	33
1.3.12 The Fission Cross-Section of ^{241}Am in the Energy Range from 10 to 1200 keV W. Hage, H. Hettlinger, S. Kumpf, F. Käppeler, K. Wisshak ...	34
2. CHARGED-PARTICLE REACTIONS	35
2.1 POLARIZED AND UNPOLARIZED DEUTERONS	35
2.1.1 Spins of Proton Hole States from Analyzing Powers of (d,τ) Reactions at 52 MeV V. Bechtold, L. Friedrich, P. Doll, K.T. Knöpfle, G. Mairle, G.J. Wagner	35
2.1.2 Fission Fragment Energy-Velocity Correlation Measurements for the $^{233}\text{U}(d,pf)$ Reaction Y. Patin, S. Cierjacks, J. Lachkar, J. Sigaud, G. Haout, F. Cocu	35
2.2 ALPHA-PARTICLE REACTIONS	37
2.2.1 $^{48}\text{Ca}-^{40}\text{Ca}$ Radius Difference from Elastic Scattering of 104 MeV Alpha-Particles H.J. Gils, E. Friedman, H. Rebel, J. Buschmann, H. Klewe-Nebenius, Z. Majka, B. Neumann	37

	Page
2.2.2	Fourier-Bessel Series Description of Alpha-Particle- Nucleus Optical Potentials and Nuclear Matter Densities E. Friedman, H.J. Gils, H. Rebel, Z. Majka 40
2.2.3	A Study of the Giant Resonance Region of ^{208}Pb by Particle-Gamma Angular Correlations W. Eyriçh, A. Hofmann, H. Rost, U. Scheib, S. Schneider, F. Vogler, H. Rebel 43
2.2.4	The Deformation of ^{26}Mg and ^{28}Si from Particle-Gamma Angular Correlations W. Eyriçh, A. Hofmann, U. Scheib, S. Schneider, F. Vogler, H. Rebel 45
2.3	^6Li -PARTICLE REACTIONS 47
2.3.1	Search for Different Components in the Giant Resonance Bumps Excited by 156 MeV ^6Li -Particle Scattering on ^{90}Zr H.J. Gils, J. Buschmann, H. Rebel, S. Zagromski, G. Bechtold, H. Klewe-Nebenius, B. Neumann, H. Faust 47
2.3.2	Giant Resonance Excitation by 156 MeV ^6Li Scattering H.J. Gils, H. Rebel, J. Buschmann, H. Klewe-Nebenius 50
2.3.3	Experimental Studies of the Reaction Mechanisms of $^{208}\text{Pb} + ^6\text{Li} \rightarrow ^{211\text{m}}, ^{212\text{m}}\text{Po}$ B. Neumann, J. Buschmann, H. Klewe-Nebenius, H. Rebel 50
2.3.4	104 MeV Alpha-Particle and 156 MeV ^6Li -Ion Scattering and the Validity of the Refined Folding Model Description Z. Majka, H.J. Gils, H. Rebel 53
2.3.5	Importance of the Density Dependence of the Nucleon- Nucleon Interaction for Elastic Scattering of Light Complex Projectiles Z. Majka, H. Rebel, H.J. Gils 55
2.3.6	N- α and N- ^6Li Microscopic Potentials Z. Majka 57

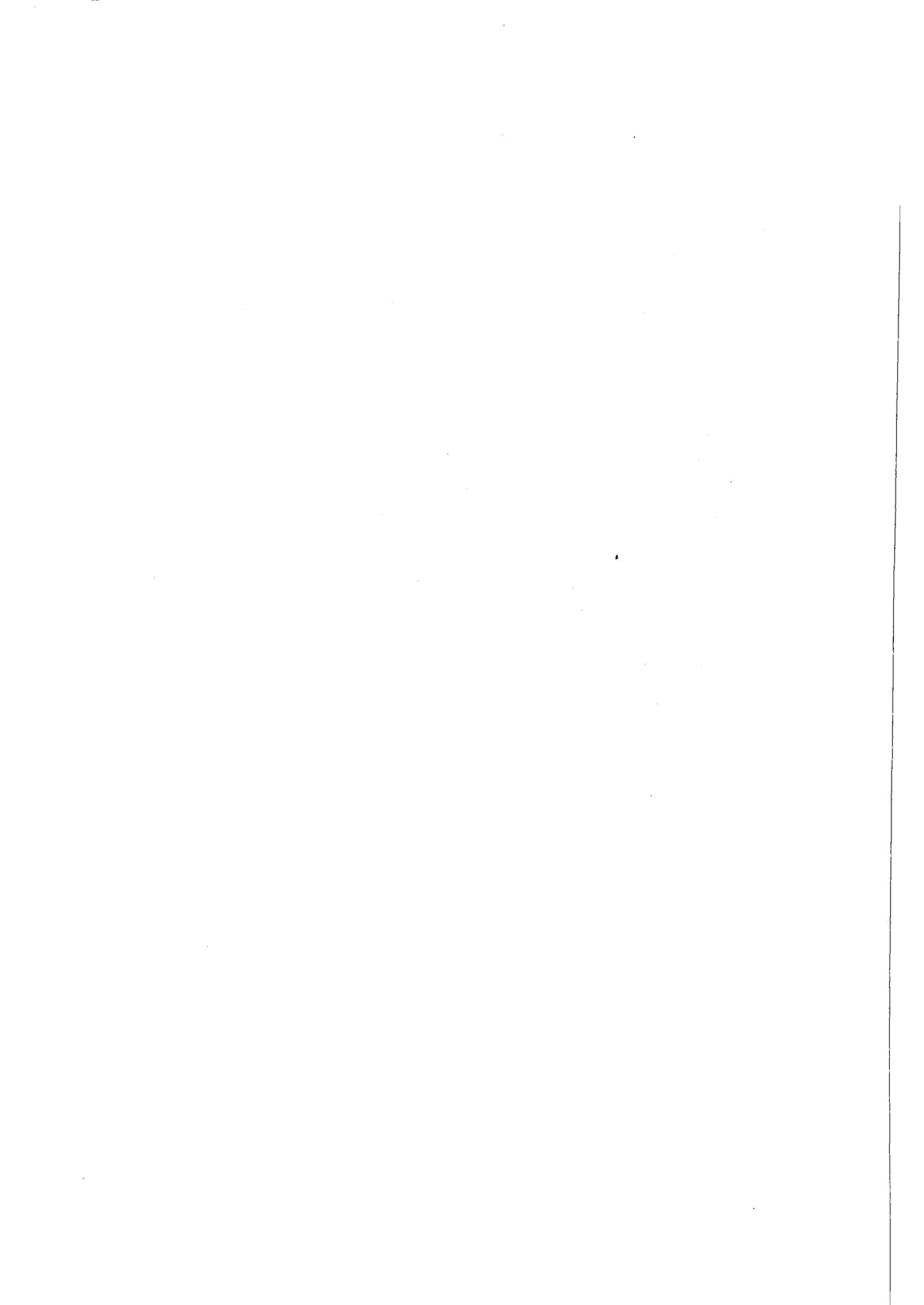
	Page
3. NUCLEAR SPECTROSCOPY	58
3.1 Experimental Studies of Hexadecapole Motion in Spherical Nuclei H. Faust, A. Hanser, H. Klewe-Nebenius, H. Rebel, J. Buschmann, H.J. Gils	58
3.2 Spectroscopic Studies of ^{137}Nd and ^{189}Ir by Means of Conversion Electron Angular Distribution-Measurements. Evidence for Hexadecapole-Deformation of Nuclei in the Transitional Regions of the Rare Earths H. Faust, J. Rieder, J. Buschmann, H. Klewe-Nebenius, H. Rebel, K. Wisshak	59
3.3 Study of the Level Structure of ^{239}U Using the Thermal Neutron Capture Reaction H.G. Börner, H.R. Koch, H. Seyfarth, T. von Egidy, W. Mampe, J.A. Pinston, K. Schreckenbach, D. Heck	61
4. THEORY	62
4.1 Induced Collective Motion: Limit of Two Fission Fragments F. Dickmann	62
4.2 Decrease of Pair-Correlations in a Deforming Nucleus F. Dickmann	65
4.3 A Variational Principle for the Energies and Widths of Unstable Nuclear States R. Beck, M.V. Mihailović, M. Nagarajan	66
4.4 Hill-Wheeler Equation for Three-Cluster Systems R. Beck	68
5. LASER SPECTROSCOPY	71
5.1 Nuclear Charge Radii and Moments of Neutron Deficient Ba- Isotopes by High Resolution Laser Spectroscopy K. Bekk, S. Göring, A. Hanser, G. Nowicki, H. Rebel, G. Schatz	71

5.2	Production of Instable Barium Samples for Laser Spectroscopic Experiments by Alpha-Particle Irradiation of Enriched Xenon and Mass Separation B. Feurer, A. Hanser	72
6.	NUCLEAR FUEL AND ELEMENTAL ANALYSIS	75
6.1	Manganese Nodule Analysis System - 'MANKA' K. Borcharding, R. Döbele, H. Eberle, I. Erbacher, J. Hauschild, J. Hübener, J. Lange, G. Müller, W. Rapp, E. Rathjen, K.-D. Rusch, A. Schäf, U. Tamm	75
6.2	Elemental and Isotopic Concentration Analyses on Nuclear Fuels Using Nondestructive Assay Techniques H. Eberle, P. Matussek, I. Michel-Piper, H. Ottmar, H. Allex	76
6.3	Experiences with the Plutonium Waste Monitor M.R. Iyer, S.J. Choithramani, P.P. Chakraborty, P. Matussek, H. Ottmar	76
6.4	Pu/U Ratio Determination from Uranium and Plutonium Isotopic Gamma Rays H. Eberle, H. Ottmar	78
6.5	Evaluation of Plutonium Isotopic Ratios Using High Resolution Gamma Spectrometry H. Eberle, M.R. Iyer, H. Ottmar	80
6.6	Branching Intensities of ²³⁹ Pu Gamma Rays H. Eberle, M.R. Iyer, H. Ottmar	83
6.7	Determination of Heavy Element Concentrations in Solutions by K-Edge Gamma Absorptiometry P. Matussek, I. Michel-Piper, H. Ottmar	85
7.	TECHNICAL DEVELOPMENT	89
7.1	CYCLOTRON	89
7.1.1	Operation Summary of the Karlsruhe Isochronous Cyclotron F. Schulz, H. Schweickert	89

7.1.2	Status of the Routine Production of ^{123}J at the Karlsruhe Isochronous Cyclotron K.H. Assmus, K. Jäger, R. Schütz, F. Schulz, H. Schweickert ...	93
7.1.3	Status of the Computer Diagnostic and Control for the Cyclotron H. Heinzmann, W. Kappel, W. Kneis, B. Kögel, Ch. Lehmann, J. Möllenbeck, H. Schweickert	95
7.1.4	Status of the New Trim Coils V. Bechtold, L. Friedrich, L. Wiss	98
7.1.5	Improvements of the Pulsing System for the Neutron Time-of-Flight Spectrometer at the Karlsruhe Cyclotron D. Erbe, G. Schmalz, F. Schulz	101
7.1.6	A Pulsing System for the External Beam of the Karlsruhe Isochronous Cyclotron M. von Hartrott, G. Haushahn, K. Heidenreich, M. Luft, H. Schweickert, E. Weihreter	102
7.1.7	Target System for the Production of ^{18}F G. Bauer, Ch. Rämer, A. Walter	104
7.1.8	First Results of Automatic On-Line Beam Optimization Procedures W. Kneis	106
7.2	VAN DE GRAAFF ACCELERATOR	109
7.2.1	Operation of the 3 MV Van de Graaff Accelerator A. Ernst, D. Roller, H. Schreiber, J. Nadasdy	109
7.2.2	Improved Synchronization of the Mobley Buncher High Frequency to the Ion Beam Pulses from the Van de Graaff Accelerator A. Ernst	110
7.2.3	A Beam Switching System for Pulsed and Mobley-Bunched Light Ion Beam A. Ernst	112
7.2.4	Realization of a Proton Microbeam with < 3 Micrometer Diameter D. Heck	115

	Page
7.3	NEUTRON PRODUCTION 117
7.3.1	Possible Improvements in the Production of keV-Neutrons F. Käppeler, G. Schatz 117
7.3.2	Development of the KARIN High Intensity Neutron Generator K.A. Schmidt, H. Dohrmann 119
7.4	COMPUTERS 120
7.4.1	Further Developments on Data Acquisition and On-Line Analysis for the Experiment Computer NOVA-2 at the Cyclotron J. Bialy, B. Kögel, W. Kneis, W. Segnitz 120
7.4.2	Standards and Proposals of Industrial Real Time FORTRAN G. Heller, W. Kneis, U. Rembold, G. Wiesner 121
7.4.3	Hardware Improvements for the NOVA-2 Computer at the Cyclotron J. Bialy, B. Kögel 121
7.4.4	Connection of the Large Neutron Spectrometer to the NOVA-2 Computer at the Cyclotron J. Bialy, B. Kögel 123
7.4.5	Status of a BASIC Compiler for a NOVA-2 Computer G. Ehret, W. Kneis 126
7.4.6	Concept of an Integrated Mega-Channel-Kicksorter G. Ehret, H. Hanak, H. Sobiesiak 128
7.4.7	A Computerized System for On-Line Data Acquisition and Evaluation P. Matussek 130
7.4.8	Final Status of "Analyzer" A.A. Naqvi, H. Sobiesiak 131
7.4.9	FASS (Fortran Analyser Software System) - an Approach to a Universal Multichannel Analyser Program H. Sobiesiak 133
7.4.10	A Load-On-Call Overlap-Manager for CGD Fortran IV H. Sobiesiak 136
7.4.11	How to Avoid Complicated IF Clause Structure in FORTRAN Real-Time Programming H. Sobiesiak, W. Kneis 137

	Page
7.4.12 Data Analysis on the Experiment Computer NOVA-2 at the Cyclotron S. Zagromski, J. Buschmann, H.J. Gils	138
7.4.13 A European Proposal for Industrial Real-Time FORTRAN W. Kneis	140
7.5 ION SOURCES AND DETECTORS	143
7.5.1 Recent Improvements of the Karlsruhe Polarized Ion Source C-LASKA V. Bechtold, L. Friedrich	143
7.5.2 The Lambshift Polarized Ion Source at the FN Tandem Van de Graaff Accelerator of the University of Cologne V. Bechtold, L. Friedrich, P. Ziegler, R. Anoil, G. Latzel, H. Paetz gen. Schieck	145
7.5.3 Monte-Carlo Calculation for the Pulse Height Weighting Function of a C_6D_6 Scintillation Detector F. Hensley	145
8. SEMINARS	148
9. PUBLICATIONS AND CONFERENCE CONTRIBUTIONS	150
9.1 Publications	150
9.2 Conference Contributions	152
9.3 Lectures and Seminars	156
10. PERSONNEL	157



1. NEUTRON PHYSICS

1.1 FUNDAMENTAL RESEARCH: NUCLEAR PHYSICS

1.1.1 A Measurement of the Total Neutron Cross-Sections of ^3He and ^4He with High Resolution between 1 and 30 MeV H.O. Klages⁺, W. Heeringa⁺, B. Haesner⁺, H. Dobiasch⁺, B. Zeitnitz⁺, G. Schmalz, B. Leugers, D. Erbe, and F. Käppeler

In view of the general progress in the theoretical description of few nucleon systems it seemed worth-while to improve also the experimental data basis for intercomparison. Therefore a series of neutron total cross section measurements with high resolution was started at the neutron spectrometer of the Karlsruhe cyclotron.

In a first run ^3He and ^4He were investigated between 1 and 30 MeV with an overall energy resolution of 0.007 ns/m using the 190 m flight path. Although data analysis is not yet completed an overall accuracy of $\lesssim 2\%$ is expected for the cross-section magnitude. The main emphasis of these measurements was laid upon the search for resonances, corresponding to states in ^4He and ^5He . In spite of our good energy resolution - e.g. $\Delta E/E = 0.1\%$

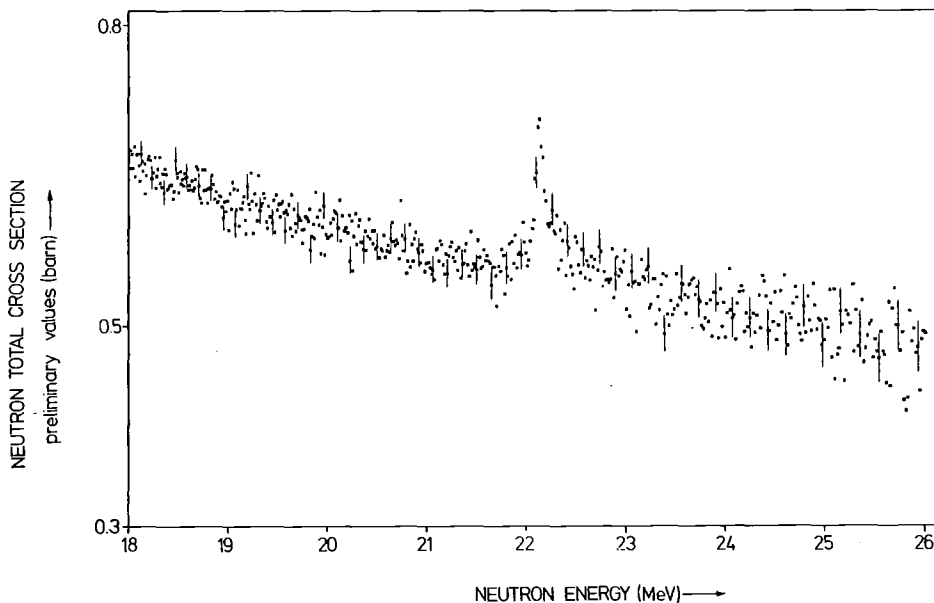


Fig. 1. The preliminary total neutron cross-section of ^4He between 18 and 26 MeV (1 ns/channel).

at 20 MeV - no additional resonances were found in both isotopes except the well known 22.16 MeV resonance in ^4He . Fig. 1 displays the total cross-section of ^4He in the energy range between 18 and 26 MeV. The energy scale was confirmed by various well known ^{12}C resonances in a separate run.

The systematic investigation of light nuclei will be continued with total neutron cross-section measurements on the hydrogen isotopes, including ^3H .

⁺ University of Bochum, present address: Institut für Kernphysik

1.1.2 Investigation of Isospin-Forbidden $T = 3/2$ Resonances in ^{13}C and ^{17}O

S. Cierjacks, D. Erbe, F. Hinterberger⁺, B. Leugers,
P. von Rossen⁺, and G. Schmalz

In the light nuclei with mass number $A = 4n + 1$ sharp $T = 3/2$ resonances are observed at higher excitation energies. As a speciality the lowest $T = 3/2$ states are bound to isospin-allowed particle decay. From a study of the isospin-forbidden particle-decay widths and other properties like excitation energies and gamma-decay widths one obtains direct access to the charge dependent effects in the nuclear states, i.e. the structure and size of isospin impurities. The investigation of proton-induced $T = 3/2$ resonances on target nuclei with $A = 4n$ from ^{12}C to ^{40}Ca yielded rich information on the isospin-forbidden decay properties of the lowest $T = 3/2$ resonances in $A = 4n + 1$, $T_3 = -1/2$ nuclei. Similar investigations of neutron-induced $T = 3/2$ resonances are only known for $^{24}\text{Mg} + n$ and $^{28}\text{Si} + n$.

In order to obtain a precise determination of the excitation energies, total widths and ground-state neutron decay widths, the lowest $T = 3/2$ levels of ^{13}C and ^{17}O were investigated as isospin-forbidden resonances in a high-resolution study of the $^{12}\text{C} + n$ and $^{16}\text{O} + n$ total neutron cross-section. The experiment was performed at the 190 m neutron time-of-flight facility of the Karlsruhe Isochronous Cyclotron. The overall time resolution of the neutron bursts as deduced from the full width at half maximum of the prompt gamma-

peak was 1.05 ns. Thus the neutron time-of-flight resolution was $\Delta t/L=5.5$ ps/m yielding an energy resolution $\Delta E/E=4.8 \cdot 10^{-4}$ at $E = 10$ MeV. A 1.019 atoms/barn thick pyrolytic graphite sample of natural carbon was used for the $^{12}\text{C}+n$ transmission experiment. A 1.200 atoms/barn thick liquid sample of natural oxygen was used for the $^{16}\text{O}+n$ transmission experiment.

The measured transmission data were analyzed using a single-level Breit-Wigner resonance formalism. In the region of a sharp resonance the nonresonant background was fitted by a quadratic approximation. The effective energy resolution was taken into account by an appropriate folding procedure.

The first $T = 3/2$ level in ^{13}C which was of special interest did not show any visible resonance anomaly. This observation yields an upper limit for the branching ratio $\Gamma_n/\Gamma \leq 0.02$ in contradiction to the value $\Gamma_n/\Gamma = 0.070 \pm 0.018$ of a previous coincidence experiment (1). Also in the region of higher excited $T = 3/2$ states of ^{13}C the measured transmission data did not show detectable resonance anomalies.

Table 1. $^{16}\text{O}+n \rightarrow ^{17}\text{O}(T=3/2)$ resonance parameters

E_R (keV)	Γ (keV)	Γ_{n_o} (keV)	E_x (keV)	J^π
6935.0 ± 0.3	3.0 ± 0.3	2.1 ± 0.1	11079.3 ± 0.9	$1/2^-$
8323.4 ± 1.6	11.1 ± 1.6	1.7 ± 0.2	12467.7 ± 1.8	$3/2^-$
8854.0 ± 1.5	4.1 ± 1.1	0.51 ± 0.07	12998.3 ± 1.7	$5/2^-$
10090.4 ± 0.6	21.5 ± 1.3	2.45 ± 0.15	14234.7 ± 1.0	$7/2^-$
10143.6 ± 3.3	6.6 ± 5.7	0.35 ± 0.19	14287.9 ± 3.4	$3/2^-$

In case of ^{17}O about ten $T = 3/2$ levels are known from ($^3\text{He},p$), ($^3\text{He},\alpha$) and (d,t) studies (1,2). From those states five $T = 3/2$ resonances were observed as anomalies in the $^{16}\text{O}+n$ transmission data. Interestingly only $T = 3/2$ states with negative parity were observed which is in accordance with shell model predictions. The results of a preliminary resonance analysis are given in Table 1. It should be noted that there are marked deviations between the present results and a previous $^{13}\text{C}(\alpha,n)$ resonance study (3).

⁺ Institut für Strahlen- und Kernphysik, University of Bonn, Germany

References

- (1) E.G. Adelberger, A.B. McDonald, C.L. Cocke, C.N. Davids, A.P. Shukla, H.B. Mak, and D. Ashery, Phys. Rev. C7 (1973) 889.
- (2) F. Ajzenberg-Selove, Nucl. Phys. A 166 (1971) 1; G. Mairle, K.T. Knöpfle, P. Doll, H. Breuer, and G.J. Wagner, Nucl. Phys. A 280 (1977) 97.
- (3) A.B. McDonald, T.K. Alexander, and O. Häusser, Nucl. Phys. A 273 (1976) 464.

1.1.3 Isobaric Analog Impurity from Total and Differential Neutron Scattering Cross-Sections of Silicon*

S. Cierjacks, S.K. Gupta⁺, and I. Schouky

Resonance parameters for four resonances in Si have been obtained by analyzing measured differential neutron scattering cross-sections combined with the total neutron cross-section in the neutron energy range 1.05-1.40 MeV and applying R-matrix single channel multilevel theory. The resonance at 1254 keV has been identified as the s-wave analog resonance in ²⁹Si. The identification also takes into account experimental radiative neutron capture data and shell model calculations for the radiative width. Estimates of the isospin mixing matrix elements are given.

* Phys. Rev. C17 (1978) 12.

⁺ Nuclear Physics Division, Bhabha Atomic Research Centre, Bombay 400-085, India.

1.1.4 Investigation of the Validity of the Valence Model for Neutron Capture in the Mass Range $40 < A < 70$

H. Beer

For a considerable number of nuclei in the mass range of the 3s giant resonance ($40 < A < 70$) the capture and total cross-sections have been measured at the Karlsruhe pulsed 3 MV Van de Graaff accelerator (1-4). In the analysis of the s-wave resonances significant correlations between reduced neutron widths and total radiation widths have been detected (1) in con-

trast to the expectations of the model of compound nucleus formation. Correlations of that type are frequently associated with a single particle capture mechanism, the valence capture (5,6) which should exhibit strong high energy E1 transitions from $s_{1/2}$ -states to low lying $2 p_{1/2,3/2}$ levels. According to this model the partial radiation widths of these transitions can easily be calculated by means of experimentally determined resonance neutron widths and (d,p)-spectroscopic factors of the final states. The total radiation widths of the resonances are then obtained by a summation over all partial radiation widths of these high energy transitions.

In the present investigation total radiation widths were calculated via the valence model for the various nuclei which have been studied experimentally at the Karlsruhe 3 MV Van de Graaff accelerator. The calculations were carried out using the formulae given by Cugnon (7). In Fig. 1 the theoretical and experimental results for the s-wave resonances of the even-even nuclei are compared by white and hatched bars, respectively. For resonances located below the 5 keV energy limit of the Van de Graaff measurements experimental values from other work were included. The experimental results of ^{54}Cr were taken from Stieglitz et al. (8)

The comparison of calculation and measurement shows that in some cases valence capture seems to be responsible for essentially all the observed radiation width. In addition, the existence of a threshold effect in neutron energy is indicated. For the neutron deficient nuclei ^{54}Fe , ^{50}Cr and ^{58}Ni the agreement between theoretical and experimental values is very good up to about 100 keV resonance energy. The transition to more neutron rich nuclei which is connected with a reduction in excitation energy seems to lower this neutron energy threshold so that for the neutron richest nuclei ^{54}Cr , ^{58}Fe and ^{64}Ni the model totally fails in predicting the experimental radiation widths.

Among the studied odd target nuclei ^{53}Cr and ^{57}Fe seem to be good candidates for a valence model capture mechanism. ^{59}Co and ^{61}Ni show sizeable valence capture only for some resonances with large neutron width whereas for the ^{47}Ti resonances the valence model fails.

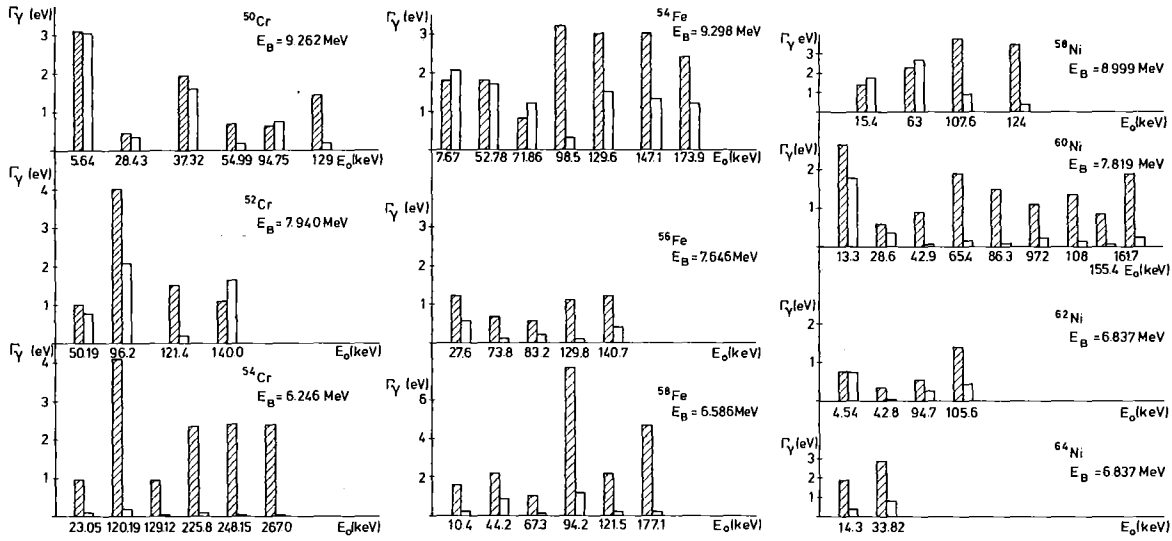


Fig. 1. Comparison of experimental and theoretical total radiation widths for the even-even nuclei of Cr, Fe and Ni (experimental values: hatched bars; theoretical values: white bars). For each resonance the neutron energy E_0 and for each nucleus the binding energy E_B are specified.

Besides the comparison with calculated total radiation widths, the existence of valence capture might also be confirmed by the study of high energy gamma transitions. In a measurement carried out at our laboratory (9) this has been done for the 27 keV resonance in ^{56}Fe , the 13.3 keV resonance in ^{60}Ni and the 15.4 and 63 keV resonances in ^{58}Ni . Only in the case of ^{60}Ni the valence capture mechanism could be confirmed in this way. Fig. 2 gives the theoretical and measured partial radiation widths for the two ^{58}Ni resonances and for the 13.3 keV resonance in ^{60}Ni .

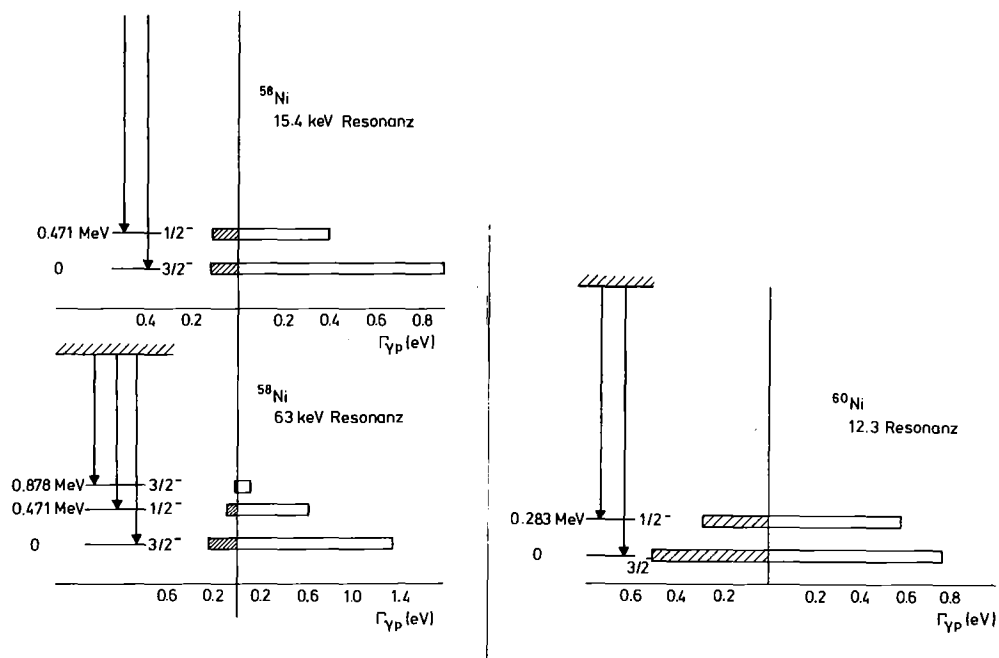


Fig. 2. Comparison of calculated and measured partial radiation widths for high energy transitions of the 13 keV ^{60}Ni resonance (right) and the 15 keV and 63 keV resonances in ^{58}Ni (left) (experimental values: hatched bars, theoretical values: white bars). For each nucleus the high energy transitions are indicated.

References

- (1) H. Beer, R.R. Spencer, Nucl. Phys. A 240, (1975) 29.
- (2) F.H. Fröhner, Report KFK 2046 (1973).
- (3) R.R. Spencer, H. Beer, Nucl. Sci. Eng. 60, (1976) 390.
- (4) L.D. Hong, H. Beer, F. Käppeler, Specialist Meeting on Neutron Data of Structural Materials for Fast Reactors, CBNM Geel, 5th - 8th December, 1977.
- (5) J.E. Lynn, Theory of Neutron Resonance Reactions, Oxford Clarendon Press, 1968.
- (6) J. Cugnon, C. Mahaux, Ann. Phys. 94, (1975) 128.
- (7) J. Cugnon, Nucl. Phys. A 263, (1976) 61.
- (8) R.G. Stieglitz, R.W. Hockenbury, R.C. Block, Nucl. Phys. A 163, (1971) 592.
- (9) H. Beer, R.R. Spencer, F. Käppeler, Z. Phys. A 284, (1978) 173.

1.1.5 Measurement of Partial Radiation Widths of High Energy Transitions from keV Capture Resonances in ^{56}Fe and $^{58,60}\text{Ni}$ *

H. Beer, R.R. Spencer⁺, and F. Käppeler

High energy gamma-ray transitions to low-lying states following neutron capture in ^{56}Fe and $^{58,60}\text{Ni}$ have been investigated for individual resonances in the neutron energy range 7-70 keV using a 50 cc Ge(Li)-detector. Partial radiation widths for s- and $\ell > 0$ wave resonances were determined. For the 47.8 keV resonance in ^{58}Ni a spin of 3/2 was derived. The gamma-ray strength for M1 transitions was found to be $(21 \pm 17) \times 10^{-9}$ and $(16 \pm 7) \times 10^{-9} \text{ MeV}^{-3}$ for ^{56}Fe and ^{58}Ni , respectively. The partial radiation widths of the studied s-wave resonances were compared with valence model calculations.

* Z. Physik A 284 (1978) 173.

⁺ Oak Ridge National Laboratory, Oak Ridge, Tennessee, 37830, USA.

1.1.6 Intermediate Structure in the Capture-to-Fission Ratio of ^{235}U between 10 and 100 keV

H. Beer and F. Käppeler

The capture-to-fission ratio of ^{235}U has been measured at the Karlsruhe pulsed 3 MV Van de Graaff accelerator with relatively high energy resolution compared to previous measurements. In the energy range from 10 to 100 keV strong intermediate structure has been observed (1). In Fig. 1 the fission-to-capture ratio from two different runs of the present work is plotted versus energy together with the fission cross-section of Ref. (2). From the comparison of the data a clear correlation between the structures in the present results and the well-known fluctuations in the fission cross-section (2,3,4,5) is immediately obvious, although the structures in the fission-to-capture ratio are much more pronounced.

The structures in the fission cross-section have first been discussed in terms of the double humped fission barrier and the channel theory of fission by Cao et al (6). Following this interpretation it has been tried several times to deduce widths and spacings of intermediate structures in the fission cross-section of ^{235}U by means of an autocorrelation analysis and to calculate with these quantities the energy difference E_{II} between the first and second well

of the fission barrier. The difficulty with this kind of analysis, however, is that strong statistical fluctuations of the reaction entrance channel are superimposed on the fission cross-section. A direct way to eliminate the influence of the entrance channel is offered by the investigation of the fission-to-capture ratio where the effects of the entrance channel cancel out. Fluctuations in the capture widths are normally small enough so that structure in the fission-to-capture ratio can be attributed to the fission channel.

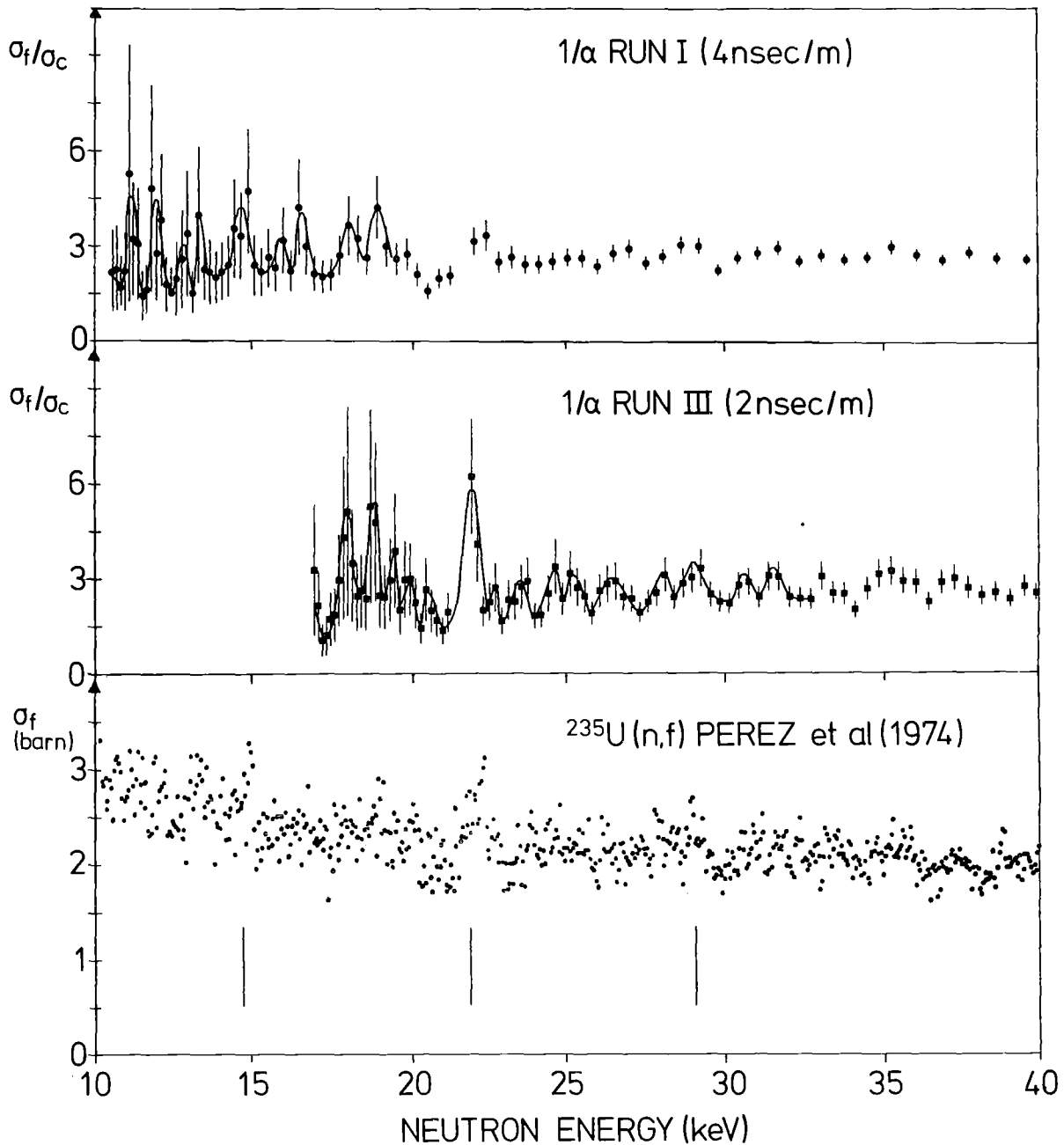


Fig. 1. The measured fission-to-capture cross-section ratio σ_f/σ_c for two different runs (middle and above) compared to the fission cross-section taken from Ref. 2 (below). The gap in the present data at 22 keV was caused by the gamma-flash.

In the energy range from 10 to 30 keV (Fig. 1) 20 resonance-like structures were determined giving an average level spacing of 1000 ± 300 eV. The corresponding level spacing distribution is well represented by a Wigner distribution within the available statistics. This behavior is to be expected if the structures are associated with subthreshold fission via a partially open fission channel. Using the level density formula with adjusted parameters given by Dilg et al (7) and the additional information that the partially open fission channel with $J = 4^-$ (8) is responsible for the intermediate structure, a value of 3.26 ± 0.14 MeV was calculated for E_{II} where the quoted uncertainty reflects the uncertainty in the average level spacing only.

This value is significantly different from earlier analyses of neutron fission cross-sections which suggested values around 2.3 MeV (6,9). Besides the fact that our value is determined from a more reliable data basis there is another argument which is in favor of our result. From theoretical calculations of potential energy surfaces, Nilsson et al (10) determined $E_{II} = 2.4$ MeV for the compound nucleus ^{236}U . Following the concept of transition states for the fission of even nuclei from Lynn (11) one finds that fission of ^{235}U with s-wave neutrons cannot proceed through the first three transition states because of spin and parity reasons. The first transition state with $I^\pi = 4^-$ is available in the $K^\pi = 1^-$ band which lies ~ 0.9 to 1 MeV higher than the lowest 0^+ state. This leads to a value of $E_{II} \sim 3.3$ to 3.4 MeV for the 4^- channel in fair agreement with our result.

References

- (1) H. Beer, F. Käppeler, Proc. Int. Conf. on the Interactions of Neutrons with Nuclei, Lowell, 1976, Vol. II, p. 1408.
- (2) R.B. Perez, G. de Saussure, E.G. Silver, R.W. Ingle, H. Weaver, Nucl. Sci. Eng. 55 (1974) 203.
- (3) B.U. Patrick, M.G. Sowerby, M.G. Schomberg, J. Nucl. Energy 24 (1970) 269.
- (4) J.R. Lemley, G.A. Keyworth, B.C. Diven, Nucl. Sci. Eng. 43 (1971) 281.
- (5) C.D. Bowman, M.L. Stetts, R.J. Baglan, Proc. Conf. on Nucl. Data for Reactors, Helsinki, 1970, Vol. II, p. 65.
- (6) M.G. Cao, E. Migneco, J.P. Theobald, Phys. Lett. 27B (1968) 409.
- (7) W. Dilg, W. Schantl, H. Vonach, Nucl. Phys. A 217 (1973) 269.

- (8) G.A. Keyworth, Proc. Int. Conf. on the Int. of Neutrons with Nuclei, Lowell (1976) Vol. I, p. 255.
- (9) D.G. Sood, N. Sarma, Nucl. Phys. A 151 (1970) 532.
- (10) S.G. Nilsson, C.F. Tsang, A. Sobiczowski, Z. Szymanski, S. Wycech, C. Constafson, I.-L. Lamm, P. Möller, B. Nilsson, Nucl. Phys. A 131, (1969) 1.
- (11) E. Lynn, The Theory of Neutron Resonance Reactions, Clarendon Press, Oxford (1968) 396.

1.1.7 (E_{kin}, γ) -Measurements on Correlated Fragments in the Fission of ^{235}U and ^{237}Np at Neutron Energies of 550, 800 and 5500 keV

R. Müller⁺, A.A. Naqvi, and F. Käppeler

The 4 parameter spectrometer for the measurement of kinetic energies and velocities of correlated fragments from neutron induced fission events has been described earlier (1). In the meantime important improvements in the experimental set-up were achieved and the final measurements on ^{235}U and ^{237}Np at 550, 800 and 5500 keV neutron energy have been completed.

One of the major improvements in the experimental set-up was the use of a vacuum tight feed-through for the mounting support of the solid state detectors which allowed for quick flight path changes between 70 and 450 mm. Frequent flight path changes during the experimental runs were important to correct for electronic drifts. The new mounting supports were water cooled which considerably improved the detector stability and the timing properties, and prolonged the detector life time by a factor of 4. In addition, one of the fragment flight tubes could be tilted sideways to account for noncollinearities in the fragment direction due to momentum transfer by the high energy neutrons.

Another improvement concerned the neutron target construction. Previously, these targets were cooled by a 1 mm thick water layer circulating on the back of the neutron producing surface. Neutrons scattered by this water layer caused slight tails in the time-of-flight spectra of the fission fragments. This effect was minimized by new low mass targets which were cooled only at their outer boundaries.

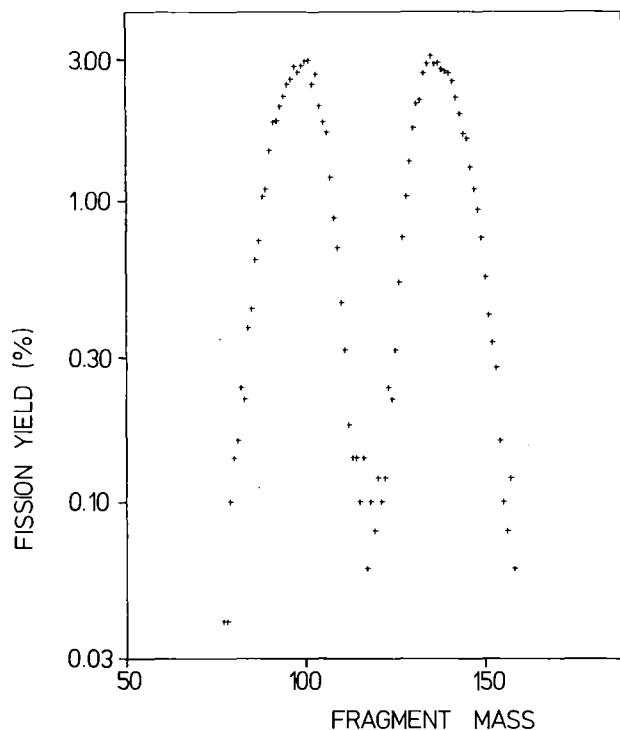


Fig. 1. Preliminary prompt fragment mass yields in the fission of ^{237}Np with 5.5 MeV neutrons.

The final measurements were carried out with fission targets of $\sim 100 \mu\text{g}/\text{cm}^2$ thickness enriched to more than 99 % ^{235}U and ^{237}Np , respectively. ^{235}U was investigated at 550 and 5500 keV neutron energy whereas in case of ^{237}Np neutron energies of 800 and 5500 keV were chosen because of the high fission threshold of this latter isotope. For each energy an overall of more than 15000 coincident fission events were observed, using 4 different but well defined flight paths. The overall time resolution achieved in the velocity determination of the fragments was ~ 600 psec. Daily energy calibration of the solid state detectors was performed by thin ^{252}Cf sources.

At present data analysis is under way. In a first step prompt fragment mass yields have been determined from the kinetic energies of correlated fragments. A preliminary distribution for the fission of ^{237}Np at 5.5 MeV is given in Fig. 1, showing a peak/valley ratio of ~ 30 .

+ University of Tübingen, Germany

1.2 FUNDAMENTAL RESEARCH: ASTROPHYSICS

1.2.1 A Capture Cross-Section Measurement on ^{58}Fe and
its Implication for the s-Process Near the Iron Seed

L.D. Hong, H. Beer, and F. Käppeler

The present neutron capture cross-section measurement covered the energy range from 7 to 200 keV. In spite of experimental difficulties with the small amount of sample material 24 resonances were determined and analyzed. The Maxwellian averaged cross-section of 24 ± 6 mb turned out to be significantly higher than previous theoretical estimates.

As ^{58}Fe is not produced in fusion reactions with charged particles this nucleus could be used as a normalization point in s-process calculations. With a simple single flux assumption it was not possible to reproduce the empirical abundances for $56 < A < 70$ whereas a good fit was obtained by an exponential flux distribution with two components. The calculated abundance distribution was found to be very sensitive to the set of capture cross-sections used in these calculations.

The seed abundance and the neutron flux parameters determined for the s-process above $A = 56$ were checked with the abundances of rare isotopes in the mass range below $A = 56$ which possibly are produced by neutron capture from neighbouring nuclei with high abundance. Contrary to previous solutions, in none of the investigated examples an overproduction was obtained.

The sum of abundances calculated for explosive nuclear burning and for the s-process exhibit a remarkably good agreement with empirical solar abundances for $56 < A < 63$ (see Fig. 1).

All these observations suggest that with the experimental capture cross-section of ^{58}Fe an improved description of the s-process near the iron seed could be achieved.

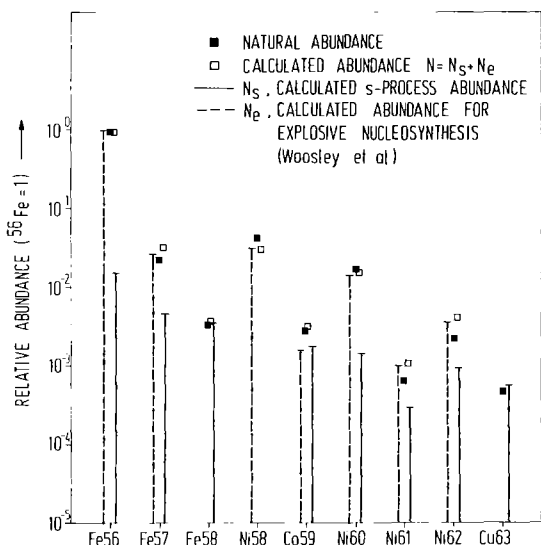


Fig. 1. Comparison between empirical solar abundances and the abundances calculated from the s-process and explosive nuclear burning.

1.2.2 The Neutron Capture Cross-Section of Natural Krypton between 10 and 200 keV

F. Hensley and F. Käppeler

The neutron capture cross-section of natural krypton was measured between 10 and 200 keV at the Karlsruhe pulsed Van de Graaff accelerator. The measurements were performed on liquid samples containing at the average 4 g of krypton (~ 1.1 l NTP), and are described in a previous report(1). Cross-sections were determined relative to ¹⁹⁷Au as a standard.

The ⁷Li(p,n)⁷Be reaction was used as a neutron source. Neutron energies were determined by time-of-flight at a distance of 70 cm from the ⁷Li target with a time resolution of 1.5 ns/m. Two C₆D₆ liquid scintillators using the Maier-Leibnitz pulse height weighting technique (2) served for the detection of prompt gamma-rays from capture events. The resulting cross-section is shown in Fig. 1. The error bars include the statistical uncertainty of 6.6 % only. The triangles represent Hauser-Feshbach statistical model calculations by Holmes, Woosley, Fowler, and Zimmerman (3).

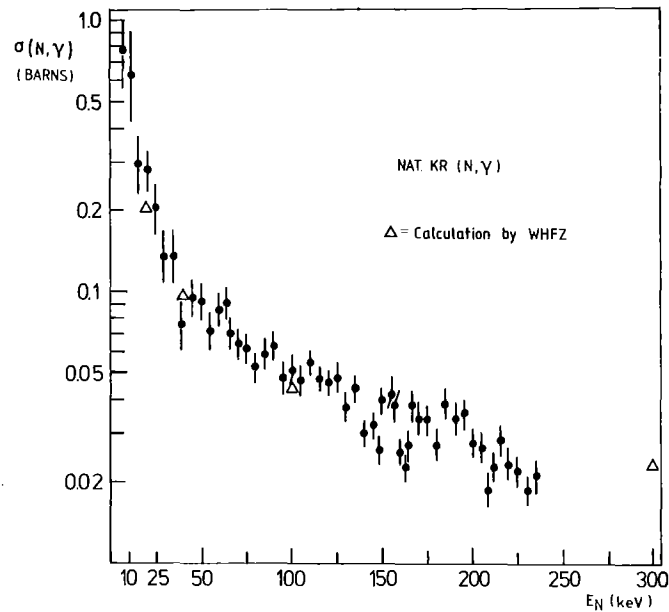


Fig. 1. Preliminary results of the capture cross-section of natural krypton.

References

- (1) F. Hensley, Report KFK 2504 (1977) 11.
- (2) R.L. Macklin, J.H. Gibbons, Phys. Rev. 190 (1967) 1007.
- (3) J.A. Holmes, S.E. Woosley, W.A. Fowler, and B.A. Zimmerman, At. Data and Nucl. Data Tables 18 (1976) 305.

1.2.3 Improvements in the Determination of Capture Cross-Sections for Neutron Energies from 5 to 200 keV

B. Leugers

The measurement of neutron capture cross-sections by C_6D_6 scintillation detectors using the pulse height weighting technique was recently established at the Karlsruhe Van de Graaff accelerator (1). In the meantime the first arrangement was improved with the aim to reduce the background, to optimize the counting rate and to improve the energy resolution.

The main problem for this kind of measurements is the background of gamma-rays generated by neutron capture in the surrounding material. For this reason a compact lead shielding was constructed containing the two C_6D_6 -detectors and the sample changer. The thickness of the lead shielding is about 20 cm in all directions. The schematic construction is given in Fig. 1. Gamma-ray production near the collimated neutron beam is avoided by using a conical guide tube of 6Li_2CO_3 which was pressed to 85 % of crystal density. 6Li was chosen because of its reasonable capture cross-section (without gamma-ray emission) and its rather low scattering cross-section. Scattered neutrons in the beam would disturb the energy resolution as the time-of-flight method is used. Outside the Li_2CO_3 -tube neutrons are moderated and absorbed in boron loaded resin and paraffin. For 400 keV neutrons sufficient collimation and shielding requires a minimum flight path of ~ 60 cm. Fig. 2 shows the time-of-flight spectrum of one detector measured in a two-hours-run with a 11.6 g ${}^{197}Au$ -sample. The signal-to-background ratio is better than 5:1 at 200 keV neutron energy. The C_6D_6 -detector has a volume of one liter and a diameter of 11.5 cm. The time resolution of this detector is 550 ps measured with a ${}^{60}Co$ source (threshold 100 keV). The total time resolution including the pulse width of the Van de Graaff accelerator is better than 800 ps. As the pulse height weighting technique is used the data of each detector were stored in a two-dimensional field of 1024 time-of-flight channels and 16 analog channels. Coincidences of the two C_6D_6 -detectors were measured in an additional time-of-flight spectrum (1024 channels) to get some information about

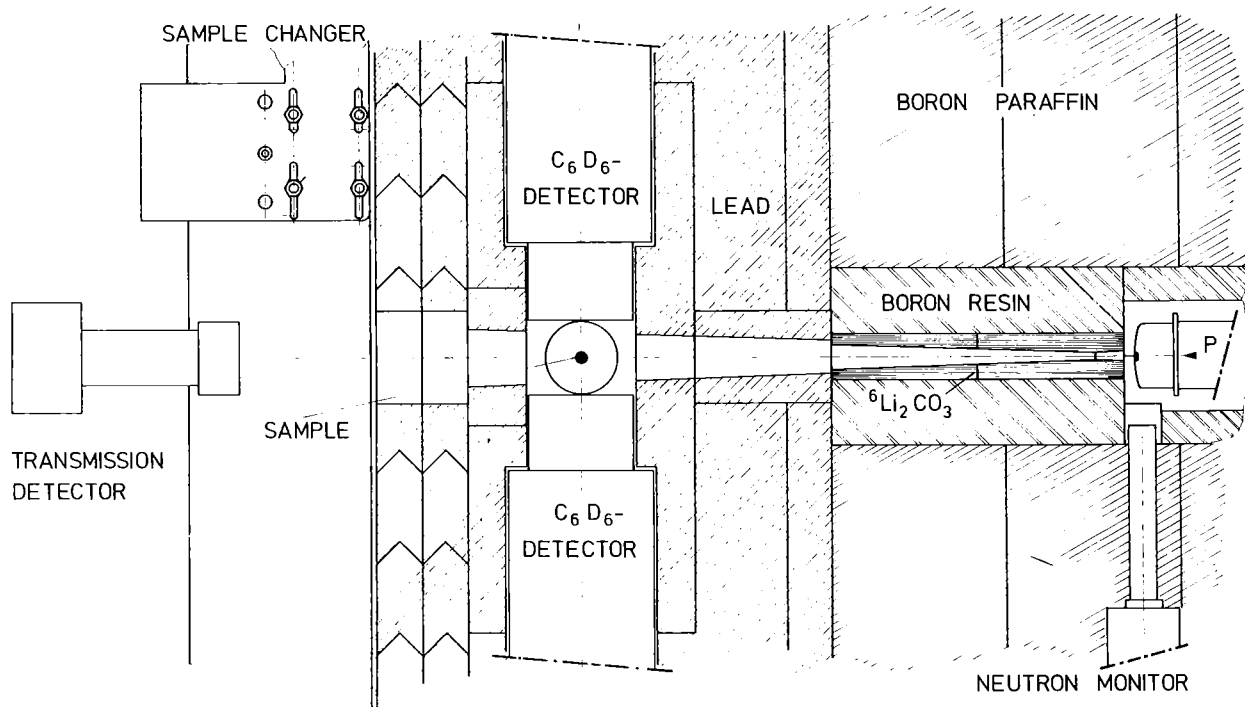


Fig. 1. Schematic design of the capture cross-section experiment.

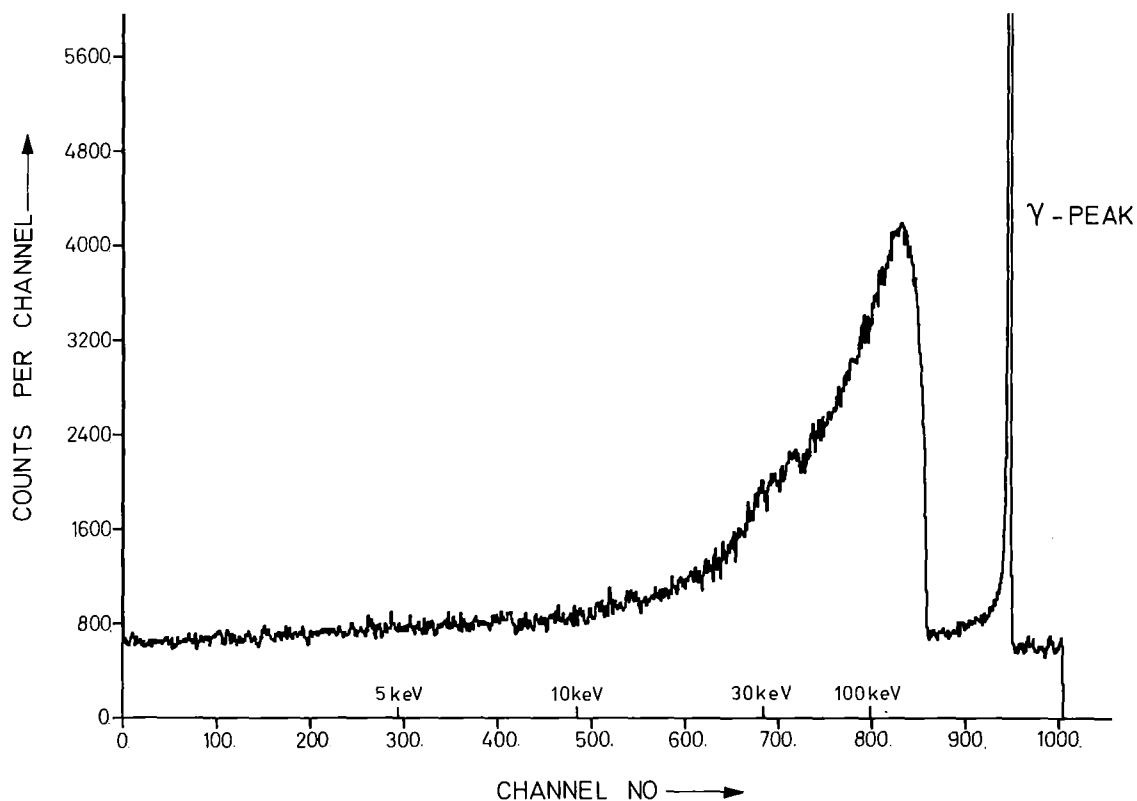


Fig. 2. Time-of-flight spectrum of capture events from a 11.6 g ^{197}Au -sample measured in a two-hours-run (0.67 ns/channel).

the average multiplicity \bar{m} of the capture events. In the same experiment a transmission measurement is made by a small ^6Li -glass detector at 1 m flight path (time resolution 1.1 ns). This time-of-flight spectrum (1024 channels) is also stored in the computer simultaneously. The total cross-section will be used to correct for the effect of scattered neutrons, although the sensitivity for scattered neutrons is pretty low (about 1 %). The sample changer has eight different positions so that different samples and background measurements can be made at the same run. The normalization to the same neutron flux is provided by an additional Li-glass detector mounted close to the target (see Fig. 1).

Measurements on samples of natural xenon and of some krypton isotopes will be carried out this year. For these measurements low mass high pressure gas targets were designed.

References

- (1) F. Hensley, Report KfK 2504 (1977) 11.

1.2.4 The Application of the Neutron Activation Method to Measure keV Neutron Capture Cross-Sections for Astrophysics

H. Beer

The neutron activation technique is a relatively simple method to measure neutron capture cross-sections. The measurement is carried out in two steps, the neutron irradiation of the sample and the detection of the induced activity with a β - or gamma-counter. Using a Van de Graaff type accelerator for the irradiations and a high resolution Ge(Li)-detector for the measurement of the activity the method turns out to be a useful tool to determine capture cross-sections important for problems of stellar nucleosynthesis. The advantages of the activation method can be summarized as follows:

- Normally no enriched samples are necessary which are sometimes expensive and difficult to get for measurements via detection of the prompt capture gamma-rays.
- The activation sample can be placed very close to the neutron target in a high flux so that only small sample amounts are needed resulting in small corrections for multiple scattering and self-shielding. For applications where no good energy resolution is necessary the method provides very accurate results.
- Partial capture cross-sections to isomeric states can be measured. These cross-sections are sometimes an indispensable means for the analysis of s-process branching points if the branching ratio is sensitively dependent on isomeric state population via neutron capture.

In the light of these arguments an experimental arrangement for the application of the neutron activation method at the Karlsruhe 3 MV pulsed Van de Graaff was set up which takes into account the special conditions of the accelerator and the aim of the measurements. A proton beam of 1 ns pulse width and 5 MHz repetition rate is used for neutron production via the ${}^7\text{Li}(p,n)$ reaction. If a proton energy 10 keV above the reaction threshold is chosen, one obtains a kinematically collimated neutron beam

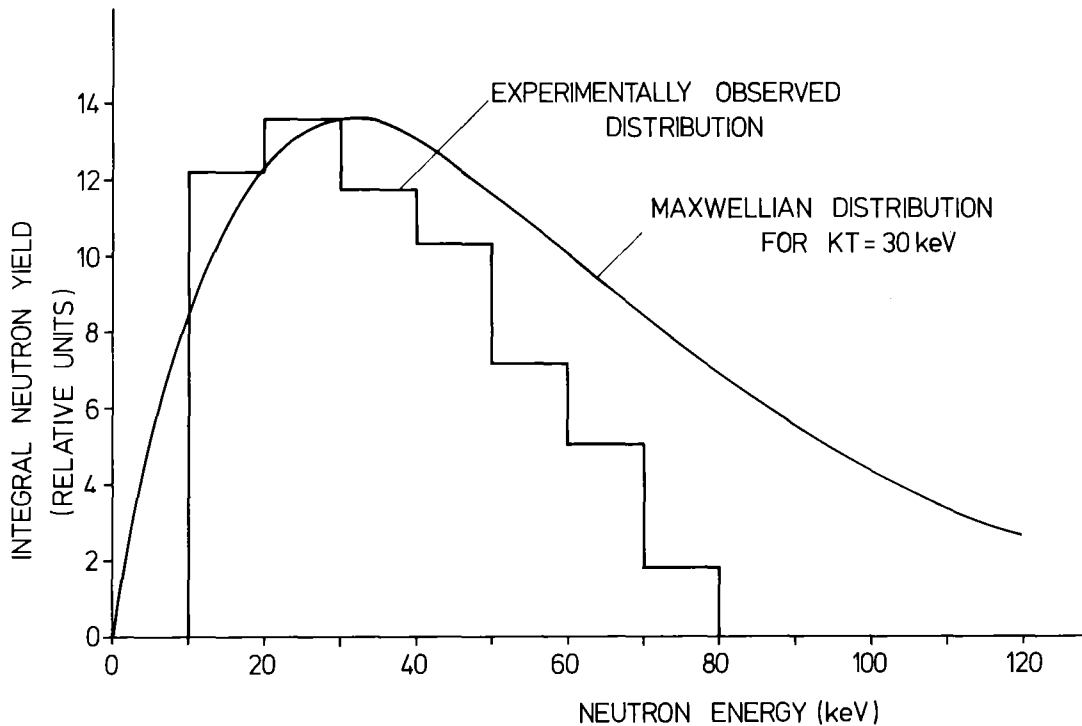


Fig. 1. The neutron flux distribution (histogram) compared to the Maxwellian distribution function.

with an energy distribution very similar to a Maxwellian distribution for $kT = 30$ keV. The difference in the distributions of Fig. 1 does not affect the resulting average cross-sections in a significant way. Assuming a $1/v$ -dependence of the differential cross-section, the resulting average cross-sections differ by only 5%, for example.

For the neutron irradiation the activation foil is placed back to back with a gold foil immediately at the neutron target. The target is cooled by heat convection to an area far outside the kinematically collimated neutron beam to avoid scattering effects. The beam spot corresponds to the dimensions of the activation foils (6 mm diameter). The time-of-flight technique is used to measure the neutron flux as a function of neutron energy during the irradiation of the samples. For this purpose a Li-glass detector is installed at a distance of 0.23 m. By means of the Fortran program FASS (1) the count rate of the Li-glass detector is periodically accumulated in a NOVA computer to obtain the fluctuations of the neutron flux as a function of time. FASS also controls the registration of the induced activity measured with a Ge(Li)-detector. Fig. 1 shows the measured neutron energy distribution from a first preliminary run together with a Maxwell distribution for $kT = 30$ keV.

Reference

- (1) H. Sobiesiak, contribution 7.4.9 of this report

1.3 NUCLEAR DATA FOR REACTORS

1.3.1 Resonance Analysis of the ^{10}B Total Cross-Section in the Energy Range from 90 to 420 keV.

H. Beer

The ^{10}B neutron absorption cross-section is one of the important standard cross-sections for neutron flux determinations. Much of the present information about this cross-section has been obtained via measurements of the ^{10}B total cross-section (1,2). The broad $7/2^+$ s-wave resonance at 370 keV is primarily responsible for the well-known $E^{-1/2}$ energy dependence of the total and (n, α) cross-sections from thermal energies up to 100 keV (3). This resonance has been analyzed from polarization and differential scattering measurements (3), but it had not been observed in the total and (n, α) cross-sections itself.

In the present investigation the total cross-section measured at the Karlsruhe pulsed 3 MV Van de Graaff accelerator (4) between 90 and 420 keV has been analyzed. Special emphasis has been placed upon a broad structure with a maximum at about 230 keV.

According to the work of Lane et al. (3) only one broad resonance is close to our investigated energy region, the $7/2^+$ s-wave resonance at 370 keV with

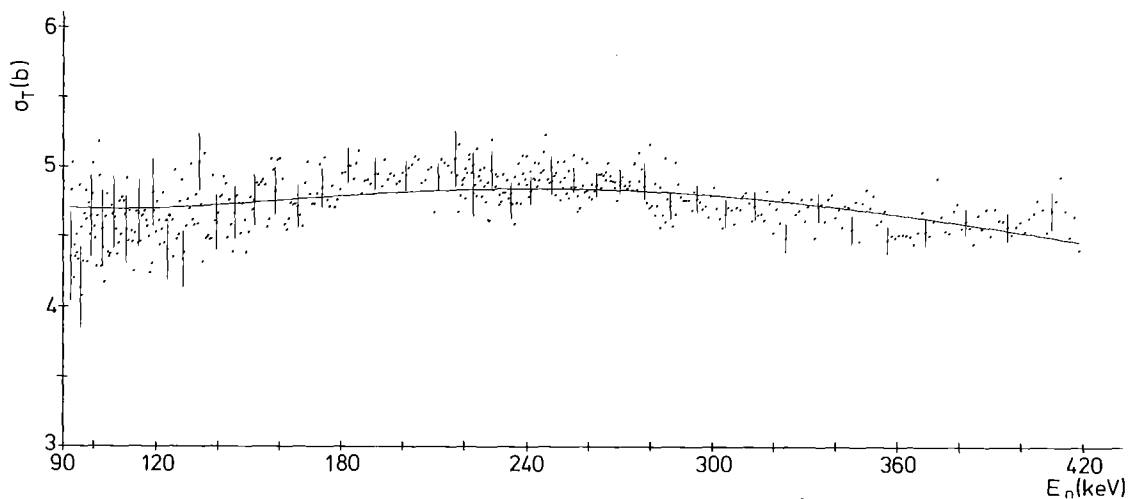


Fig. 1. The neutron total cross-section data of ^{10}B and an R-matrix shape fit represented by the full black curve. The uncertainty indicated at each 10^{th} data point is only the statistical uncertainty.

a neutron width of 770 keV and a total alpha-width of 114 keV.

In order to check whether the broad structure in the total cross-section corresponds to this s-wave resonance an R-matrix analysis was performed using the resonance parameters of Ref. 3 . Besides neutron scattering only alpha-decay has to be considered as the contributions of other decay processes, i.e. (n,p), (n,t) and (n, γ) which are also energetically possible are negligibly small (1). Following Lane et al. (3) the variation in the alpha-penetrability was neglected and the alpha-widths were assumed to be constant . In this approximation an R-matrix multilevel analysis with the Fortran IV code FANAL (5) could be carried out treating the total alpha-decay width formally like the total radiation width. The result of our calculation shown in Fig. 1 together with the experimental data indicates that the observed structure can easily be explained with the $7/2^+$ s-wave resonance at 370 keV.

References

- (1) F.P. Mooring, J.E. Monahan, C.M. Huddleston, Nucl. Phys. 82, (1966) 16.
- (2) M.G. Sowerby, B.H. Patrick, C.A. Uttley, K.M. Diment, Proc. Int. Conf. on Nucl. Data for Reactors, Helsinki, 1970, p. 161, Vol. I.
- (3) R.O. Lane, S.L. Hausladen, J.E. Monahan, A.J. Elwyn, F.P. Mooring, A. Langsdorf, jr., Phys. Rev. C4, (1971) 380.
- (4) R.R. Spencer, H. Beer, and F.H. Fröhner, Report KFK 1518.
- (5) F.H. Fröhner, Report KFK 2129 (1976).

1.3.2 Precision Measurements of Neutron Resonance Energies of Carbon and Oxygen between 3 and 15 MeV

S. Cierjacks, D. Erbe, G. Schmalz, and B. Leugers

In recent years neutron energy standards have been requested to remove existing discrepancies in neutron cross-sections which obviously originated from discrepancies in energy for different spectrometers. In order to provide a set of carefully selected standard resonance energies, the INDC in 1975 set up a Standard Subcommittee, which presently has almost finalized its task (2). Some representative standard resonances and their present accuracies selected by the INDC-Subcommittee are listed in Table 1.

Table 1. Resonances suggested as energy standards for the MeV-range

	Isotope	Nominal Energy (MeV)	$\Delta E/E$
recommended by INDC subcommit- tee	O-16	1.651 ± 0.002	1.2×10^{-3}
	Mg-24	1.709 ± 0.002	1.2×10^{-3}
	C-12	2.818 ± 0.004	1.4×10^{-3}
	O-16	3.211 ± 0.003	1.0×10^{-3}
	C-12	6.293 ± 0.008	1.3×10^{-3}
	C-12	12.1 ± 0.1	8.2×10^{-3}
this work	O-16	3.2117 ± 0.0002	6.2×10^{-5}
	C-12	6.295 ± 0.003	4.8×10^{-4}
	C-12	12.090 ± 0.010	8.2×10^{-4}
	O-16	4.5944 ± 0.0004	8.7×10^{-5}
	C-12	4.9368 ± 0.0004	8.1×10^{-5}
	O-16	5.3695 ± 0.0005	9.3×10^{-5}

Between 1 MeV and 10 MeV a total of 43 standard resonance energies were proposed having typically an accuracy of $\Delta E/E_R \sim 10^{-4}$. However, in the MeV region accuracies of only $\Delta E/E_R \sim 10^{-3}$ were obtained which decrease to almost 10^{-2} at 10 MeV. In the present work new precision measurements of carbon and oxygen resonances were made, which represent an improvement of previous resonance energy determinations by more than one order of magnitude.

Transmission measurements for both elements were carried out at the 190 m flight path of the Karlsruhe fast neutron spectrometer, using a 250 ps channel width for data accumulation. A largely decreased neutron pulse width of 0.7 ns was employed throughout the experimental runs. The relative uncertainties $\Delta E/E$ are dependent on $\Delta t/t$ and $\Delta \ell/\ell$, where t is the total flight-time of the neutrons to traverse the flight path of the length ℓ . The length of the 190 m flight path was measured by an electro-optical method with an accuracy of ± 1.2 mm, giving a value $\Delta \ell/\ell = 6 \times 10^{-6}$. Thus the major contribution to the energy uncertainty comes from the total time uncertainty which is $4 \times 10^{-5} < \Delta t/t < 10^{-4}$ for neutron energies between 3 and 15 MeV.

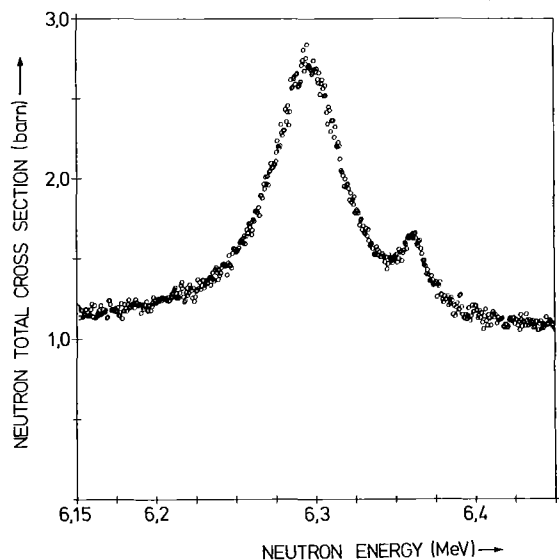


Fig. 1. The total neutron cross-section of carbon with resonances at 6.295 and 6.360 MeV.

The upper part of Table 1 gives the resonance energies recommended by the INDC subcommittee for the MeV range. In the mid part the present results are listed which show considerably better accuracy and in the lower part some more resonances are quoted which might also be suited as energy standards, as they are sharp, well isolated and exhibit an excursion of at least 30 % over the flat part of the cross-section.

Finally, it should be noted that we found a small resonance nearby the 6.295 MeV resonance in carbon which might cause a slight shift in energy if it cannot be resolved experimentally. Fig. 1 gives an impression of this possibility.

References

- (1) G.D. James, Symposium on Neutron Standards and Applications, Gaithersburg, USA, March 1977, NBS Special Publication 493, p. 319-328.

1.3.3 Investigation of s-Wave Resonances and a Possible Doorway State in Fe below 850 keV*

S. Cierjacks and I. Schouky

High resolution total and differential elastic neutron scattering cross-sections for Fe were determined with the Karlsruhe fast neutron time-of-flight

facility. Thick sample transmission measurements were carried out with an improved spectrometer resolution of 0.015 ns/m in the range from 0.4-30 MeV. From the highly resolved transmission data s-wave resonance parameters were determined by applying single channel, multilevel R-matrix theory. The assignments of spins and parities were verified by a study of the resonance shapes and the symmetry properties of resonances obtained in the scattering cross-sections for ten scattering angles between $20^\circ \leq \theta_{c.m.} \leq 150^\circ$ from 0.4 to 1 MeV. As a first step in our work assigning resonance parameters for all observed resonances in this range, the shapes of the candidates for s-wave resonances were compared with the shapes of precalculated s-wave standard resonances. The s-wave resonance data in the range from 500-850 keV indicate strong evidence for the existence of a second fragmented s-wave doorway resonance near 770 keV.

* Proc. of a NEANDC/NEACRP Specialists Meeting on Neutron Data of Structural Materials for Fast Reactors, CBNM Geel, Belgium, Dec. 5-8 (1977), to be published.

1.3.4 A Possibility to Investigate the 27.7 keV Capture Resonance in ^{56}Fe Avoiding Effects of Detector Neutron Sensitivity
F. Käppeler

Very recent capture cross-section measurements on structural materials (1) came up with resonance parameters which showed severe discrepancies of up to 100 % as compared to earlier measurements. Therefore, it was one of the recommendations of the NEANDC/NEACRP Specialists Meeting on Structural Materials at Geel (2) to investigate carefully, whether these discrepancies were caused by unexpected high neutron sensitivities of the gamma-ray detectors used in the various measurements. Even small neutron sensitivities could cause large effects as the ratio of scattering and capture widths is up to 10^3 for resonances in structural materials. Such an effect is particularly crucial in measurements where the flight path between neutron source and capture sample is much longer than the distance between capture sample and gamma detector. In this case the interval in the time-of-flight spectrum corresponding to a resonance is much larger than the time which those neutrons scattered by the same

resonance need to be captured in the detector or its environment. Thus, there is no possibility to distinguish between gamma rays from neutron capture in the sample and from scattered neutrons which are captured in the detector or nearby. By an experimental technique used previously for the measurement of capture cross-sections on various actinide isotopes (3), disturbing effects of neutron sensitivity can be avoided. Fig. 1 gives a schematic sketch of the experimental set-up.

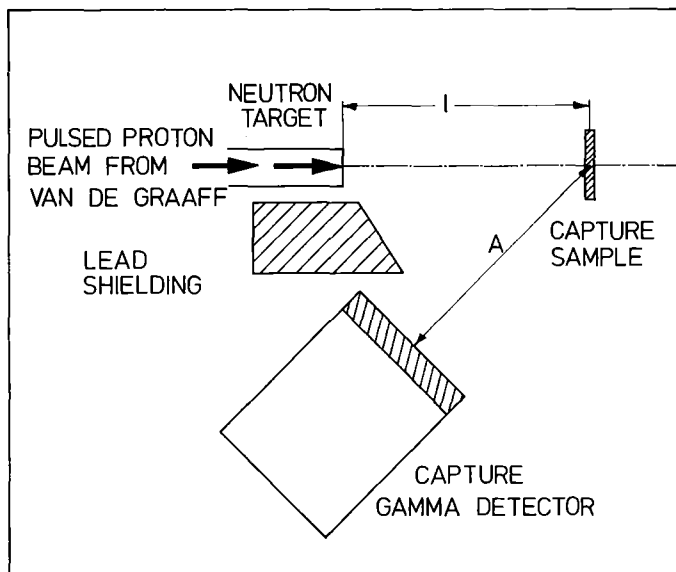


Fig. 1. Experimental set-up for the accurate determination of keV capture resonances avoiding the effect of detector neutron sensitivity.

The main point is the fact that neutron production in direct reactions such as ${}^7\text{Li}(p,n)$ or $\text{T}(p,n)$ yields kinematically collimated neutrons in a certain energy range just above the reaction threshold. Therefore no additional collimator is to be used, and the flight path between neutron target and capture sample can be reduced to a few cm. Fast pulsing of the proton beam still provides sufficient energy resolution in time-of-flight measurements to resolve particular resonances. The effect of scattered neutrons can clearly be discriminated by time-of-flight as now the distance between sample and detector is equal to or larger than the flight path between neutron source and sample.

Actual measurements are planned on an enriched ${}^{56}\text{Fe}$ sample with special emphasis on the large resonance at 27,7 keV. All the relevant parameters for this experiment are summarized in Table 1.

Table 1. Summary of the relevant experimental parameters which are characteristic for an investigation of the ^{56}Fe resonances between 20 and 40 keV.

Experimental parameters	
Proton energy	$E_p = 1885 \text{ keV}$
Resulting neutron spectrum	$20 < E_n < 39 \text{ keV}$
Opening angle of neutron cone	$\theta_{\text{max}} = 38 \text{ deg}$
Overall time resolution	$\Delta t \lesssim 1 \text{ nsec}$
Distance neutron target-sample	$l = 10 \text{ cm}$
Energy resolution at 30 keV	$\Delta E/E = 1.2 \text{ keV}$
Neutron time-of-flight between target and sample	$38 < t < 50 \text{ nsec}$
Earliest arrival of scattered neutrons at the detector:	
for $A = 10 \text{ cm}$	$t = 76 \text{ nsec}$
for $A = 20 \text{ cm}$	$t = 114 \text{ nsec}$

References

- (1) B.J. Allen and A.R. de L. Musgrove, Proc. of a NEANDC/NEACRP Specialists Meeting on Neutron Data of Structural Materials in Fast Reactors, CBNM Geel, Belgium, December 5-8 (1977), to be published.
- (2) Recommendations of Working Group B, Proc. of a NEANDC/NEACRP Specialists Meeting on Neutron Data of Structural Materials in Fast Reactors, CBNM Geel, Belgium, December 5-8 (1977), to be published.
- (3) K. Wisshak and F. Käppeler, Nucl. Sci. Eng. 66 (1978) 363.

1.3.5 A Measurement of the Total Neutron Cross-Section of Iron-58 in the Energy Range from 7 to 325 keV*

H. Beer, L.D. Hong, and F. Käppeler

The total neutron cross-section of ^{58}Fe has been determined in the energy range from 7 to 325 keV by a transmission measurement using samples enriched by the ^{58}Fe isotope. The data have been shape-fitted by means of an R matrix multilevel formalism to extract resonance parameters for s and $\ell > 0$ wave resonances. The s-wave strength function was determined to $S_0 = (4.3 \pm 1.9) \times 10^{-4}$.

*Nucl. Sci. Eng. 67 (1978) 184.

1.3.6 Neutron Total Cross-Sections for ^{240}Pu and ^{242}Pu in the Energy Range from 10 to 375 keV

F. Käppeler, L.D. Hong, and H. Beer

The isotopes ^{240}Pu and ^{242}Pu are inevitable constituents in the fuel cycle of the fast breeder reactor. Fast neutron cross-sections of these isotopes deserve, therefore, special attention in the design of these systems. As, in the fast energy range above 10 keV, experimental data of their total cross-sections are only available for ^{240}Pu from 116 keV up to 1.5 MeV in increments of 25 keV (1), transmission measurements on ^{240}Pu and ^{242}Pu were carried out at the Karlsruhe pulsed 3 MV Van de Graaff accelerator. The present measurements covered the energy range from 10 to 375 keV. Using the time-of-flight technique an improved energy resolution of 0.8 ns/m was achieved compared to the measurement reported in Ref. 1. The neutron time-of-flight spectra with and without sample were recorded with a ^6Li -glass detector at a flight path of about 5 m. Details of the experimental arrangement can be found elsewhere (2). The Pu samples consisted of plutonium oxide powder (PuO_2) which was pressed into thin walled Al-cannings. The samples were enriched in ^{240}Pu and ^{242}Pu to 98.3 and 77.16%, respectively. Therefore, besides the oxygen content impurities of other Pu isotopes had to be taken into account in the analysis. In addition the data had to be corrected for small impurities of Al from the cannings. The corrections were calculated using cross-sections from KEDAK and ENDF/B-IV data files. In Figures 1 and 2 the results of the measurements in the original energy resolution are displayed.

For comparison the KEDAK and ENDF/B-IV evaluation and the experimental values of Smith et al (1) have been included. Above 140 keV deviations between the evaluated data and the present results lie within our quoted uncertainties. Below 140 keV the evaluated data are lower than our values. The ^{240}Pu total cross-section of Smith et al (1) is in good agreement with our results.

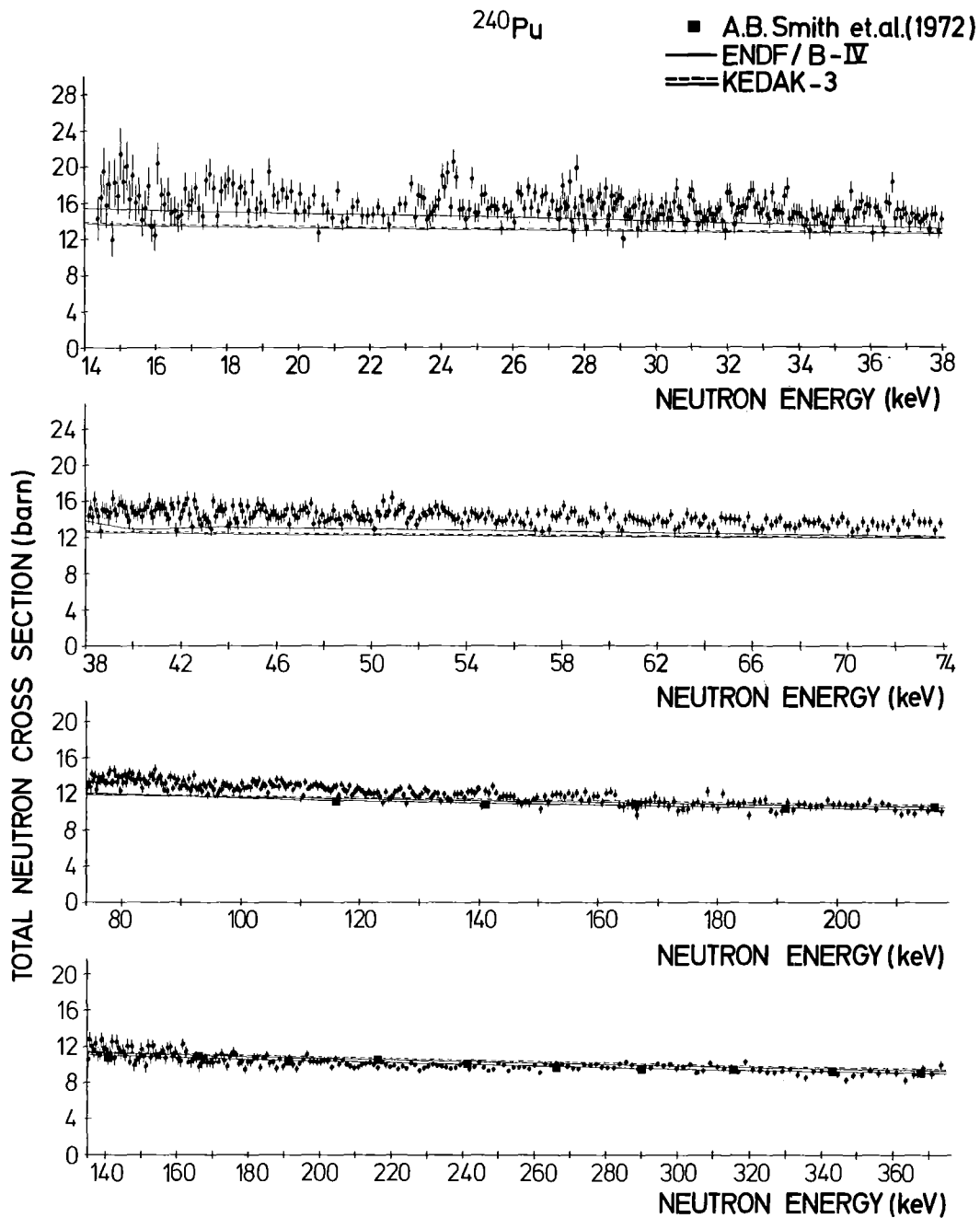


Fig. 1. The total neutron cross-section of ^{240}Pu in the energy range from 14 to 375 keV.

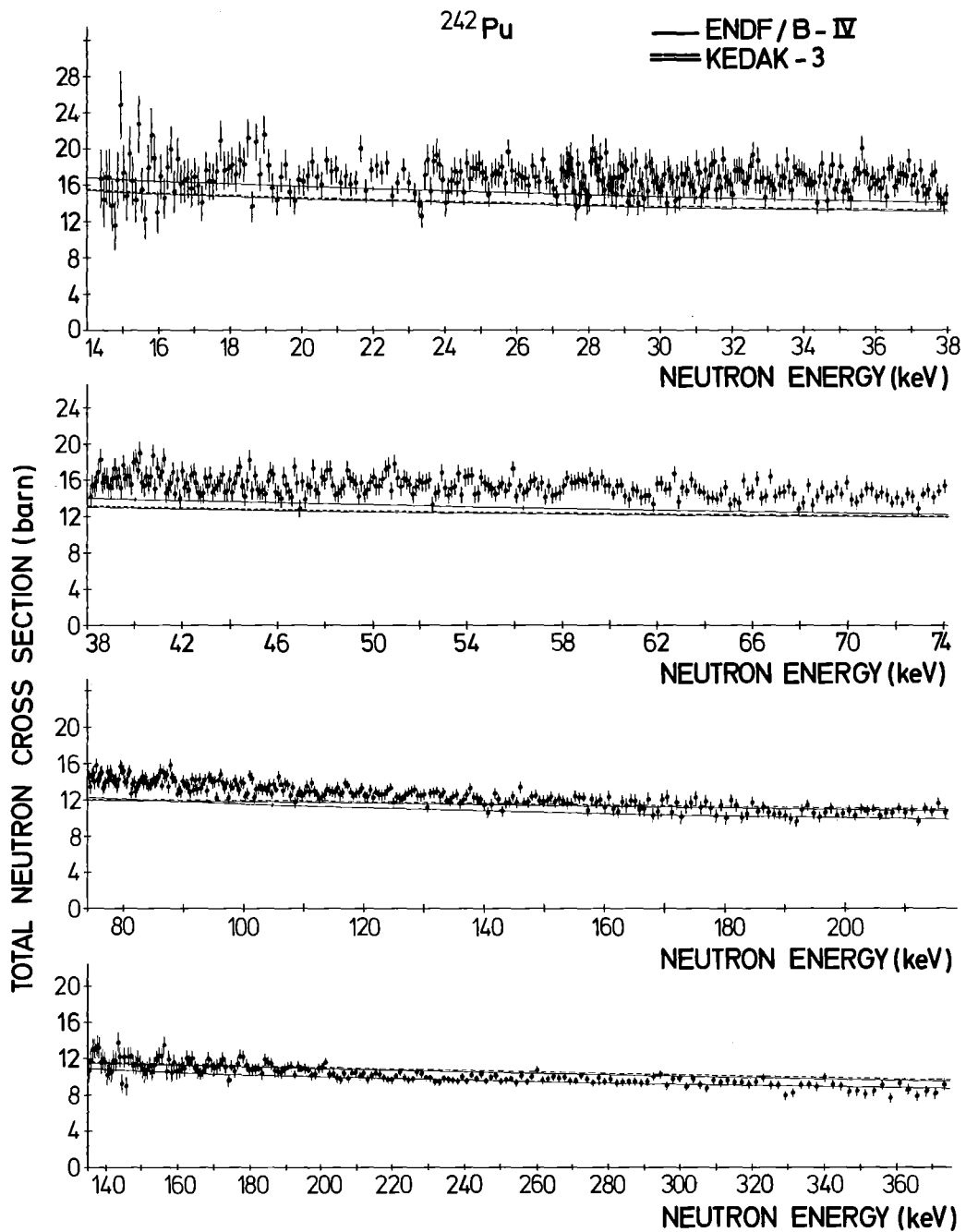


Fig. 2. The total neutron cross-section of ^{242}Pu in the energy range from 14 to 375 keV.

References

- (1) A.B. Smith, P. Lambropoulos, J.F. Whalen, Nucl. Sci. Eng. 47 (1972) 19.
- (2) H. Beer, L.D. Hong, F. Käppeler, Nucl. Sci. Eng. (accepted for publication).

1.3.7 Recent Capture Cross-Section Measurements at Karlsruhe*

H. Beer, F. Hensley, L.D. Hong, F. Käppeler, B. Leugers, and K. Wisshak

A short description of the techniques and detectors used recently at Karlsruhe for neutron capture cross-section measurements between 5 and 300 keV is given. Special emphasis is laid on the possibilities provided by the fast time resolution of Moxon-Rae and total energy detectors in connection with the subnanosecond pulsing system of the Karlsruhe Van de Graaff accelerator. The main subjects of the present work - actinide build-up and nuclear astrophysics - are illustrated by the examples of capture cross-section measurements on plutonium isotopes and on krypton.

*Proc. of a Topical Conference on "Techniques of Capture Cross-Section Measurements", Oak Ridge, 5 April 1978, to be published.

1.3.8 Neutron Capture Cross-Section Ratios of ^{240}Pu and ^{242}Pu versus ^{197}Au in the Energy Range from 50 to 250 keV*

K. Wisshak and F. Käppeler

The neutron capture cross-sections of ^{240}Pu and ^{242}Pu were measured in the energy range from 50 to 250 keV, using ^{197}Au as a standard. Neutrons were produced via the T(p,n) reaction with the Karlsruhe 3 MV pulsed Van de Graaff accelerator. Capture events were detected by a Moxon-Rae detector. A flight path as short as 66 mm was used in the measurements in order to obtain a sufficient signal-to-background ratio. An overall uncertainty of 7 to 11 % was obtained for ^{240}Pu and of 10 to 15 % for ^{242}Pu . In the region of overlap between 50 and 90 keV the presented data agree with our previous results. They confirm the existing data for ^{240}Pu . Discrepancies up to 30 % for ^{240}Pu and ^{242}Pu were found to the evaluated file ENDF/B-IV while KEDAK 3 fits the experimental data reasonably well.

*Accepted for publication in Nucl. Sci. Eng.

1.3.9 Neutron Capture Cross-Section Measurement of ^{241}Am in the Energy Range from 10 to 250 keV

K. Wisshak and F. Käppeler

For the capture cross-section measurement of ^{241}Am the same experimental method was applied as used recently for the plutonium isotopes 240 and 242 (1). The high activity of ^{241}Am , however, called for a more careful sample preparation. A sintered pellet of 3.6 g AmO_2 , 17.7 mm in diameter and 2.2 mm thick was prepared, which was welded in a 0.15 mm thick stainless steel canning.

In the low energy range from 10 to 90 keV several runs have been performed using flight paths between 50.0 and 66.4 mm. In the high energy range

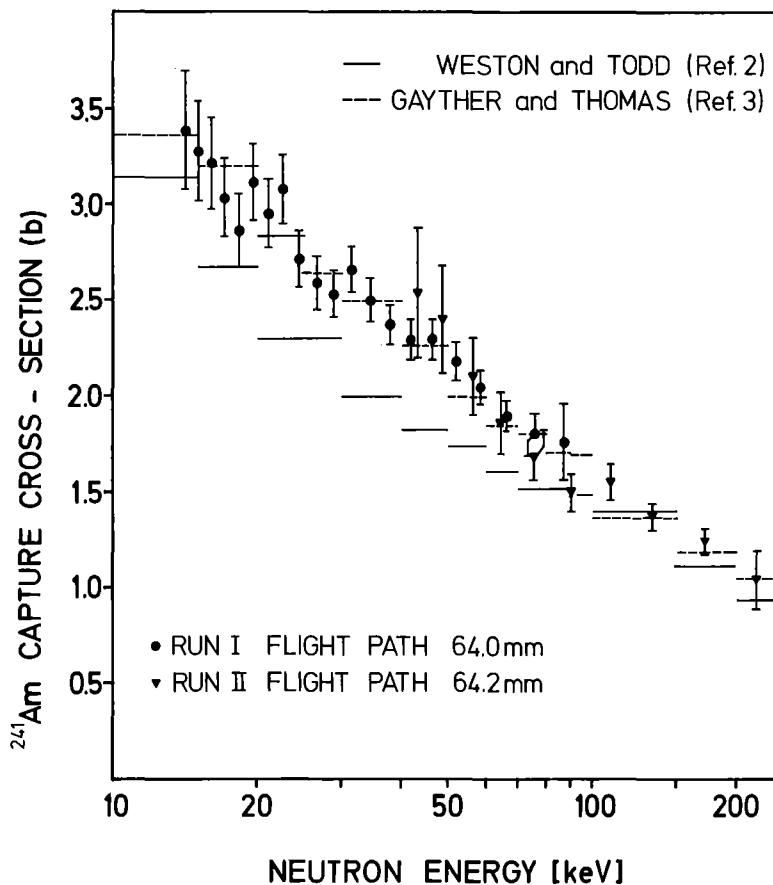


Fig. 1. Preliminary data for the capture cross-section of ^{241}Am . The absorption cross-section of References 2 and 3 are plotted for comparison.

from 50 to 250 keV data were taken at a flight path of 64.2 mm. The effect to background ratio achieved was nearly the same as in the previous measurements on plutonium samples. The data evaluation is facilitated by the fact that the correction for fission events is very small and that no isotopic impurities had to be taken into account. Therefore, the systematic uncertainties are smaller than in the previous experiments.

In Fig. 1 preliminary values for the capture cross-section of ^{241}Am are given. The values are obtained by multiplying the experimental ratios of one run at low energies and the run at high energies with the evaluated cross-section of gold taken from ENDF/B-IV. The error bars indicate the uncertainty of the measured ratio only. The total uncertainty is 4-6% for the data points between 20 and 160 keV and increases to $\sim 10\%$ at lower and higher energies.

Since the fission cross-section of ^{241}Am is several orders of magnitude smaller than the capture cross-section, a comparison is made in Fig. 1 to the measurements of the absorption cross-section from Weston and Todd (2) and Gayther and Thomas (3). Our data seem to confirm the latter measurements.

From the fission neutron spectra determined in this measurement the fission cross-section of ^{241}Am can be determined only roughly since it is known from gamma-ray measurements that the sample contains about 1% ^{239}Pu .

References

- (1) K. Wisshak and F. Käppeler, Nucl. Sci. Eng. 66, (1978) 363.
- (2) L.W. Weston and J.H. Todd, Nucl. Sci. Eng. 61, (1976) 356.
- (3) D.B. Gayther and B.W. Thomas, Proc. of a Conf. on Neutron Physics, Kiev 1977, and private communication.

1.3.10 A Measurement of the Subthreshold Neutron Fission Cross-Section of ^{240}Pu in the Energy Range from 10 to 250 keV*

K. Wisshak and F. Käppeler

The subthreshold fission cross-section of ^{240}Pu was measured in the energy range from 10 to 250 keV, using ^{235}U as a standard. Neutrons were produced via the $^7\text{Li}(p,n)$ and $\text{T}(p,n)$ reactions with the Karlsruhe 3 MV pulsed Van de Graaff accelerator. Fission events were registered by detecting fission neutrons with a NE 213 liquid scintillator with pulse-shape discriminator equipment. The high neutron flux available at flight paths of ~ 67 and 135 mm allowed for a statistical accuracy of 1-3 % together with a moderate energy resolution of ~ 10 to 20 ns/m. The overall accuracy achieved is between 7 and 9 %. The data show a distinct structure in the cross-section as indicated with poor statistics in previous measurements.

*Accepted for publication in Nucl. Sci. Eng.

1.3.11 Measurement of the ^{239}Pu and ^{240}Pu Fission Cross-Sections Relative to the ^{235}U Fission Cross-Section and the Scattering Cross-Section $\text{H}(n,p)$ in the Neutron Energy Range from 0.5 to 20 MeV*

K. Kari

The fission cross-section ratios $\sigma_f(^{239}\text{Pu})/\sigma_f(^{235}\text{U})$ and $\sigma_f(^{240}\text{Pu})/\sigma_f(^{235}\text{U})$ were measured in the energy range from 0.5-20 MeV by the neutron time-of-flight spectrometer installed at the Karlsruhe isochronous cyclotron. The simultaneous measurement of the neutron flux by a new telescopic proton recoil counter allowed to determine also the absolute fission cross-section of ^{239}Pu as well as the relative shape of the ^{240}Pu fission cross-section. An improved gas scintillation counter assembly was used to record the fission events; it allowed to detect fission events in the presence of a very high alpha background of about 10^6 events/s.

The excitation functions of the fission cross-sections between 1 and 20 MeV are interpreted on the basis of the direct (n,f) fission process and the competing fission channels of the (n,n'f) and (n,2nf) types.

*Report KfK 2673 (1978).

1.3.12 The Fission Cross-Section of ^{241}Am in the Energy Range from 10 to 1200 keV

W. Hage⁺, H. Hettinger⁺, S. Kumpf⁺, F. Käppeler, and K. Wisshak

The measurements of the ^{241}Am fission cross-section via fission neutron and fission fragment detection which were described in the preceding progress report (1) are now completed. The data analysis is also almost finished but we still have some problems with the determination of the sample masses. Therefore no final results can be communicated at present but we hope that they will soon be available.

⁺JRC Euratom, Ispra, Italy

References

- (1) W. Hage, H. Hettinger, S. Kumpf, F. Käppeler, and K. Wisshak, Report KFK 2504 (1977) 27.

2. CHARGED-PARTICLE REACTIONS

2.1 POLARIZED AND UNPOLARIZED DEUTERONS

2.1.1 Spins of Proton Hole States from Analyzing Powers of (d, τ) Reactions at 52 MeV*

V. Bechtold, L. Friedrich, P. Doll⁺, K.T. Knöpfle⁺⁺, G. Mairle⁺⁺,
and G.J. Wagner⁺⁺

Large and characteristic vector-analyzing powers of the (\vec{d},τ) reactions on ^{16}O , ^{28}Si and ^{40}Ca at 52 MeV have been observed and utilized to determine the spins of 1p hole states in ^{15}N and ^{27}Al and of 1d hole states in ^{39}K . The results are pertinent to the empirical determination of the 1p and 1d spin-orbit splittings.

* Physics Letters 72B (1977) 169

⁺ Present address: Lawrence Berkeley Laboratory

⁺⁺ Max Planck-Institut für Kernphysik, Heidelberg, Germany

2.1.2 Fission Fragment Energy-Velocity Correlation Measurements for the $^{233}\text{U}(d,pf)$ -Reaction*

Y. Patin⁺, S. Cierjacks, J. Lachkar⁺, J. Sigaud⁺, G. Haout⁺,
and F. Cocu⁺

A new experimental method is proposed to determine, as a function of excitation energy of the fissioning nucleus, the mass and energy distributions of the fragments for both pre- and post-neutron emission. From these distributions also the average number of neutrons emitted by the fission fragments as a function of initial fragment masses can be derived. The method is based on the measurement of both fragment kinetic energies and velocities in charged-particle induced fission through reactions such as (d,pf) where the emitted charged particle is used as starting time for the fragment velocity determination. The major interest lies in the precision of about 0.5 amu in the pre-neutron mass determination. Details of the experimental arrangement and the method of data analysis are given.

Typical experimental results obtained from the $^{233}\text{U}(\text{d},\text{pf})$ reaction are shown and compared with previous results from thermal neutron fission.

* submitted to Nucl. Instr. Meth.

+ Centre d'Etudes de Bruyères-le-Châtel, Service de
Physique Nucléaire

2.2 ALPHA-PARTICLE REACTIONS

2.2.1 $^{48}\text{Ca}-^{40}\text{Ca}$ Radius Difference from Elastic Scattering of 104 MeV Alpha-Particles

H.J. Gils, E. Friedman⁺, H. Rebel, J. Buschmann,
H. Klewe-Nebenius⁺⁺, Z. Majka⁺⁺⁺, and B. Neumann

In contrast to our knowledge about charge or proton distributions, respectively, the information about the radial distributions of the neutrons or of the total nucleon density is rather scarce and less certain. This is due to the lack of knowledge about the strong interaction involved in the experimental processes providing such information and because of a considerable model dependence of the analyses. Nevertheless, there are great efforts to determine the radial shape of the neutron distributions preferentially in neutron rich nuclei such as ^{48}Ca and ^{208}Pb . There, a remarkable difference between proton and neutron densities may be expected. The results of the different methods, however, are contradictory in some cases, and it seems worthwhile to continue these efforts by improving the experimental information and the methods of the analyses.

Among the various experimental methods medium energy alpha-particle scattering is a promising tool because the reaction mechanism has been demonstrated to be sufficiently well understood in terms of refined microscopic calculations (1). The analyses have been shown to provide reliable information about the radial shape of nuclei if the experimental data satisfy some necessary conditions such as high angular accuracy and a wide range of scattering angles from very small values up to the region far beyond the nuclear rainbow.

In order to determine the radius difference of the total nucleon densities of $^{48}\text{Ca}-^{40}\text{Ca}$ and to extract the radius difference of the neutrons and protons of ^{48}Ca the elastic scattering of 104 MeV alpha-particles was measured at the Karlsruhe Isochronous Cyclotron. The experimental cross sections range from $\theta_{\text{Lab}} = 2.5^\circ$ to 110° in steps of 0.5° (up to 60°) and of 1.5° (larger angles), respectively. The total uncertainty of the absolute angular scale was estimated to be smaller than 0.1° .

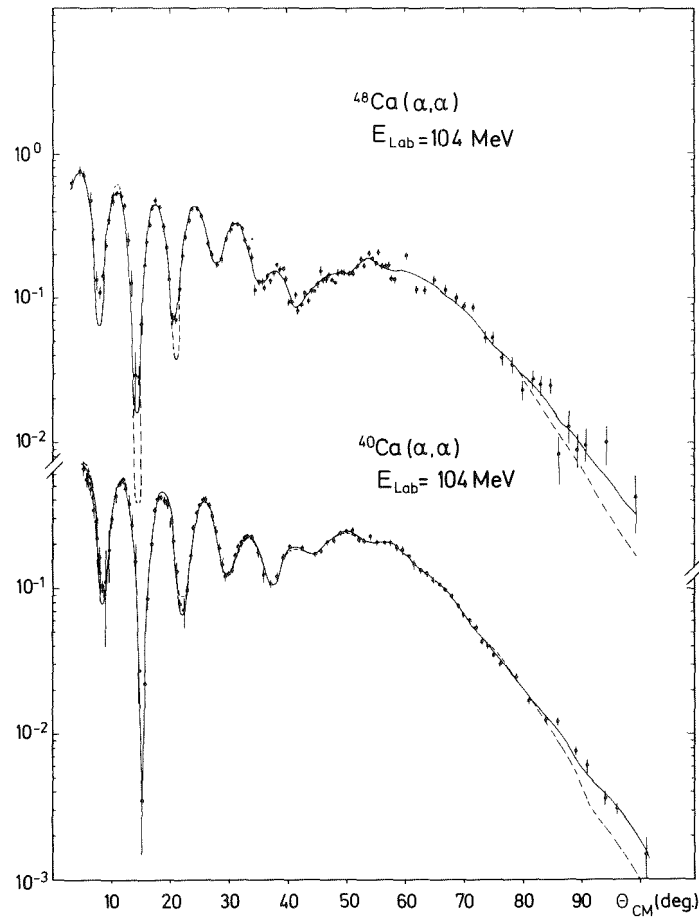


Fig. 1. Measured differential cross sections (normalized to the Rutherford cross sections) for elastic 104 MeV alpha-particle scattering from $^{40,48}\text{Ca}$

- Fourier-Bessel potential analyses
- Density dependent folding model calculations.

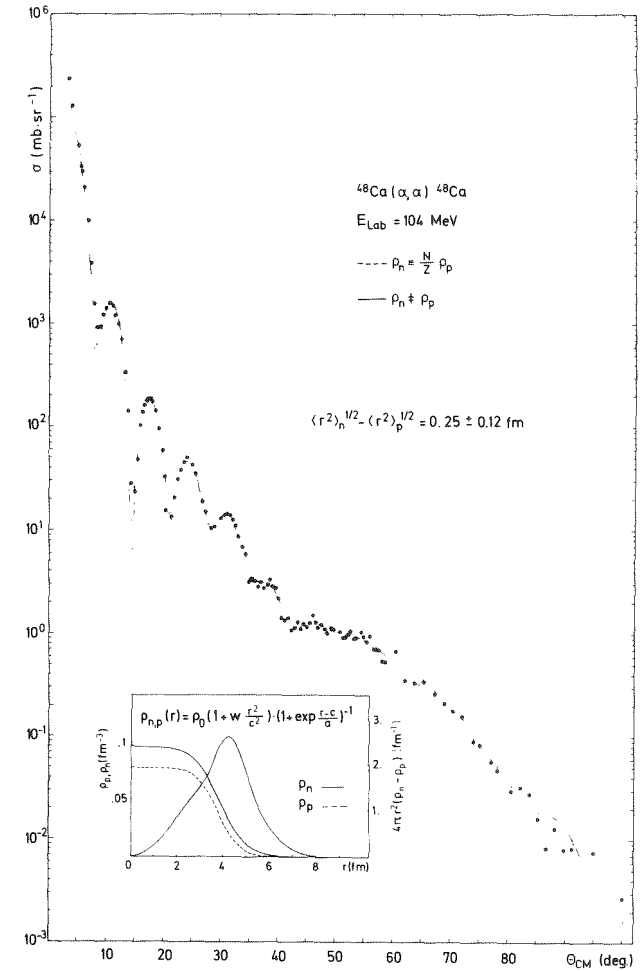


Fig. 2. Influence of the neutron density on the calculated scattering cross sections of ^{48}Ca

- $\rho_n \neq \frac{N}{Z} \rho_p$ best fit
- $\rho_n \equiv \frac{N}{Z} \rho_p$

Inset: Proton and neutron densities and weighted difference.

The differential cross sections normalized to the Rutherford scattering cross sections are displayed in Fig. 1. The data were analyzed by several procedures:

- i) optical potential analyses with conventional Saxon-Woods form, Saxon-Woods squared potential, and Fourier-Bessel-series (FB) potential (2);
- ii) folding model analyses with a density dependent effective interaction, Fermi-shaped and Fourier-Bessel-series densities.

The solid curves in Fig. 1 are the results of the FB-potential analyses whereas the dashed curves are the theoretical cross sections using the density dependent folding model with three parameter Fermi distributions. All analyses consistently yield the difference

$$\Delta r_m (48-40) = 0.17 \pm 0.07 \text{ fm}$$

between the rms radii of the total nucleon densities. The error given is that one of the FB potential analyses (c.f. contrib.2.2.2).

In Fig. 2 we compare the folding model calculation for ^{48}Ca assuming $\rho_n = \frac{N}{Z} \rho_p$ (dashed curve) with the best fit result for $\rho_n \neq \frac{N}{Z} \rho_p$ (solid curve) varying the parameters of ρ_n . The experimental cross sections clearly favour a larger radius for the neutrons. The corresponding neutron and proton densities and the radially weighted difference $4\pi r^2(\rho_n - \rho_p)$ - indicating a "neutron halo" - are displayed in the inset. The analyses result in the difference

$$\Delta r_{n-p} (48) = 0.25 \pm 0.12 \text{ fm}$$

between the rms radii of neutrons and protons. The radii differences obtained are - within the error bars - in agreement with previous investigations (3). However, one should notice that previous analyses appreciably underestimate the uncertainties of the results due to the use of a specific simple functional form for the density distributions (c.f. contrib.2.2.2).

⁺ Racah Institute of Physics, The Hebrew University of Jerusalem

⁺⁺ Institut für Radiochemie

⁺⁺⁺ Permanent address: Jagellonian University, Cracow, Poland

References

- (1) Z. Majka, H.J. Gils, H. Rebel; Report KFK 2622 (1978).
- (2) E. Friedman and C.J. Batty; Phys. Rev. C17 (1978) 34.
- (3) G.D. Alkhozov et al., Phys. Lett. 57B (1975) 47, Nucl. Phys. A 274 (1976) 443;
A. Chaumeaux, V. Layly, and R. Schaeffer, Phys. Lett. 72B (1977) 33.

2.2.2 Fourier-Bessel Series Description of α -Particle-Nucleus Optical Potentials and Nuclear Matter Densities

E. Friedman⁺, H.J. Gils, H. Rebel, and Z. Majka⁺⁺

In optical model descriptions of elastic scattering usually there is some residual dependence of the results on the particular choice of the parametrized form for the potential. The Saxon-Woods (SW) form has been widely and very successfully used to describe optical potentials for nucleons as well as for composite projectiles. However, this form gives an implicit coupling between the surface region and the interior of the potential and this could introduce undesirable constraints in the analysis. Some attempts have been made to improve the SW form e.g. by using the square of the SW form factor (1) or by adding an additional term to the SW potential which is centered at the nuclear surface. Both procedures yield a distinctly better representation of elastic scattering cross sections (e.g. for 104 MeV alpha particles), in particular when large scattering angles beyond the nuclear rainbow are included in the data.

A special case of the latter method is presented in this contribution the main aim of which is to remove the coupling between the surface and interior part of the potential and to provide realistic estimates of the errors of the potentials at each radial point. Following descriptions of nuclear charge distributions (2) we choose a Fourier-Bessel (FB) expansion of the real potential (3), namely

$$V(r) = -V_0 / (1 + e^x) - \sum_{n=1}^N b_n j_0(q_n r)$$

where $x=(r-r_0 \cdot A^{1/3})/a$ and V_0 , r_0 and a are the parameters of the best-fit SW potential. $j_0(q_n r)$ are spherical Bessel functions and $q_n = n\pi/R$, where R is a suitable chosen cut-off radius beyond which the extra term of the potential vanishes.

The refined parametrization described was applied to the analysis of elastic scattering of 104 MeV alpha particles from $^{40,48}\text{Ca}$ measured at the Karlsruhe Isochronous Cyclotron (4). The FB potentials obtained are displayed in Fig. 1. The shaded areas are the error bands determined from the covariance matrix of the FB coefficients (3). They indicate that the potential shape is well determined for $r > 2$ fm. Only the very interior of the potential ($r < 2$ fm) is less certain.

When performing folding model analyses of elastic scattering in order to determine nucleon density distributions a similar coupling between the surface and interior regions of the density distributions occur when choosing common parametrizations such as two or three parameter Fermi distributions (5). In order to remove this we introduce the FB expansion also to nucleon density distributions in folding model analyses (4).

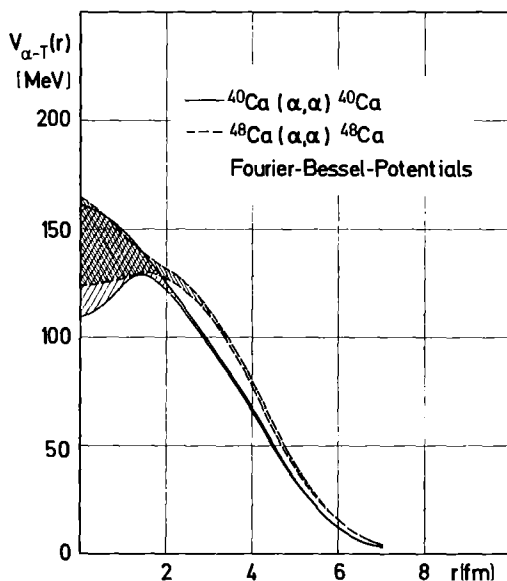


Fig. 1. Real best-fit optical potentials $^{40,48}\text{Ca}(\alpha, \alpha)$. The shaded areas indicate the error bands obtained by the FB analysis. The rms radii of the potentials are $\langle r^2 \rangle^{1/2}(40) = 4.38 \pm 0.04$ fm and $\langle r^2 \rangle^{1/2}(48) = 4.59 \pm 0.04$ fm, respectively.

Results for folding model analyses are presented in Fig. 2. The total nucleon density of ^{48}Ca has a remarkably larger radial extension than that of ^{40}Ca . The bump of $\rho_m(48)$ at $r \sim 3$ fm possibly indicates the location of the $f_{7/2}$ neutrons. The remarkably larger error band in the interior region of ^{48}Ca is due to the poorer quality of the data in the scattering region beyond 40° . This is a clear indication that for a reliable determination

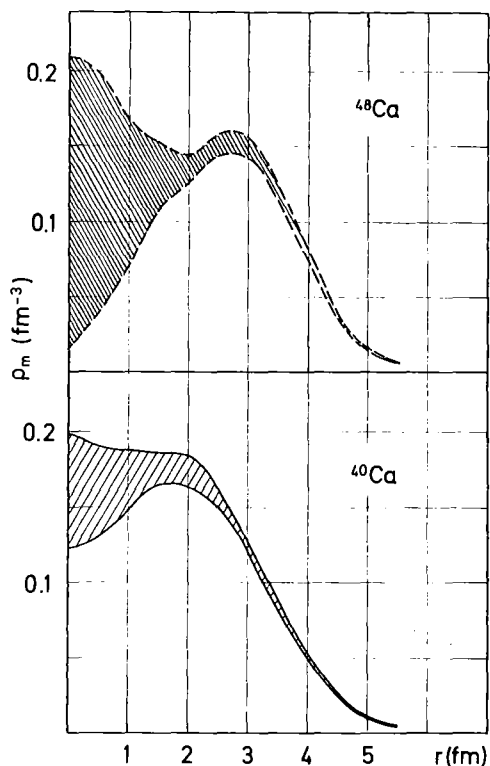


Fig. 2. Nuclear matter density distributions from a combined folding model and Fourier-Bessel analysis. The rms radii of the presented distributions are
 $\langle r^2 \rangle^{1/2}(40) = 4.37$ fm and
 $\langle r^2 \rangle^{1/2}(48) = 4.49$ fm, respectively.

of nuclear matter radii by alpha-particle scattering it is necessary to carefully measure cross sections not only in the diffraction region but far beyond it.

⁺Racah Institute of Physics, The Hebrew University of Jerusalem

⁺⁺Permanent address: Jagellonian University, Cracow, Poland

References

- (1) Z. Majka and T. Srokowski; Acta Phys. Pol. B9 (1978) 53.
- (2) B. Dreher, J. Friedrich, K. Merle, H. Rothhaas and G. Lührs, Nucl. Phys. A 235 (1974) 219.
- (3) E. Friedman and C.J. Batty, Phys. Rev. C17 (1978) 34.
- (4) Contribution 2.2.1 of this report.
- (5) H.J. Gils and H. Rebel; Phys. Rev. C13 (1976) 2159;
H.J. Gils, H. Rebel, J. Buschmann, H. Klewe-Nebenius, G.P. Nowicki, W. Nowatzke; Z. Phys. A 279 (1976) 55.
E. Friedman and C.J. Batty; Phys. Rev. C16 (1977) 1425.

2.2.3 A Study of the Giant Resonance Region of ^{208}Pb by Particle-Gamma Angular Correlations

W. Eyrich⁺, A. Hofmann⁺, H. Rost⁺, U. Scheib⁺, S. Schneider⁺,
F. Vogler⁺, and H. Rebel

Giant multipole resonances (GMR) are often studied by inelastic alpha-particle scattering. More detailed information about GMRs can be obtained from angular correlation experiments, in which the scattered particles and particles from the decay of the GMR are measured in coincidence. By this method which leads to a drastic reduction of the background it should be easier to identify new GMRs, to assign multipolarities and strengths.

Moreover it should be possible to extract additional information on the structure of the GMRs from the angular correlation function.

In heavy nuclei the GMRs cannot decay by charged particle emission because of the mostly negative Q-values and the high Coulomb barriers. They decay mainly by emission of neutrons and gamma-quanta. Here α' - γ angular correlation experiments seem to be a powerful tool for the investigation of the GMRs. In order to show this we have started an $(\alpha, \alpha'\gamma)$ angular correlation experiment on ^{208}Pb at the Karlsruhe cyclotron. The experiment is performed with a multidetector arrangement consisting of four Si(Li) alpha-particle detectors and two Ge(Li) gamma-detectors.

In ^{208}Pb two isoscalar GMRs around 10.9 MeV and 13.7 MeV excitation energy are known from alpha-particle scattering experiments. From the anal-

yses of these experiments there is strong evidence of E2 for the lower resonance and some indication of a "breathing mode" for the resonance at 13.7 MeV. It is one aim of our correlation experiment to decide this unambiguously.

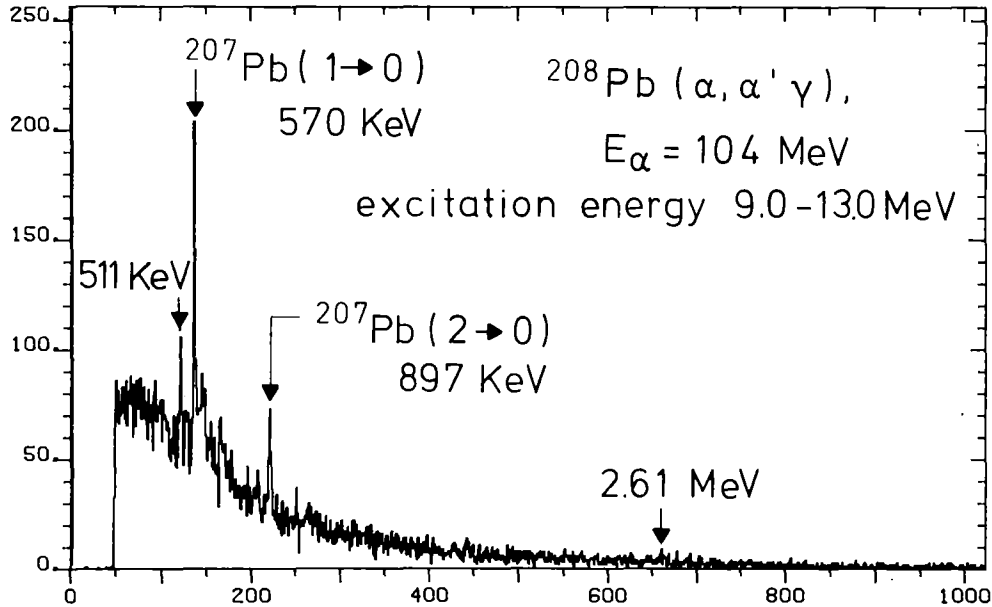


Fig. 1. Gamma-spectrum coincident to alpha-particles scattered from ^{208}Pb at excitation energies between 9 and 13 MeV.

Figure 1 shows a gamma-spectrum coincident to the scattered alpha-particles in an excitation range 9-13 MeV. The spectrum is dominated by two peaks at 570 keV and 897 keV belonging to the lowest gamma-transitions in ^{207}Pb . At the transition energies of ^{208}Pb (especially from the first excited state to the groundstate) there is practically no enhancement. That means that the resonance at 10.9 MeV decays nearly to 100% by emission of neutrons. In the alpha-particle spectrum coincident to the gamma-peaks at 570 keV and 897 keV, respectively, the background in the region of the giant resonances is suppressed by a factor of 5-7. This facilitates the analyses of the spectra very much. The in-plane alpha-gamma angular correlation $^{208}\text{Pb}(\alpha, \alpha') ^{208}\text{Pb}^* \xrightarrow{n} ^{207}\text{Pb}^*(\gamma_{1 \rightarrow 0}) ^{207}\text{Pb}$ of the resonance at 10.9 MeV shows an anisotropic pattern compatible with the assumption of E2. It can be suspected from preliminary calculations that the pattern of the correlation function is extremely sensitive to the microscopic structure of the GMR. The corresponding correlation function of the resonance at 13.7 MeV seems to be isotropic. The statistical errors, however, are still too large for a definite statement on this resonance.

⁺Physikalisches Institut der Universität Erlangen-Nürnberg, Germany

2.2.4 The Deformation of ^{26}Mg and ^{28}Si from Particle-Gamma Angular Correlations

W. Eyrich⁺, A. Hofmann⁺, U. Scheib⁺, S. Schneider⁺, F. Vogler⁺, and H. Rebel

Particle-gamma angular correlations provide more detailed information about reaction mechanisms and nuclear structure than differential cross sections. In the special case of $(\alpha, \alpha_1 \gamma)$ angular correlations on even-even nuclei it is possible to determine the individual reaction amplitudes, which describe the transitions to the various magnetic substates of the excited residual state. Therefore $(\alpha, \alpha_1 \gamma)$ angular correlation measurements are especially suitable for the study of reaction and structure models and their parameters.

The "in-plane" angular correlation function for alpha-particle scattering and the spin sequence $0^+ - 2^+ - 0^+$ is given by

$$W(\Theta_\alpha = \frac{\pi}{2}, \phi_\alpha; \Theta_\gamma = \frac{\pi}{2}, \phi_\gamma) = A(\phi_\alpha) + C(\phi_\alpha) \cdot \sin^2 2 \cdot (\phi_\gamma - \phi_2(\phi_\alpha)).$$

The quantities A, C and ϕ_2 which depend on the alpha-particle scattering angle ϕ_α are simply related to reaction amplitudes (1).

We continued the $(\alpha, \alpha' \gamma)$ angular correlation measurements of s-d-shell nuclei (2) and measured the in-plane correlation on ^{26}Mg and ^{28}Si (4). The experiments were performed with a multidetector arrangement consisting of four Si(Li) alpha-particle detectors and two Ge(Li) gamma-detectors. The data were analyzed in terms of coupled channels on the basis of the symmetric rotator model in the frame of the extended optical model. The correlation data, especially the amplitude C of the angular correlation function, were found to be very sensitive to the sign of the intrinsic quadrupole deformation (2). The characteristic prolate-oblate effects turned out to be independent of the potential parameters used.

In Figure 1 the correlation amplitudes C are shown for ^{24}Mg , ^{28}Si and ^{26}Mg . The curves represent CC calculations with the parameters resulting from the best fits to the respective differential cross sections for prolate and oblate deformation. For ^{24}Mg and ^{28}Si prolate and oblate deformation, respectively, is favored already in the best fits to the elastic and inelastic cross sections (3). The drastic prolate-oblate effects in the correlation amplitude C allow an unambiguous decision on the deformation sign (2).

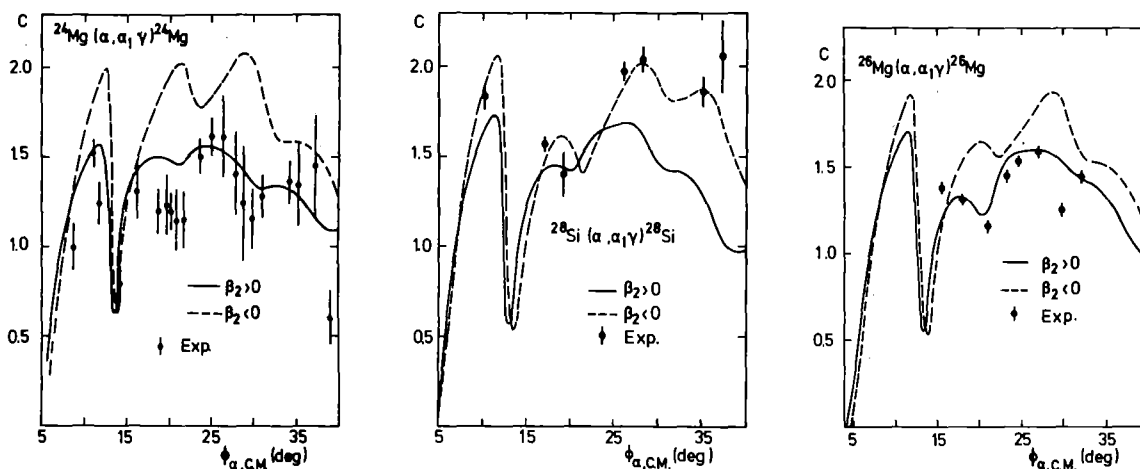


Fig. 1. Experimental correlation amplitudes C of the reactions ^{24}Mg , ^{28}Si , $^{26}\text{Mg}(\alpha, \alpha_1 \gamma)$ and coupled channels predictions for prolate and oblate deformation.

In contrast to ^{24}Mg and ^{28}Si the sign of the quadrupole deformation of ^{26}Mg was not definitely assigned. From the cross sections, which again are described very well by CC calculations (3), no indication about the deformation sign can be obtained. Obviously the correlation data (Fig. 1) clearly favor prolate deformation for ^{26}Mg .

⁺Physikalisches Institut der Universität Erlangen-Nürnberg, Germany

References

- (1) H. Wagner, A. Hofmann, and F. Vogler; Phys. Lett. 47B (1973) 497.
- (2) W. Eyrych, A. Hofmann, U. Scheib, S. Schneider, F. Vogler, and H. Rebel; Phys. Lett. 63B (1976) 406, Nucl. Phys. A287 (1977) 119, and J. Phys. Soc. Japan 44 (1978) Suppl. p.640-643.
- (3) H. Rebel, G.W. Schweimer, G. Schatz, J. Specht, R. Löhken, G. Hauser, D. Habs, and H. Klewe-Nebenius; Nucl Phys. A182 (1972) 145.

2.3 ${}^6\text{Li}$ -PARTICLE REACTIONS

2.3.1 Search for Different Components in the Giant Resonance Bumps Excited by 156 MeV ${}^6\text{Li}$ -Particle Scattering on ${}^{90}\text{Zr}$

H.J. Gils, J. Buschmann, H. Rebel, S. Zagromski, G. Bechtold, H. Klewe-Nebenius⁺, B. Neumann, and H. Faust⁺⁺

The isoscalar quadrupole giant resonance (GR) has been studied extensively by p-, d-, τ - and α -particle scattering in recent years (1). However, in order to interpret the measured spectra quantitatively serious difficulties arise from the considerable continuum background on which the GR bumps are superimposed. Recently, it has been shown that this background is drastically reduced when exciting the GR by scattering of high energy (>100 MeV) ${}^6\text{Li}$ -projectiles (2). This is mainly due to the low lying α -d break-up threshold of the ${}^6\text{Li}$ -particle preventing two effects which are disadvantageous for GR observation: preequilibrium emission of the probing particle from compound nucleus formation and projectile excitation. Thus ${}^6\text{Li}$ -scattering appears to be an excellent tool for more detailed studies of shape, components and multipolarities of giant resonances.

The most interesting questions in this field currently discussed (1,3,4,5) are the evidence of the monopole giant resonance ("breathing mode") and of the location and strength of giant resonances of higher multipolarities (octupole, hexadecapole) which are predicted by microscopic theories (4,5).

Concerning L=4 transitions ${}^{90}\text{Zr}$ is of particular interest because of its strongly reduced collectivity of the low-lying hexadecapole strength. From the simple sum rule point of view the missing L=4 transition strength thus should be located in the GR region. In fact, in an attempt of a consistent description of low-lying states and giant resonances in ${}^{90}\text{Zr}$ (5) a considerable amount of E4 strength is predicted to be located at the low energy tail of the E2 giant resonance at about 11 MeV.

We started to search this giant resonance component (and perhaps other multipolarities) by scattering of 156 MeV ${}^6\text{Li}$ -particles from ${}^{90}\text{Zr}$. The main experimental difficulties arose from the fact that - due to a coupled channel prediction - the angular distribution of an E4 component should remarkably

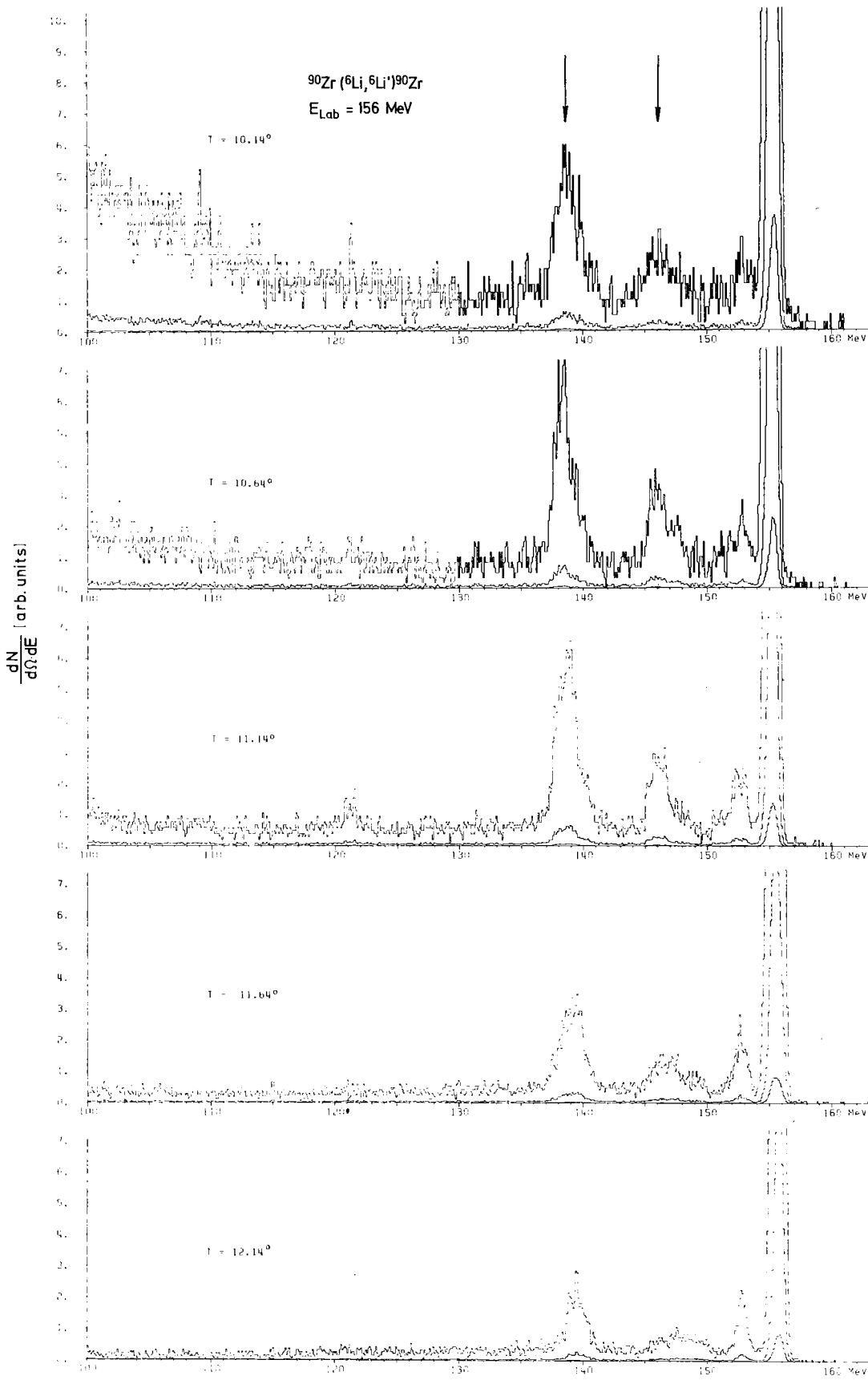


Fig. 1. Spectra of scattered ${}^6\text{Li}$ particles from ${}^{90}\text{Zr}$ taken at different scattering angles. The arrows indicate the giant resonance regions at about 7.5 and 15 MeV excitation energy.

deviate from that of an E2 GR only at very forward scattering angles ($\lesssim 10^\circ$) where elastic scattering is strongly dominating and the hydrogen contamination peak is disturbing the spectra. In addition, one has to determine and to control very carefully the energy calibration in order to assure that possible changes in the shape of the GR bumps are not due to electronic instabilities. We performed this by repeated measurements of elastic scattering from ^{12}C positioning the elastic scattering peak into the GR region of ^{90}Zr by choosing a suitable scattering angle (6).

As an example of the experimental results, Fig. 1 displays spectra of scattered ^6Li between $\Theta_{\text{Lab}} = 10^\circ$ and 12° clearly showing the well-known isoscalar quadrupole giant resonance at $E_x \sim 15$ MeV and additionally a bump at $E_x \sim 7.5$ MeV split into different components. This is assumed to be the $L = 3$ GR (4).

The shape of the GR bump at 15 MeV varies significantly with increasing scattering angle indicating that the different contributions at the centre, the low energy tail and the high energy slope may have different multipolarities. Similar features are observed for the excitation peak around $E_x = 7.5$ MeV.

The quantitative analysis of the spectra confirms the location and strength of the predicted E4 GR at about 12 MeV. However, before convincing results can be presented, more data have to be included to improve the statistical accuracy.

⁺Institut für Radiochemie

⁺⁺Physikalisches Institut der Universität Heidelberg

References

- (1) D.H. Youngblood, J.M. Moos, C.M. Rozsa, J.D. Bronson, A.D. Bacher, and D.R. Brown; Phys. Rev. C13 (1976) 934.
K.T. Knöpfle, G.J. Wagner, H. Breuer, M. Rogge and C. Mayer-Böricke, Phys. Rev. Lett. 35 (1975) 779.
M.N. Harakeh, K. van der Borg, T. Ishimatsu, H.P. Morsch and A. van der Woude; Phys. Rev. Lett. 38 (1977) 676.

- (2) H.J. Gils, H. Rebel, J. Buschmann, and H. Klewe-Nebenius;
Phys. Lett. 68B (1977) 427.
R. Pardo, R.G. Markham, W. Benenson, A.I. Galonsky, and E. Kashy;
Phys. Lett. 71B (1977) 301.
- (3) N. Marty, M. Morlet, A. Willis, V. Comparat, and R. Frascaria;
Proc. Int. Symp. on Highly Excited States in Nucl., Jülich, 1975,
Vol. 1, p. 17.
J.S. Dehesa, S. Krewald, J. Speth, and A. Faessler; Phys. Rev. C15
(1977) 1858.
- (4) J. Wambach, V.A. Madsen, G.A. Rinker, and J. Speth; Phys. Rev. Lett.
39 (1977) 1443.
- (5) W. Knüpfer; private communications.
- (6) S. Zagromski, J. Buschmann, and H.J. Gils, contribution 7.4.12 of this
report.

2.3.2 Giant Resonance Excitation by 156 MeV ${}^6\text{Li}$ Scattering*
H.J. Gils, H. Rebel, J. Buschmann, and H. Klewe-Nebenius⁺

The excitation of the giant quadrupole resonance in ${}^{208}\text{Pb}$ has been observed by inelastic scattering of 156 MeV ${}^6\text{Li}$ ions. The continuum background in the giant resonance region of the measured ${}^6\text{Li}$ spectra proves to be strongly reduced as compared to the spectra obtained by inelastic scattering of lighter projectiles, which makes ${}^6\text{Li}$ scattering a promising tool for more detailed studies.

* Phys. Lett. 68B (1977) 427.

⁺ Institut für Radiochemie

2.3.3 Experimental Studies of the Reaction Mechanisms
of ${}^{208}\text{Pb} + {}^6\text{Li} \rightarrow {}^{211\text{m}}, {}^{212\text{m}}\text{Po}$

B. Neumann, J. Buschmann, H. Klewe-Nebenius⁺, and H. Rebel

During the investigations of ${}^6\text{Li}$ induced reactions at the Karlsruhe Isochronous Cyclotron we have encountered the problem to discriminate between different reaction paths leading to the same final nucleus. This problem arises when e.g. ${}^{208}\text{Pb}$ is bombarded by ${}^6\text{Li}$ -ions and the

production cross-sections of $^{211m,212m}\text{Po}$ are determined by observing the alpha-decay of these nuclides. A competition of following processes is expected:

- ($^6\text{Li}, xn+yp$) compound or precompound processes
- direct particle transfer (e.g. alpha-transfer)
- break-up of the ^6Li projectile ($^6\text{Li} \rightarrow \alpha + d$) with capture of a fragment into highly excited levels of the target nucleus and subsequent deexcitation via compound and precompound processes (we call this particular reaction type "internal break-up" (1)).

An experimental discrimination between these processes is possible due to different recoil energies of the product nuclei. While for $E_{\text{Li}} = 156$ MeV the fusion nucleus recoils with $E_{\text{R}} = 4.5$ MeV, the recoil energy of ($\alpha + ^{208}\text{Pb}$) compound nucleus formed via "internal break-up" is below 1.8 MeV. Assuming a forward peaked angular distribution for the direct ($^6\text{Li}, d$)-reaction, the recoil for the alpha-particle transfer is below 0.7 MeV.

In our measurements the produced $^{211m,212m}\text{Po}$ nuclei have been detected by their long-lived alpha-activity. Using a target thin enough for all reaction products to escape, we have varied the thickness of a ^{12}C -catcher foil behind the target and measured the range of the recoils in the carbon foils. The catcher foils were mounted on a slider movable pneumatically between the irradiation position just behind the (fixed) target and the measuring position in front of a thin surface barrier detector appropriate for the alpha-spectroscopy. Irradiation period and recording of the alpha-particle spectra during four time intervals have been controlled electronically.

Fig. 1 shows the measured ^{211m}Po alpha-activity as a function of the thickness of the ^{12}C catcher foils. Most of the ^{211m}Po recoil nuclei ($\sim 90\%$) have a range of about $90 \mu\text{g}/\text{cm}^2$ in ^{12}C corresponding to a recoil energy of 1.8 MeV. The same result is obtained from an analysis of the energy shifts of the alpha-peak due to the different thickness of the catcher foils in which the recoils are stopped before emitting the decay alpha-particle. Only less than 10% of the observed ^{211m}Po recoils have energies of about 4.5 MeV. These results confirm the conclusions of Kropp et al (1).

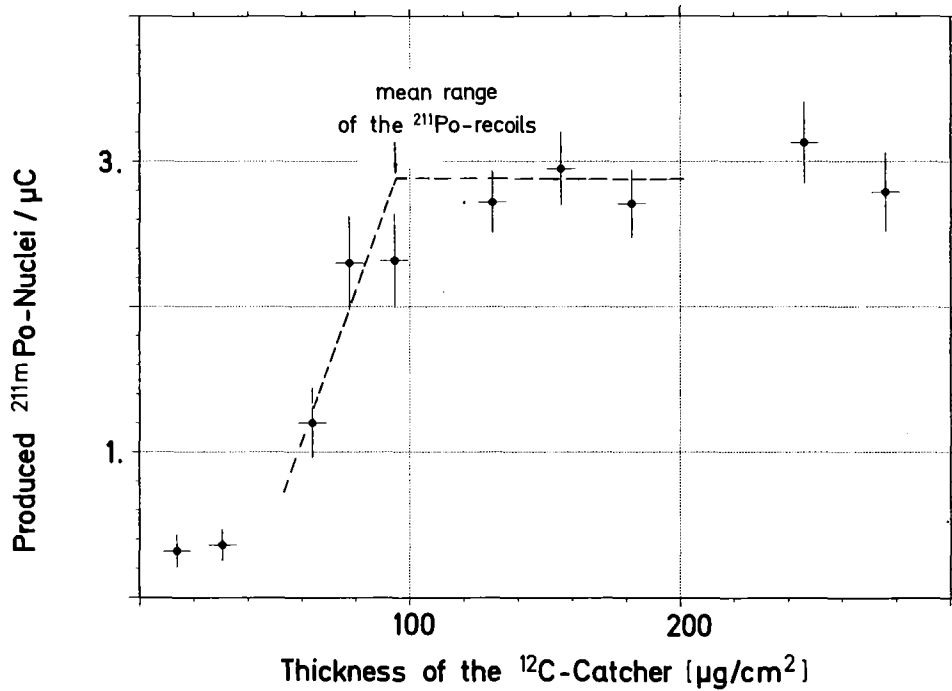


Fig. 1. Absorption curve for ^{211m}Po recoil nuclei. The dotted line is the expected curve for ^{211m}Po nuclei, produced by the internal break-up process.

who suggested that the "internal break-up" process is the dominating reaction channel when bombarding heavy nuclei by high energy ^6Li -projectiles.

The total cross-section for ^{211m}Po production amounts to 200 μb . Looking for the much weaker ^{212m}Po production a constant $^{211m}\text{Po}/^{212m}\text{Po}$ ratio for all catcher foils is observed. From this it might be concluded that for both reactions the contributions of the different reaction channels are at least similar. The total cross-section for the ^{212m}Po production is found to be 8 μb . An upper limit of 0.7 μb is estimated for the direct transfer branch.

⁺Institut für Radiochemie

References

- (1) J. Kropp, H. Klewe-Nebenius, H. Faust, J. Buschmann, H. Rebel, H.J. Gils, and K. Wisshak, Z. Phys. A 280 (1977) 61; KfK-Report 2223 (1975).

2.3.4. 104 MeV Alpha-Particle and 156 MeV ${}^6\text{Li}$ -Ion Scattering and the Validity of the Refined Folding Model Description

Z. Majka[†], H.J. Gils, and H. Rebel

The experimental basis of our investigation is provided by recent experiments of elastic scattering of 104 MeV alpha-particles from ${}^{40,48}\text{Ca}$ (1) and 156 MeV ${}^6\text{Li}$ -ions from ${}^{40}\text{Ca}$ (2) where the differential cross-sections have been carefully measured with high angular accuracy up to the angular region where the diffraction pattern is strongly damped and in the case of ${}^{40,48}\text{Ca}$ (α,α) into the region of the exponential fall-off. Precise and accurate determinations of the angular distributions are a quite necessary prerequisite of any refinements of the current reaction models.

First, the experimental data have been described in terms of a modified phenomenological optical model (real and imaginary potentials in Woods-Saxon squared form) and excellent fits have been obtained. Subsequently we tested the following versions of the folding model for complex projectile scattering:

i. Simple double folding

$$U_{\text{PT}}^{\text{S}}(\mathbf{r}) = \iint d\vec{Z}_P d\vec{Z}_T \rho_P(\vec{Z}_P) \rho_T(\vec{Z}_T) t^{\text{NN}}(\vec{r}_{\text{NN}}) \quad (1)$$

ii. Projectile-nucleon (target folding) and nucleon-target (projectile folding) approaches

$$U_{\text{PT}}^{\text{X}}(\mathbf{r}) = \int d\vec{Z}_Y \rho_Y(\vec{Z}_Y) U_{\text{X-N}}(\vec{R}_X) \quad (2)$$

where

$$U_{\text{X-N}}(\vec{R}_X) = \int d\vec{Z}_X \rho_X(\vec{Z}_X) t_{\rho}^{\text{NN}}(\vec{r}_{\text{NN}}, \rho_X) + \int d\vec{Z}_X \rho_X^{\text{MIX}}(\vec{Z}_X, \vec{R}_X) t_{\rho}^{\text{NN}}(\vec{r}_{\text{NN}}, \rho_X) \quad (3)$$

X = P(T); Y = T(P)

iii. Double folding with sudden and intermediate density dependence

$$U_{\text{PT}}^{\text{SD/IM}}(\mathbf{r}) = \iint d\vec{Z}_P d\vec{Z}_T \rho_P(\vec{Z}_P) \rho_T(\vec{Z}_T) t_{\rho}^{\text{NN}}(\vec{r}_{\text{NN}}, \rho^{\text{TOTAL}}) \quad (4)$$

where $\rho^{\text{TOTAL}} = \rho_P + \rho_T$ (sudden approximation)

$\rho^{\text{TOTAL}} = m\rho_P + \rho_T$ (intermediate approximation)

$0 < m < 1$

The quantities ρ and ρ^{MIX} are nucleon point density distribution and mixed density, respectively, and t^{NN} is an effective nucleon-nucleon interaction.

The one-nucleon exchange effects are included in the procedure (ii) only, and procedures (ii) and (iii) include density dependence of the effective nucleon-nucleon interaction using different approaches.

Applying the microscopic potentials for the description of the measured differential cross sections one has to add an imaginary part in phenomenological way, and a normalization factor λ_R for the depth of the real potential has been introduced.

The results of the studies may be summarized by the following statements:

1. The procedures (ii) provide considerably better fits to the experimental data compared to the simple double folding model (i). However, a renormalization of the real part of the potential by a factor $\lambda_R < 1$ proved to be necessary. Moreover, the effects of the density dependence of the nucleon-nucleon interaction and one-nucleon-exchange are stronger for the projectile folding procedure.

2. One-nucleon-exchange effects are of minor importance as compared to the density dependence of nucleon-nucleon-interactions.

3. Satisfactory fits to the experimental data of alpha-particle scattering can be obtained with a normalization factor $\lambda_R = 1$ if the nucleon-nucleon interaction depends on the density resulting from both colliding nuclei $\rho^{\text{TOTAL}} = 0.5 \rho_\alpha + \rho_T$ (intermediate compression, see contrib. 2.3.5). In contrast, for ${}^6\text{Li}$ scattering in spite of the assumption of the total compression ($\rho = \rho_{\text{Li}} + \rho_T$) a normalization factor of the real potential smaller than 1 is required by the best fit.

4. When introducing a neutron density distribution $\rho_n \neq N/Z \cdot \rho_p$ for ${}^{48}\text{Ca}$ significantly better fits to the experimental cross section have been obtained.

⁺Permanent address: Institute of Physics, Jagellonian University, Cracow, Poland

References

- (1) J. Buschmann, H.J. Gils, H. Rebel, Z. Majka and S. Zagromski, to be publ.
- (2) J. Buschmann, H.J. Gils, H. Rebel, S. Zagromski, G. Bechtold, H. Klewe-Nebenius, H. Faust, B. Neumann, Verhandlungen DPG 4/1978, S. 945.

2.3.5 Importance of the Density Dependence of the Nucleon-Nucleon Interaction for Elastic Scattering of Light Complex Projectiles

Z. Majka⁺, H. Rebel, and H.J. Gils

Although double folding procedures predict almost correctly the shapes of the complex projectile-target nucleus potentials they are less successful in predicting the strength of the potentials. Recently, Satchler et al. (1) found that folded potentials on the basis of a new "realistic" effective nucleon-nucleon interaction (2) reproduce the ion-ion potentials (within 10 %) such as required for a reasonable description of the scattering ¹²C and ¹⁶O. However, such a potential fails for ⁶Li scattering (3) and the authors conclude that ⁶Li scattering has a behaviour quite different from the scattering of other complex nuclear particles.

In this contribution we consider the application of the "realistic" nucleon-nucleon interaction (2) for the 104 MeV alpha-particle and 156 MeV ⁶Li scattering. We compare with predictions of a refined folding model approach (4) and with recently measured differential cross sections covering a wide angular range (5).

The real part of the projectile-target potential is calculated using a double-folding model procedure

$$V_{PT}^{(i)}(r) = \int \int d\vec{z}_P d\vec{z}_T \rho(\vec{z}_P) \rho(\vec{z}_T) t^{(i)}(\vec{s}) \quad (1)$$

where $\rho_P(\vec{z}_P)$ and $\rho_T(\vec{z}_T)$ are the densities of the projectile and target nucleus, respectively, and $t^{(i)}(\vec{s})$ is an effective nucleon-nucleon interaction. Indices "i" refer to various procedures in calculating the potentials:

- a. Bertsch et al. (B) "realistic" effective N-N interaction (2).
- b. Density independent Kallio-Koltveit (KK) effective N-N interaction (6)
- c. Density dependent Green (G) effective N-N interaction (7). For this particular interaction we assume that the value of the density in the overlap region of the colliding nuclei is given by

$$\rho = m \cdot \rho_P(\vec{z}_P) + \rho_T(\vec{z}_T) \quad (2)$$

where the coefficient m ($0 \leq m \leq 1$), allows to change the value of the compression of the nuclear matter.

Applying the microscopic potentials for the description of the measured differential cross sections of elastic alpha-particle and ⁶Li scattering one

has to add an imaginary part iW (surface and volume part with Woods-Saxon squared form) in a phenomenological way. Moreover, a normalization factor λ_R for the depth of the real folded potential has to be introduced.

Results of our calculations can be summarized by the following statements (4):

i. In the case of 104 MeV alpha-particle scattering satisfactory description, especially of large angle scattering, can be obtained only by use of the density dependent effective N-N interaction. For 156 MeV ${}^6\text{Li}$ scattering agreement is considerably better for the density dependent effective N-N interaction, as well.

ii. For alpha-particle scattering the best fit to the measured differential cross sections has been obtained with a normalization factor $\lambda_R = 1$ and with compression coefficient $m = 0.5$. In contrast, for ${}^6\text{Li}$ scattering, even with the maximum value of the compression of the nuclear matter in the overlap region (sudden approximation) the calculated potential has to be renormalized by a factor $\lambda_R < 1$.

⁺Permanent address: Institute of Physics, Jagellonian University, Cracow, Poland.

References

- (1) G.R. Satchler and W.G. Love, Phys. Lett. 65B (1976); G.R. Satchler, Nucl. Phys. A 279 (1977); R.M. Wieland, R.G. Stokstad, G.R. Satchler, and L.D. Rickertsen, Phys. Rev. Lett. 37 (1976) 1458.
- (2) G. Bertsch, J. Borysowicz, H. McManus and W.G. Love, Nucl. Phys. A 284 (1977) 399; G.R. Satchler and W.G. Love, Phys. Lett. 65B (1976) 415.
- (3) G.R. Satchler and W.G. Love, to be publ. in Phys. Lett., private communication.
- (4) Z. Majka, H.J. Gils, and H. Rebel, Report KfK 2622 (1978), Proc. 3rd Int. Conference on Clustering Aspects of Nuclear Structure and Nuclear Reactions, Manitoba, Canada, June 19-23, 1978, p. 1316.
- (5) E. Friedman, H.J. Gils, and H. Rebel, to be published; J. Buschmann, H.J. Gils, H. Rebel, S. Zagromski, G. Bechtold, H. Klewe-Nebenius, H. Faust, and B. Neumann; to be published.
- (6) A. Kallio and K. Kolltveit; Nucl. Phys. 53 (1964) 87.
- (7) A.M. Green; Phys. Lett. 24B (1967) 384.

2.3.6 N- α and N- ^6Li Microscopic Potentials*

Z. Majka⁺

The nucleon-alpha and nucleon-lithium potentials are generated from Green density dependent effective nucleon-nucleon interaction using microscopic model with antisymmetrization effects included. A phenomenological parametrization and the energy dependence of the potentials are derived.

*Phys. Lett. 76B (1978) 161

⁺Permanent address: Institute of Physics, Jagellonian University,
Cracow, Poland

3. NUCLEAR SPECTROSCOPY

3.1 Experimental Studies of Hexadecapole Motion in Spherical Nuclei*

H. Faust⁺, A. Hanser, H. Klewe-Nebenius⁺⁺, H. Rebel,
J. Buschmann, and H.J. Gils

The $0^+ \rightarrow 4_1^+$ hexadecapole transitions in ^{60}Ni and ^{140}Ce have experimentally been investigated by means of alpha-particle scattering as well as by spectroscopy of the electromagnetic decay of the 4_1^+ states. In the case of ^{60}Ni an upper limit of 1×10^{-7} was found for the branching of the E4 and E2 cascade decays of the 4_1^+ state by conversion electron spectroscopy.

It corresponds to an enhancement factor $G_4 < 9.0$ s.p.u., while the alpha-particle scattering measurements result in $G_4 = (5.5 \pm 0.8)$ s.p.u.. In ^{140}Ce the $4_1^+ \rightarrow 0^+$ cross-over gamma-decay has been observed with an enhancement of $G_4 = (11.8 \pm 0.7)$ s.p.u. in very good agreement with the value $G_4 = (13 \pm 2)$ s.p.u. from the alpha-particle scattering experiments. The evaluation of the alpha-particle scattering cross sections is based on a specific reaction model (folding model). The experimental results from the direct ($4_1^+ \rightarrow 0^+$) decay are considered to be an empirical test of model dependence of the procedures extracting $L = 4$ transition rates from alpha-particle scattering. Compiling several similar results the consistency of the methods applied as well as the evidence and some implications of hexadecapole motion in spherical nuclei are discussed briefly.

* J. Phys. G.: Nucl. Phys. 4 (1978) 247; Report KfK 2470

⁺ Physikalisches Institut der Universität Heidelberg, Germany

⁺⁺ Institut für Radiochemie

3.2 Spectroscopic Studies of ^{137}Nd and ^{189}Ir by Means of Conversion Electron Angular Distribution-Measurements. Evidence for Hexadecapole-Deformation of Nuclei in the Transitional Regions of the Rare Earths

H. Faust⁺, J. Rieder⁺, J. Buschmann, H. Klewe-Nebenius⁺⁺, H. Rebel, and K. Wisshak

We investigated the $11/2^-$ high-spin bands of the transitional nuclei ^{137}Nd (N=77) and ^{189}Ir (Z=77) populated via compound-nuclear reactions (α , 7n+p) and (d, 5n), respectively at the beam of the Karlsruhe Isochronous Cyclotron. For the determination of the multipolarities of the prompt transitions in the high-spin bands considered a new experimental method has been applied. This method is based on the combined information extracted from the gamma- and conversion electron-angular distributions (1). The quantities measured are the coefficients $A_2(\gamma)$ and $A_2(e^-)$ of the angular distribution function $W(\Theta_{\gamma,e}) = 1 + A_2 P_2(\cos\Theta) + A_4 P_4(\cos\Theta) \dots$

It can be seen that the measurements of both angular distributions provide strong arguments for particular multipolarities of pure and mixed dipole and quadrupole transitions.

The measurements result in level schemes of the $11/2^-$ bands in ^{185}Ir and ^{137}Nd shown in Figure 1. The striking similarity of the level structure of both nuclei is obvious.

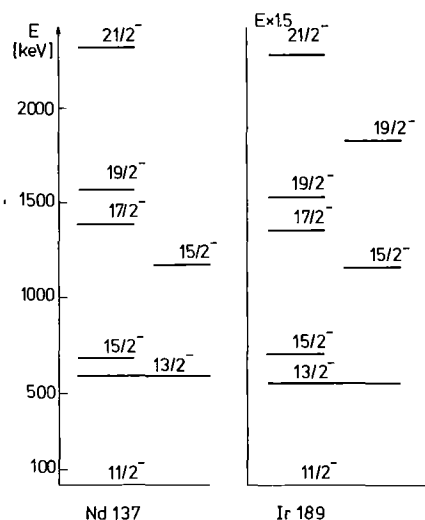


Fig. 1. Level values for the $11/2^-$ bands in ^{137}Nd and ^{189}Ir . The energy scale of ^{189}Ir has been stretched by a factor of 1.5.

It is found that observed level schemes cannot be satisfactorily described by the Coriolis-Coupling model involving quadrupole deformation only, even when admitting triaxial deformation as suggested by Meyer ter-Vehn (3). Alternatively to the triaxial deformation we considered hexadecapole deformations of the core and looked for possible effects to the level structure within the framework of the Coriolis-Coupling model. First calculations with the deformation parameters β_2 and β_4 adequately adjusted result in very good agreement between theoretical predictions and experimental observation (1). An example is presented in Fig. 2 which compares for ^{189}Ir the prediction on the basis of the triaxial rotator model with that of an axial-symmetric model but including β_4 deformation.

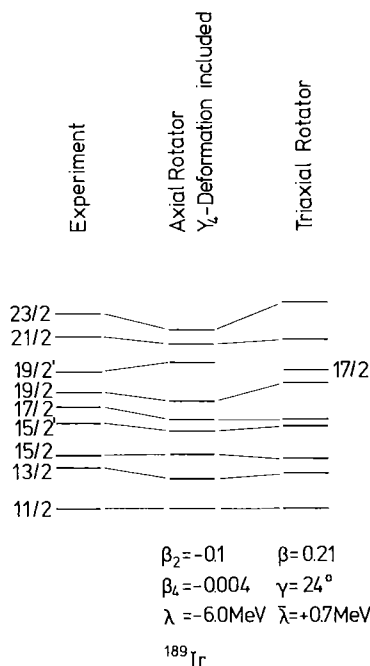


Fig. 2. Fits to the experimental levels in the $11/2^-$ band in ^{189}Ir . In the calculations with β_4 -deformation the Fermi level has been deduced from the measurements of Price et al. (4).

⁺Physikalisches Institut der Universität Heidelberg

⁺⁺Institut für Radiochemie

References

- (1) H.R. Faust, PhD Thesis, Heidelberg (1978).
- (2) S. André, J. Boutet, J. Rivier, J. Treherne, J. Jastrzebski, J. Lukasiak, Z. Sujkowski, and C. Sebille-Schück, Nucl. Phys. A 243 (1975) 229.
- (3) J. Meyer ter-Vehn, Nucl. Phys. A 249 (1975) 111, 141.
- (4) R.M. Price, D.G. Burke, and M.W. Johns, Nucl. Phys. A 176 (1971) 338.

3.3 Study of the Level Structure of ^{239}U Using the Thermal Neutron Capture Reaction*

H.G. Börner⁺, H.R. Koch⁺, H. Seyfarth⁺, T. von Egidy⁺⁺, W. Mampe⁺⁺,
J.A. Pinston⁺⁺, K. Schreckenbach⁺⁺, and D. Heck

For the investigation of vibrational states in odd A nuclei we have studied the level structure of ^{239}U by the $^{238}\text{U} (n_{\text{thermal}}, \gamma)$ reaction. Various complementary measurement techniques as curved-crystal, anti-Compton, γ - γ coincidence and conversion electron spectroscopy have been applied.

The resulting data have been used to establish the deexcitation scheme of ^{239}U up to ~ 1.3 MeV and to make spin assignments. Most of the levels are interpreted in terms of the Nilsson model. The data also indicate the presence of the Nilsson states $|501\downarrow|$ and $|750|$. Three members of the β -vibrational band built on the $|631\downarrow|$ state and one member of the β -vibration built on the $|622\uparrow|$ ground state have been identified through transitions with strong E0 admixtures. The octupole vibrational state built on the $|631\downarrow|$ band is proposed at 815 keV.

* Z. Physik A 286, (1978) 31

⁺ Institut für Kernphysik, Kernforschungsanlage Jülich, Germany

⁺⁺ Institut Laue-Langevin, Grenoble, France

4. THEORY

4.1 Induced Collective Motion: Limit of Two Fission Fragments

F. Dickmann

The relative momentum and kinetic energy of two fission fragments or two heavy ions as functions of their relative velocity are determined by the reduced mass. This quantity is known for a given mass division and therefore serves to test theoretical procedures aiming at a description of the collective motion of nucleons in the fission process or heavy ion reactions.

We employ a static Two-Center-Oscillator Hamiltonian $\hat{H}(x_i, p_i, \alpha_j)$, which depends on the nucleon coordinates x_i , momenta p_i and up to five parameters α determining the shape of the single particle potential. The Hamiltonian also contains a residual nucleon-nucleon interaction of the simplest pairing force type. For an even-even nucleus the BCS-groundstate $\phi(\alpha)$ of the static Hamiltonian is even under time reversal. Thus, the expectation values of time odd operators, for instance the center of mass momentum \hat{P}_x and the angular momentum \hat{L} , vanish. In order to introduce dynamic features into the model the time odd momentum operator $\hat{P}_\alpha = -i\hbar\partial/\partial\alpha$ which generates a change of the parameter α is coupled with a Lagrange parameter $\dot{\alpha}$ to the Hamiltonian. We determine the normalized state vector $\phi(\alpha, \dot{\alpha})$ which minimizes the expectation value $\langle\phi(\alpha, \dot{\alpha})|\hat{H} - \dot{\alpha}\hat{P}_\alpha|\phi(\alpha, \dot{\alpha})\rangle$ of the constrained Hamiltonian. The increase of the energy and the momentum associated with the collective velocity $\dot{\alpha}$ are

$$\Delta E = \langle\phi(\alpha, \dot{\alpha})|\hat{H}|\phi(\alpha, \dot{\alpha})\rangle - \langle\phi(\alpha)|\hat{H}|\phi(\alpha)\rangle \quad (1a)$$

$$\text{and } P_\alpha = \langle\phi(\alpha, \dot{\alpha})|\hat{P}_\alpha|\phi(\alpha, \dot{\alpha})\rangle \quad (1b)$$

In the case of a translation the parameter α is the position of the center of the single particle potential. The static single particle wave functions ψ_ℓ depend on α in the form

$$\psi_\ell(x, \alpha) = \psi_\ell(x - \alpha) \quad (2)$$

We now use the center of mass position operator \hat{X} to induce a center of mass motion (1) and investigate whether the state vector

$$\phi(\alpha, k) = e^{ik(\hat{X} - \alpha)}\phi(\alpha)$$

yields a stationary value of the constrained Hamiltonian. The expectation

value of any operator \hat{O} referring to a system of A nucleons is

$$\langle \phi(\alpha, k) | \hat{O}(\hat{x}_i, \hat{p}_i, \alpha) | \phi(\alpha, k) \rangle = \langle \phi(\alpha) | \hat{O}(\hat{x}_i, \hat{p}_i + \frac{\hbar k}{A}, \alpha) | \phi(\alpha) \rangle$$

Thus the expectation value of the center of mass momentum \hat{P}_x is $\hbar k$ and due to eq. (2) the expectation value of the operator \hat{P}_α is $-\hbar k$. For the constrained Hamiltonian we obtain

$$\begin{aligned} G(\{\phi\}) &= \langle \phi(\alpha, k) | \hat{H}(\hat{x}_i, \hat{p}_i, \alpha) - \dot{\alpha} \hat{P}_\alpha | \phi(\alpha, k) \rangle \\ &= \langle \phi(\alpha) | \hat{H}(\hat{x}_i, \hat{p}_i + \frac{\hbar k}{A}, \alpha) - \dot{\alpha} (\hat{P}_\alpha - \hbar k) | \phi(\alpha) \rangle \end{aligned}$$

If we assume for a moment that the Hamiltonian depends on the single particle momenta only via the kinetic energy operator $\hat{T} = \sum_{i=1}^A \hat{p}_i^2 / 2m$ we obtain

$$G(\{\phi\}) = \frac{(\hbar k)^2}{2mA} + \dot{\alpha} \hbar k + \langle \phi(\alpha) | \hat{H}(x, p, \alpha) + \frac{\hbar k}{Am} \hat{P}_x - \dot{\alpha} \hat{P}_\alpha | \phi(\alpha) \rangle$$

Since $\phi(\alpha)$ is the BCS groundstate of the Hamiltonian \hat{H} , the expectation values $G(\{\phi\})$ are stationary with respect to first order variations of $\phi(\alpha)$ if the operators $\frac{\hbar k}{Am} \hat{P}_x$ and $\dot{\alpha} \hat{P}_\alpha$ have the same two quasiparticle matrix elements. This is the case if $\dot{\alpha} = -\hbar k / Am$ because of eq. (2).

Thus we have shown that the driving potential $\hbar k / Am \hat{P}_\alpha$ induces a collective motion for which the expectation value of the momentum is $\langle P_\alpha \rangle = \hbar k$ and that the energy increases relative to the static case by the amount $\Delta E = (\hbar k)^2 / 2mA$. The procedure therefore yields the correct inertial parameter, the total mass $M = Am$. The above consideration can be applied as well to the relative motion of two nuclei showing that the inertial parameter is the reduced mass.

By assuming that the only momentum dependence of the Hamiltonian is in the single particle kinetic energy operator we have so far disregarded the spin-orbit coupling. This term does not commute with the center of mass position operator, it violates Galilei's principle. Though the expectation value of the spin-orbit term is independent of the momentum k , the two quasiparticle matrix elements of this term are nonzero and therefore give rise to a first order perturbation whose magnitude has been studied numerically.

For post scission shapes the Two Center Shell Model reduces to two separated Nilsson Hamiltonians. The contributions of neutrons and protons to the momentum and kinetic energy are additive. We have performed a calculation

for the asymmetric system of 40 protons in the light and 52 protons in the heavy fission fragment of ^{236}U . For the velocity $\dot{\alpha} = v_H - v_L$ chosen for the relative motion the kinetic energy and momentum were expected to be

$$T = \Delta E = \frac{1}{2} m \frac{Z_L Z_H}{Z_L + Z_H} \dot{\alpha}^2 = 6.04957 \text{ MeV.}$$

$$P = m \cdot \frac{Z_L Z_H}{Z_L + Z_H} \dot{\alpha} = 2.56912 \text{ h/fm.}$$

With the values $\kappa = \mu = 0$ for the Nilsson parameters (no spin orbit- and l^2 -terms) the above theoretical values could be reproduced numerically from eqs. (1) with the accuracy

$$\Delta T/T = 6.5 \cdot 10^{-3} \text{ and } \Delta P/P = 1.3 \cdot 10^{-4} \quad (3)$$

Using the values $\kappa=0.03$ and $\mu = 0.65$ we obtained

$$\Delta T/T = 4.1 \cdot 10^{-2} \quad \Delta P/P = 5.3 \cdot 10^{-2} \quad (4)$$

Eqs. (3) demonstrate the accuracy of the computer calculation. The larger discrepancies exhibited in eqs. (4) reflect the violation of Galilei's principle by the model Hamiltonian.

In view of the small deviation of all calculated results from the exact values we conclude that both the simple static model and the method to induce a collective motion are useful tools for the study nuclear collective degrees of freedom unless a physical phenomenon is very sensitive to a violation of general invariance principles.

Reference

- (1) D.J. Thouless, Nucl. Phys. 21 (1960), 225-232.

4.2 Decrease of Pair-Correlations in a Deforming Nucleus

F. Dickmann

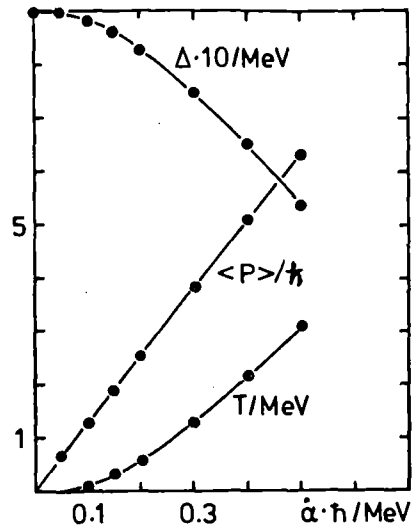
The pairing force acts between nucleons in time reversed states. Pairing correlations are inhibited in excited states with high quantum numbers of a time-odd operator. The best known example of the phenomenon is the Coriolis-Antipairing effect (1), observed in states of high angular momentum.

We investigate theoretically the case of a rapidly deforming nucleus. A deformed Nilsson and Pairing Model is used to generate the BCS ground-state $\phi(\alpha)$ of the nucleus. The parameter α is ratio of the major to the minor axes of the equipotential lines which characterize the static deformation of the nucleus. The groundstate $\phi(\alpha, \dot{\alpha})$ of the nucleus deforming with finite velocity $\dot{\alpha}$ is obtained by minimizing the expectation value of the constrained Hamiltonian

$$\hat{H}_{\text{Nilsson}}(\alpha) + \hat{H}_{\text{Pair}} - \dot{\alpha} \hat{P}_{\alpha} \quad (1)$$

The time-odd momentum operator $\hat{P}_{\alpha} = \frac{\hbar}{i} \frac{\partial}{\partial \alpha}$ generates a change of the deformation α of the static groundstate $\phi(\alpha, \dot{\alpha}=0)$. Our ansatz for the dynamic groundstate $\phi(\alpha, \dot{\alpha})$ is a single BCS state such that the occupation probability of an eigenstate $\psi_{\rho}(\alpha, \dot{\alpha})$ of the single particle operator $H_{\text{Nilsson}}(\alpha) - \dot{\alpha} P_{\alpha}$ depends only on the single particle energy $\epsilon_{\rho}(\alpha, \dot{\alpha})$. The single particle energies $\epsilon(\alpha, \dot{\alpha})$ are pairwise degenerate like in the static case $\dot{\alpha}=0$, however the associated single particle states

Fig. 1.
The energy increase T , momentum $\langle P \rangle$ and pairing gap Δ for the protons of ^{236}U as a function of the velocity $\dot{\alpha}$ of deformation.



$\psi_{\ell}(\alpha, \dot{\alpha})$ and $\psi_{\ell}^{-}(\alpha, \dot{\alpha})$ are not time reversed partners. The time reversed state corresponding to $\psi_{\ell}(\alpha, \dot{\alpha})$ is $\psi_{\ell}^{-}(\alpha, -\dot{\alpha})$.

We have performed a numerical calculation for the 92 protons of ^{236}U . The results are presented in Fig. 1. The pairing gap Δ is seen to decrease appreciably as the kinetic energy T of the collective motion increases.

From this result we infer for the collective deformation of a fissioning nucleus: if, as expected, the odd-even effects in the fine structure of the fission fragment mass and charge distributions is due to pairing, the strong calculated decrease of the pairing correlation sets a lower limit for the pre-scission kinetic energy of the fragments.

Reference

- (1) B.R. Mottelson and J.C. Valatin, Phys. Rev. Lett. 5 (1960) 511.

4.3 A Variational Principle for the Energies and Widths of Unstable Nuclear States

R. Beck, M.V. Mihailović⁺ and M. Nagarajan⁺⁺

A variational method for the determination of the positions (E_n) and the widths (Γ_n) of decaying states of a (A+B) particle system is developed. We are seeking for the stationary values of the complex eigenvalue W and the corresponding wave-functions ψ defined by the equation

$$(H-W)\psi(\underline{x}) = 0, \quad (1)$$

where \underline{x} represents all coordinates of (A+B) particles and H is the Hamiltonian of the system,

$$H = -\frac{\hbar^2}{2m} \sum_{i=1}^{A+B} \nabla_i^2 + \sum_{\substack{ij=1 \\ i < j}}^{A+B} V_{ij}$$

where V_{ij} is the two-body interaction.

ψ satisfies the nonlinear boundary condition on a chosen surface of radius R

$$\left. \frac{\partial \psi}{\partial r_j} \right|_{r_j=R} = \tilde{\psi}^{(j)}(\underline{x}, q) \quad (2)$$

where $\tilde{\psi}^{(j)}(\underline{x}, q)$ is related to the trial function ψ (see eq. (10)). In eq. (2), r_j is the radial coordinate of the j^{th} particle, $j = 1 \dots (A+B)$. The quantity $q = \sqrt{2\mu/\hbar^2 \cdot W}$ is complex, μ is the reduced mass of the systems A and B. We define the functionals

$$N(\psi^+, \psi) = \int d\underline{x} \psi^+(\underline{x}) \psi(\underline{x}) \quad (3)$$

$$F(\psi^+, \psi) = \int d\underline{x} \left[\frac{\hbar^2}{2m} \sum_{j=1}^{A+B} \nabla_j \cdot \psi^+ \cdot \nabla_j \cdot \psi + \psi^+ \nabla \psi \right] - \frac{\hbar^2}{2m} \sum_{j=1}^{A+B} \int d\underline{x}^{(j)'} \int d\Omega_j \left[(r_j \cdot \psi^+) (r_j \tilde{\psi}) + (r_j \psi) (r_j \tilde{\psi}^+) \right]_{r_j=R} \quad (4)$$

where $d\underline{x} = d\underline{x}_1 \dots d\underline{x}_{A+B}$, $d\underline{x}^{(j)'} = d\underline{x}_1 \dots d\underline{x}_{j-1} d\underline{x}_{j+1} \dots d\underline{x}_{A+B}$

It can be shown that the variational equation

$$\delta |F(\psi^+, \psi) - W \cdot N(\psi^+, \psi)| = 0 \quad (5)$$

is equivalent to the equations (1) and (2).

The trial functions to be used in the variational principle eq. (5) will be of two types. One can use a single Slater determinant

$$\psi = \det \{ \phi_\lambda(\underline{x}_j) \} \quad (6)$$

where the variation of ψ can be done by the variation of the single particle functions ϕ_λ . A second choice of the trial function will be a superposition of two center cluster functions $\phi_\alpha(\underline{x}, \underline{s})$

$$\psi = \sum_\alpha \int d\underline{s} f_\alpha(\underline{s}) \phi_\alpha(\underline{x}, \underline{s}) \quad (7)$$

where \underline{s} denotes the separation of the two potential wells and α characterizes a given many-particle configuration. In equation (7), the generator weight function $f_\alpha(\underline{s})$ is treated as variational parameter.

The boundary condition defined by eq. (2) is different from the boundary condition conventionally used in terms of channels. For example, in a one-channel case, it is assumed that the decaying state satisfies a boundary condition of the form

$$\left. \frac{d}{d\rho} \psi \right|_{\rho=R_c} = \left. \hat{L}_L(q) \psi \right|_{\rho=R_c} \quad (8)$$

where ρ is the separation of the centers of mass of the two nuclei in the channel and $\hat{L}_L(q)$ is the logarithmic derivative of an outgoing spherical Coulomb function of order L . L is the orbital angular momentum of relative motion of the two nuclei. It is implicitly assumed that the derivatives of ψ with respect to all other coordinates go to zero asymptotically. The corresponding radial derivatives with respect to the particle coordinates will be

$$\frac{d}{dr_j} \psi = \alpha(j) \cos \theta_j \frac{d}{d\rho} \psi \quad (9)$$

$$\alpha(j) = \left\{ \begin{array}{ll} \frac{1}{A} & ; j = 1 \dots A \\ -\frac{1}{B} & ; j = (A+1) \dots (A+B). \end{array} \right\}$$

where θ_j is the angle between the vectors \underline{r}_j and $\underline{\rho}$ and goes to 0 or π in the limit of large separation ρ . If we replace $\cos \theta_j$ by its average value ± 1 depending upon whether the j^{th} particle belongs to the nucleus A or B we get from eqs. (2), (8) and (9)

$$\psi^{(j)}(\underline{x}, q) = \left\{ \begin{array}{l} \frac{1}{A} \hat{L}_L(q) \psi(\underline{x}, q) \\ \frac{1}{B} \hat{L}_L(q) \psi(\underline{x}, q) \end{array} \right\} \quad \text{for } j = \left\{ \begin{array}{l} 1 \dots A \\ (A+1) \dots (A+B) \end{array} \right\} \quad (10)$$

⁺ Institut Jožef Stefan, Ljubljana, Jugoslavia

⁺⁺ Daresbury Laboratory, Warrington, England

4.4 Hill-Wheeler Equation for Three-Cluster Systems

R. Beck

The cluster structure and molecular aspects in light nuclei are studied on the basis of the Generator Coordinate Method (GCM) (1). For nuclei like ${}^9\text{Be}$ or ${}^{11}\text{B}$ one might expect three cluster structures to be important, e.g. ${}^9\text{Be} = \alpha + \alpha + n$ and ${}^{11}\text{B} = \alpha + \alpha + {}^3\text{H}$. This feature may be accounted for in

the GCM by choosing a trial function which is a superposition of three-center shell model wave-functions $|\phi_{\kappa}(\xi, \eta)\rangle$ corresponding to different configurations κ .

$$|\psi^{JM\pi}\rangle = \sum_{\kappa\kappa} \int d\xi d\eta f_{\kappa\kappa}^{J\pi}(\xi, \eta) P_{MK}^{J\pi} |\phi_{\kappa}(\xi, \eta)\rangle$$

In this equation the Jacobi-coordinates ξ and η specify the relative distances of the three potential wells and $P_{MK}^{J\pi}$ is a projection operator onto a state with angular momentum JM and parity $\pi(2)$. The weight function $f_{\kappa\kappa}^{J\pi}(\xi, \eta)$ is expanded into bipolar harmonics B

$$f_{\kappa\kappa}^{J\pi}(\xi, \eta) = \sum_{\hat{L}\hat{M} L_1 L_2} f_{\kappa\kappa}^{J\pi}(\hat{L} L_1 L_2 \xi \eta) B_{\hat{L}\hat{M}}^{L_1 L_2}(\hat{\xi} \hat{\eta})$$

depending on two directions $\hat{\xi}$ and $\hat{\eta}$.

Minimization of the energy $E^{J\pi}$ of the state $|\psi^{JM\pi}\rangle$ with respect to the weight function $f_{\kappa\kappa}^{J\pi}(\hat{L} L_1 L_2 \xi \eta)$ leads to a Hill-Wheeler integral equation

$$0 = \sum_{\kappa' \kappa' L_1' L_2'} \int \xi'^2 d\xi' \eta'^2 d\eta' \left[H_{\kappa\kappa, \kappa' \kappa'}^{J\pi}(L_1 L_2 L_1' L_2'; \hat{L}; \xi \eta \xi' \eta') - E^{J\pi} N_{\kappa\kappa, \kappa' \kappa'}^{J\pi}(L_1 L_2 L_1' L_2'; \xi \eta \xi' \eta') \right] f_{\kappa' \kappa'}^{J\pi}(\hat{L} L_1' L_2' \xi' \eta')$$

which has to be satisfied for all $\{\kappa\kappa L_1 L_2 \xi \eta\}$.

The calculation of the integral kernels

$$\begin{aligned} & \left(\begin{matrix} N \\ H \end{matrix} \right)_{\kappa\kappa, \kappa' \kappa'}^{J\pi}(L_1 L_2 L_1' L_2'; \hat{L}; \xi \eta \xi' \eta') \\ & = \int d\hat{\xi} d\hat{\eta} d\hat{\xi}' d\hat{\eta}' B_{\hat{L}\hat{M}}^*(L_1 L_2 \hat{\xi} \hat{\eta}) \langle \phi_{\kappa}(\xi, \eta) | \left(\begin{matrix} 1 \\ H \end{matrix} \right)_{\kappa\kappa}^{J\pi} | \phi_{\kappa'}(\xi', \eta') \rangle \\ & * B_{\hat{L}\hat{M}}(L_1' L_2' \hat{\xi}' \hat{\eta}') \end{aligned}$$

where \hat{M} and \hat{M}' are dummy indices is in progress. If we consider only clusters consisting of nucleons in relative s-states the projection of angular momentum becomes comparatively simple. For brevity we give only the normalization Kernel N. N turns out to be a determinant which may be expanded into a sum of terms of the same structure concerning their dependence on ξ, η, ξ' and η' :

$$\begin{aligned}
 & N_{\kappa K, \kappa' K'}^{J\pi} (L_1 L_2 L'_1 L'_2 ; \xi \eta \xi' \eta') \\
 &= (4\pi)^2 (2J+1) \exp \left\{ -\alpha \left[\frac{A_1 (A_2 + A_3)}{\sum_i A_i} (\eta^2 + \eta'^2) + \frac{A_2 A_3}{A_2 + A_3} (\xi^2 + \xi'^2) \right] \right\} \\
 & * \sum_{l_1 \dots l_4} i_{l_1}(\alpha a_1 \xi \xi') i_{l_2}(\alpha a_2 \xi \eta') i_{l_3}(\alpha a_3 \eta \xi') i_{l_4}(\alpha a_4 \eta \eta') \\
 & * (2l_1+1) (2l_2+1) (2l_3+1) (2l_4+1) \frac{1}{2} (1 + \pi(-)^{\sum_j l_j}) \begin{pmatrix} \hat{L} & S & J \\ (K-\gamma)\gamma & -K & \end{pmatrix} \\
 & * \begin{pmatrix} \hat{L} & S & J \\ (K'-\gamma') & \gamma' & -K' \end{pmatrix} (-)^{K-K'} \begin{pmatrix} l_1 & l_2 & L_1 \\ 0 & 0 & 0 \end{pmatrix} \begin{pmatrix} l_1 & l_3 & L'_1 \\ 0 & 0 & 0 \end{pmatrix} \begin{pmatrix} l_2 & l_4 & L'_2 \\ 0 & 0 & 0 \end{pmatrix} \\
 & * \begin{pmatrix} l_3 & l_4 & L_2 \\ 0 & 0 & 0 \end{pmatrix} \left\{ \begin{matrix} L_2 & \hat{L} & L_1 \\ l_3 & L'_1 & l_1 \\ l_4 & L'_2 & l_2 \end{matrix} \right\}
 \end{aligned}$$

In this equation α is related to the oscillator parameter of the single particle orbits. The nucleon numbers of the three clusters are denoted by A_1 , A_2 and A_3 and the parameters a_i ($i=1\dots 4$) are simple functions of these. s is the resultant spin to which $\sum_{j=1}^3 A_j$ individual particle spins have been coupled and γ (γ') is its 3-component corresponding to the configuration κ (κ'). The functions i_l are spherical Bessel functions of imaginary argument $i_l(z) = i^l j_l(iz)$.

References

- (1) H. Horiuchi, Progr. Theoretical Physics 43 (1970) 375.
- (2) N. MacDonald, Advances in Physics, 19 (1970) 371.

5. LASER SPECTROSCOPY

5.1 Nuclear Charge Radii and Moments of Neutron Deficient Ba-Isotopes by High Resolution Laser Spectroscopy

K. Bekk, S. Göring, A. Hanser, G. Nowicki, H. Rebel, and G. Schatz

The measurements of isotope shifts (IS) and hyperfine structure (A- and B-factors) of neutron deficient Ba-isotopes ($N < 82$) have been continued. The experiments are based on the observation of the resonance fluorescence of the BaI $6s^2 \ ^1S_0 - 6s6p \ ^1P_1$ transition when induced in a well-collimated atomic beam by the light of high resolution tunable CW dye lasers. The measurements aimed at information about nuclear moments and variations of nuclear charge radii of isotopes and isomers lighter than ^{138}Ba produced by charged particle or neutron irradiation of appropriate targets. Up to now the radioactive nuclides and isomers ^{133g}Ba , ^{133m}Ba , ^{131g}Ba and ^{128g}Ba have been investigated in addition to remeasurements of all stable Ba isotopes thus providing a coherent set of data. The accuracy of the resulting differences of the rms charge radii is affected by the poor accuracy of the presently available muonic - or electronic X-ray data (1,2) which are needed for the determination of the specific mass shift. Nevertheless, the results reveal interesting features of the charge distributions of neutron deficient nuclei showing increasing deformation with decreasing neutron number and a prominent odd-even staggering (larger than theoretically predicted (3)).

Table 1. Experimental results of IS relative to ^{138}Ba , charge radii and deformation differences of neutron deficient Ba nuclides

Atomic Number	IS (MHz)	$\delta\langle r^2 \rangle$ (10^{-2} fm^2)	$\delta\langle \beta^2 \rangle$ (10^{-2})
137	215.0(7)	-4.9 (2)	0.69 (2)
136	128.9(5)	-3.4 (3)	2.09 (4)
135	260.9(7)	-6.6 (5)	3.00 (6)
134	143.0(5)	-4.4 (7)	4.50 (7)
133g	250.0(9)	-7.1 (9)	5.48 (10)
133m	202.0(10)	-6.0 (9)	5.59 (10)
132	167.9(5)	-5.7 (10)	6.93 (12)
131	249.2(21)	-7.7 (12)	8.02 (13)
130	207.3(7)	-7.2 (14)	9.40 (16)
128	271.1(8)	-9.3 (18)	11.87 (20)

Table 2. Experimental results of hyperfine constants and nuclear moments of neutron deficient Ba nuclides.

Atomic Number	A (MHz)	B (MHz)	μ/μ_N	Q (b)
137	-109.8(4)	49.7(4)	0.93582(2)	0.28(3)
136				
135	- 98.3(4)	32.5(4)	0.82656(2)	0.18(2)
134				
133g	273.3(8)		-0.775(2)	
133m	29.1(9)	195.9(9)	-0.907(28)	1.10(3)
132				
131	249.2(18)		-0.716(5)	
130				
128				

The extraction of the magnetic moments μ and the electric quadrupole moments Q used the accurate values for $^{135,137}\text{Ba}$ given in literature (4,5) Tabs. 1,2 present the IS shifts $\Delta\nu$ relative to ^{138}Ba and the observed A- and B-factors. The rms deformation differences $\delta\langle\beta^2\rangle$ are deduced from $\delta\langle r^2\rangle$ by comparing with the uniform charged sphere ($R=1.2\cdot A^{1/3}$). Compared to measured $B(E2, 0^+ - 2^+)$ values the extracted $\delta\langle\beta^2\rangle$ values show the well-known IS discrepancy indicating that the variation of $\delta\langle r^2\rangle$ cannot be fully explained by a deformation effect.

References

- (1) K. Heilig and A. Steudel; Atomic Data and Nuclear Data Tables 14, (1974) 613.
- (2) O.I. Sumbaev et al.; Sov. Journ. of Nucl. Phys. 9, (1969) 529.
- (3) B.S. Reehal and R.A. Sorenson; Nucl. Phys. A 161, (1971) 385.
- (4) I.J. Ma and G. zu Putlitz; Z. Phys. A 277, (1976) 107.
- (5) L. Olschewski; Z. Physik 249, (1972) 205.

5.2 Production of Instable Barium Samples for Laser Spectroscopic Experiments by Alpha-Particle Irradiation of Enriched Xenon and Mass Separation

B. Feurer and A. Hanser

Isotopically pure samples in the order of magnitude of one nanogram are required for the laser spectroscopic studies on neutron deficient barium

isotopes in progress at our institute. For production of samples of ^{135m}Ba , ^{129m}Ba , and ^{126}Ba enriched xenon is irradiated with the alpha-particle beam of our cyclotron. Because of the gaseous target substance, the high cost of enriched xenon, and with regard to a succeeding electromagnetic mass separation a special experimental arrangement has been developed.

The principle: The alpha-particle beam is running through a small tantalum tube filled with xenon. Barium atoms produced by (α, xn) reactions diffuse to the wall and are adsorbed there. After the irradiation the xenon is condensed in a small lockable appendix vessel by liquid nitrogen cooling. Then the tantalum tube loaded with barium is closed with two matching caps, thus forming the oven ampoule of the mass separator ion source (see Fig. 1).

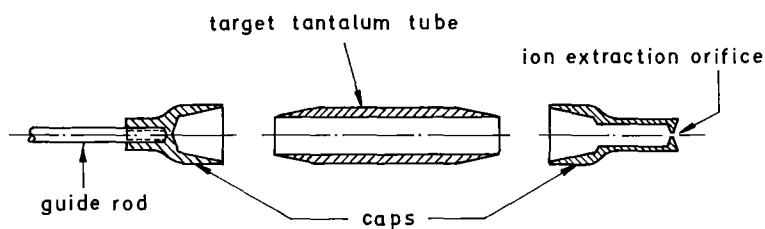


Fig. 1. Exploded view of the mass separator oven ampoule.

The xenon target: The tantalum tube enclosing the target xenon and collecting the produced barium atoms has a length of 30 mm and an inner diameter of 5.5 mm. A xenon pressure of 4 bars results in a target thickness of 70 mg/cm^2 . The beam enters and leaves the xenon-filled volume through windows of 5μ thick Havar foils. Between the two foils air is blown for cooling. The tantalum tube is embedded in a water-cooled two-piece copper bloc. Thin indium foils between the target tube and the copper provide good heat transfer. A thick collimating diaphragm ($4 \text{ mm } \emptyset$) in front of the tube is shielding the wall of the tube from direct irradiation by the alpha-particle beam. The target arrangement was tested by alpha-particle irradiations up to $8 \mu\text{A}$ (measured in a Faraday cup behind the target) at $E_{\alpha} = 104 \text{ MeV}$. From the barium activity collected in the tantalum tube and estimated cross sections for the (α, xn) reactions we can deduce that the collection efficiency is higher than 50%, possibly near 100%.

The mass separation: The electromagnetic mass separation was performed using an ion source with "surface-volume ionization" (1). For the operation of this type of ion source the oven ampoule which has a small ion extraction orifice (and the central part of which being the target tantalum tube; see Fig. 1) only has to be heated up to about 3000°K. For monitoring the mass separation 0.3 µg stable barium had been distributed over the inner surface of the tantalum tube before irradiation (in the case of preparing ^{135m}Ba samples enriched ^{138}Ba with < 0.02% ^{135}Ba is used). The mass separation procedure takes 5-10 minutes, the efficiency is 30-35%.

The sample quantities: In runs irradiating ^{136}Xe (enriched to 92%) for 16 hours with a 4 µA alpha-particle beam at $E_{\alpha} = 56$ MeV mass separated samples of 3-4 ng ^{135m}Ba (~3 mCi) have been obtained for the spectroscopic experiments. For ^{129m}Ba and ^{126}Ba we expect sample quantities of about 0.2-0.3 ng (~4 mCi) if we use xenon with ~60% ^{129}Xe .

Reference

- (1) A. Latuszynski and V.I. Raiko, Nucl. Instr. Meth. 125 (1975) 61.

6. NUCLEAR FUEL AND ELEMENTAL ANALYSIS

6.1 Manganese Nodule Analysis System - 'MANKA'*

K. Borcharding⁺, R. Döbele⁺⁺, H. Eberle, I. Erbacher⁺⁺⁺,
J. Hauschild⁺⁺, J. Hübener⁺⁺, J. Lange⁺⁺, G. Müller⁺⁺,
W. Rapp⁺, E. Rathjen⁺⁺, K.-D. Rusch⁺, A. Schäf⁺⁺, and U. Tamm⁺⁺

This paper is the final report on the development of the manganese nodule analysis system 'MANKA'. The work was performed at the Nuclear Research Center Karlsruhe from 1972 to 1976 to enable the in-situ-determination of the metal contents of manganese nodules.

A detailed description is given of the neutron capture gamma-spectroscopy with a ²⁵²Cf-source, the sledlike instrument carrier for the system component, which had to be designed for a water depth of 6500 m, and these components themselves.

On the electronic side these components include modules for data acquisition and conditioning and the transmission of data and control signals by the coaxial towing cable between sled and ship. Along with the hardware, the computer programmes are described which control the instrumentation on the sled and, immediately after gathering the spectroscopic data, compute the metal contents of the nodules.

The sled is an intermediate step on the way to a comprehensive manganese nodule exploration system. The tests on land and sea, as well as the deep sea test with the German research vessel "Valdivia" southeast of the Hawaiian Islands and their results are discussed. Finally an outlook is given on possibilities for further development.

* Report KFK 2537 (1977).

+ Abteilung Datenverarbeitung und Instrumentierung

++ Abteilung Reaktorbetrieb und Technik

+++ Laboratorium für Isotopentechnik

6.2 Elemental and Isotopic Concentration Analyses on Nuclear Fuels Using Nondestructive Assay Techniques*

H. Eberle, P. Matussek, I. Michel-Piper, H. Ottmar, and H. Allex⁺

Nondestructive assay (NDA) techniques based on the detection of X-rays and isotopic gamma rays have been investigated and applied both to elemental and isotopic concentration measurements on uranium and plutonium materials. In particular, the spectrometry of gamma rays from the natural radioactivity has been employed for fissile isotope concentration measurements in uranium and plutonium fuels, whereas both the analysis of induced X rays and the K-edge gamma densitometry technique have been used for elemental concentration measurements. Examples for the practical application of the analysis techniques are given.

* Proc. of the Discussion Meeting on Characterization and Quality Control of Nuclear Fuels, Kernforschungszentrum Karlsruhe, Germany, June 1978, to be published in Journal of Nuclear Materials.

⁺ Reaktorbrennelement Union GmbH, Hanau, Germany

6.3 Experiences with the Plutonium Waste Monitor

M.R. Iyer⁺, S.J. Choithramani⁺, P.P. Chakraborty⁺, P. Matussek, and H. Ottmar

The Plutonium Waste Monitor installed at the Bhabha Atomic Research Centre (BARC), Bombay, India, under the Indo-German Collaboration Program was field tested for performance and improvements. The monitor as reported earlier (1) employs passive gamma spectroscopy with a 5" dia. x 2" thick NaI detector. Two peak windows around 208 keV and 382 keV along with suitable Compton windows are used to give direct display of the ²⁴¹Pu and ²³⁹Pu contents in waste containers (15 cm x 21 cm). A set of six standards containing plutonium in the range of 0.05 to 2 g were used for calibration and the multipliers for the four windows thus obtained were set on the up/down scalers in the system. ²³⁹Pu content down to about 10-20 milligrams could be assayed.

The normal window for ^{239}Pu determination uses a range of 375-470 keV, i.e. the upper half of the 400 keV complex in the plutonium gamma spectrum. It was seen from a computer program (2) that samples having more than 90 % ^{239}Pu content will have only 10 % or less contribution to the counts in the full 400 keV complex from other isotopes. Based on this a procedure to check the interference of other gamma emitters in the samples was evolved. A window at 290 - 470 keV was set in the MCA in addition to the normal 4 windows and the ^{239}Pu contents were obtained using both the full 400 keV complex and the upper half of the complex. The calibration constants for the two cases were derived separately using the standards. The ^{239}Pu content estimated by using these two windows served as an effective method to check for ensuring that there is no contamination from other radioactivities. In the case of interference the ratio of these two measured quantities would be different from unity.

The measured $^{241}\text{Pu}/^{239}\text{Pu}$ ratio served as an index of attenuation in the samples since the approximate ratio for the type of material measured was known. A more realistic procedure to correct for self and matrix attenuation using 100 keV, 208 keV and 400 keV peaks is in progress.

The measurements also showed that few tens of microcuries of interfering activities could be handled in the system. This involves the identification of the interfering activity using the MCA and setting up suitable additional windows for subtracting the effect of these interferences. The corrected plutonium content and the amount of interfering activity could then be arrived at.

⁺ Bhabha Atomic Research Centre, Bombay, India

References

- (1) M.R. Iyer, P. Matussek, H. Ottmar, and S.J. Choithramani, Report KFK 2504 (1977) p. 88.
- (2) M.R. Iyer and H. Ottmar, Report KFK 2321 (1976).

6.4 Pu/U Ratio Determination from Uranium and Plutonium Isotopic Gamma Rays

H. Eberle and H. Ottmar

Previously we reported on Pu/U ratio measurements using the X-ray fluorescence analysis technique (1). There is an alternative method to determine the Pu/U ratio nondestructively in U-Pu fuel mixtures which employs the analysis of isotopic gamma rays from uranium and plutonium. We tested this technique for Pu/U ratio measurements on mixed-oxide fuel pins.

Mixed U-Pu fuel materials commonly occur as mixtures of plutonium and either highly enriched uranium or low enriched, natural and depleted uranium. Both material categories require the analysis of different gamma rays for Pu/U ratio measurements. In the former case where plutonium is mixed with highly enriched uranium, the abundant gamma rays from ^{235}U and $^{239,241}\text{Pu}$ in the low energy region (129-208 keV) are preferably employed for the analysis. Fig. 1 shows the gamma spectrum in the energy region of interest for this material category.

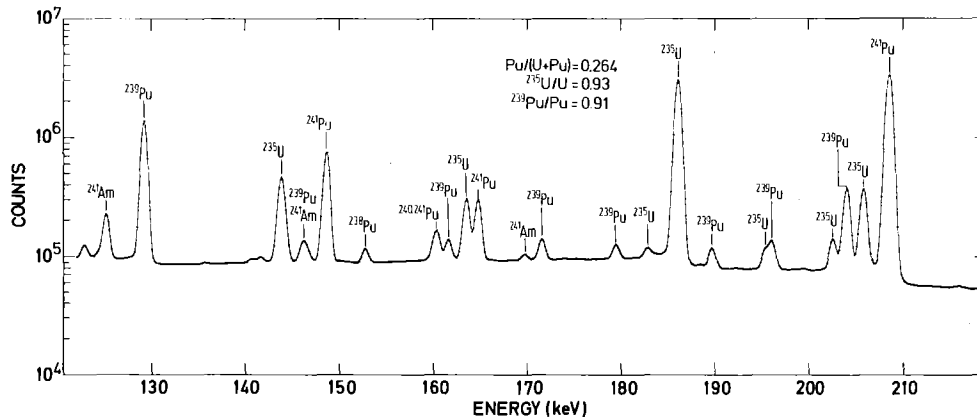


Fig. 1. Low-energy gamma spectrum from a mixture of plutonium and highly enriched uranium.

If, however, plutonium is mixed with low enriched, natural or even depleted uranium, this energy region can no longer be used for the analysis, because the plutonium activity then overrides the ^{235}U gamma signature. In this case the less abundant ^{238}U and ^{239}Pu gamma rays in the higher energy region (600-800 keV) must be employed for the Pu/U ratio analysis. Fig. 2 shows the gamma spectrum in this energy region taken from a fuel pin having 7 % plutonium mixed to natural uranium. The ^{238}U

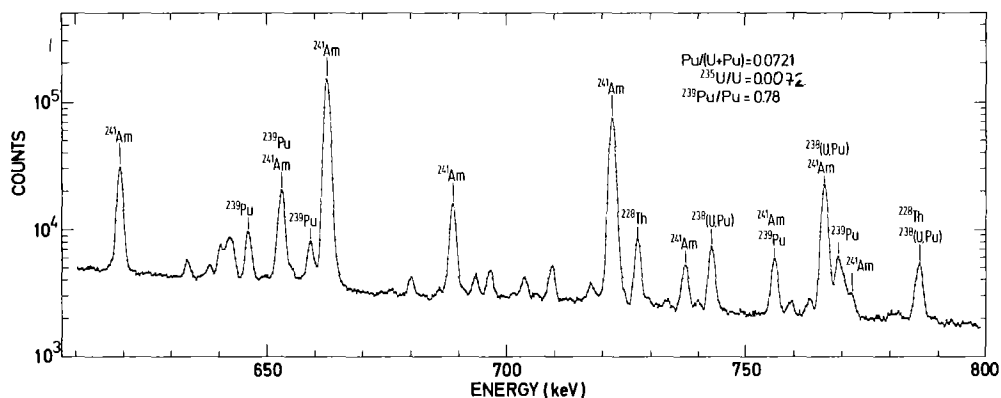


Fig. 2. High-energy gamma spectrum from a mixture of plutonium and natural uranium.

gamma rays at 743, 766 and 786 keV arise from the decay of the daughter product ^{234}Pa to ^{234}U . Unfortunately, the same gamma rays are also emitted by ^{238}Pu which decays directly to ^{234}U . For an atom ratio $^{238}\text{U}/^{238}\text{Pu} = 10^4$, which is a typical value for recycled LWR fuel ($\sim 3\%$ Pu in U_{nat} , ^{238}Pu isotopic abundance $\sim 0.3\%$), ^{238}Pu contributes approximately 30% to the observed peak intensity of the ^{238}U gamma rays.

Similar conditions were present with the mixed-oxide fuel pins which we have analyzed for Pu/U ratios. The pins contained natural uranium enriched with a few percent of plutonium. For the evaluation of the Pu/U ratio we have selected the ^{239}Pu and ^{238}U gamma rays at 646 keV and 743 keV, respectively, because these gamma rays show the least interferences from other gamma rays. The relative detection probability for both gamma energies was established using the known photon yields for the ^{241}Am gamma rays observed in this energy region. Table 1 summarizes the results obtained from 3 fuel pins.

Table 1. Pu/U ratio analysis from isotopic gamma rays 646 keV (^{239}Pu) and 743 keV (^{238}U).

Sample	Pu/U		Gamma-Book
	Book Value	Gamma Measur.	Book (%)
Pin	0.0239	0.0219	- 8.4
Pin	0.0448	0.0420	- 6.3
Pin	0.0777	0.0717	- 7.7

The evaluation of the Pu/U ratio from the observed peak intensity ratio of the ^{239}Pu and ^{238}U gamma rays requires, of course, a detailed knowledge of the uranium and plutonium isotopic composition (in particular a very accurate knowledge of the ^{238}Pu isotopic abundance), and of the absolute branching intensities of the gamma rays involved in the analysis. The observed bias between the measured values and the reported book values probably results from uncertainties in the necessary a priori information. In general, we found that the Pu/U ratio analysis from high-energy isotopic gamma rays is much more time-consuming than the previously reported X-ray fluorescence analysis technique.

References

- (1) H. Eberle and H. Ottmar, Report KFK 2504 (1977) p. 81.

6.5 Evaluation of Plutonium Isotopic Ratios Using High Resolution Gamma Spectrometry

H. Eberle, M.R. Iyer⁺, and H. Ottmar

High-resolution gamma spectrometry is becoming an alternative or complementary tool to mass spectrometry for the isotopic analysis of plutonium. With the exception of ^{242}Pu , all plutonium isotopes of interest emit useful gamma rays which can be used for isotopic ratio measurements. In addition, gamma spectrometry can also account accurately for ^{241}Am , if present.

Work is in progress for the study and evaluation of this analysis technique. We started with the analysis of plutonium samples of widely different isotopic compositions, ranging from low-burnup to high-burnup plutonium. Among these samples the NBS 946, 947 and 948 have been measured. Two different detector system have been employed for the measurements: a small planar diode (1.3 cm^3 , FWHM 550 eV at 122 keV) and a coaxial diode of medium size (18 cm^3 , FWHM 720 eV at 122 keV). Fig. 1 displays, as an example, gamma spectra taken with the planar detector from low-burnup and high-burnup plutonium samples. The selected energy region

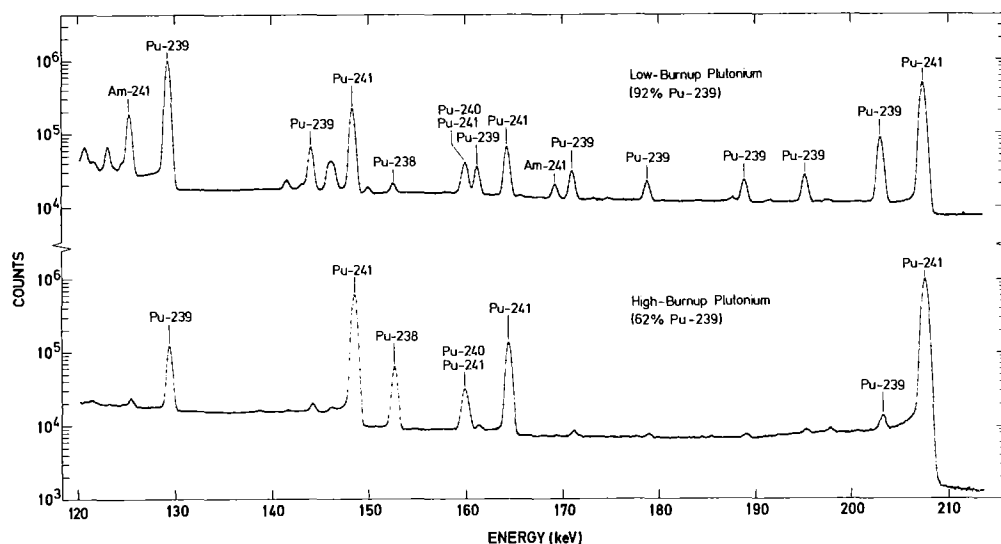


Fig. 1: High-resolution gamma spectra from low-burnup and high-burnup plutonium

(120 keV - 210 keV) provides information on all isotopes of interest. Both material types show relatively strong gamma lines from ²³⁹Pu and ²⁴¹Pu, while the ²⁴⁰Pu gamma line (160.3 keV) is less pronounced and interferes with gamma lines from ²³⁹Pu and ²⁴¹Pu. ²³⁸Pu provides a clean peak (152.8 keV) in gamma spectra from higher burnup plutonium.

In the present isotopic analysis work the peak areas of single gamma peaks or groupings of unresolved leaks have been determined by the channel summation method. For the subtraction of background counts underneath the peaks, a smooth, step-like background line was calculated from the measured spectrum. The net peak area ratios, corrected for efficiency, were then converted into isotopic ratios using published absolute gamma-branching intensities and half-lives (1,2).

Table 1 summarizes the results from isotopic ratio measurements on 5 different plutonium samples as obtained from the spectrum analysis using the channel summation method. Since in the plutonium gamma spectrum gamma rays from ^{241}Pu happen to be energetically close to gamma rays from the other plutonium isotopes, it appears advantageous to determine primarily the isotopic ratios $^{238}\text{Pu}/^{241}\text{Pu}$, $^{239}\text{Pu}/^{241}\text{Pu}$ and $^{240}\text{Pu}/^{241}\text{Pu}$. The following gamma rays have been used for the evaluation of these ratios.

$^{238}\text{Pu}/^{241}\text{Pu}$ ratio. This ratio was evaluated using gamma rays at 148 (^{241}Pu) and 152 keV (^{238}Pu). With one exception (NBS 948), the gamma values are systematically lower than the values from the destructive analysis. This deviation is most probably due to a bias in the absolute gamma-branching intensity values of the two gamma rays. In order to better define this bias, more accurate isotopic standards are required, because for the present isotopic standards the stated uncertainties of the ^{238}Pu abundances range between 2 % (NBS 946, 947) and 10 % (NBS 948).

$^{239}\text{Pu}/^{241}\text{Pu}$ ratio. Gamma rays in the energy region from 332 to 422 keV have been used for the evaluation. This is a fruitful energy region for $^{239}\text{Pu}/^{241}\text{Pu}$ ratio measurements on plutonium samples with ^{241}Pu abundances from approximately 1 % upwards. For those samples the gamma values turn out to be approximately 3 % lower than the actual values, possibly again indicating a small bias in the branching intensities of the gamma rays involved.

Table 1. Comparison of plutonium isotopic ratios from gamma analysis and destructive analysis (DA). The values in parantheses are percentage deviations between both data sets.

Sample	$^{238}\text{Pu}/^{241}\text{Pu}$		$^{239}\text{Pu}/^{241}\text{Pu}$		$^{240}\text{Pu}/^{241}\text{Pu}$	
	DA	Gamma	DA	Gamma	DA	Gamma
NBS 948	0.0295	0.0321(+8.7)	255.3	260.7 (+2.1)	22.14	20.60 (-7.0)
NBS 946	0.0786	0.0760(-3.3)	27.90	27.10(-2.9)	4.068	3.682(-9.5)
NBS 947	0.0827	0.0805(-2.7)	22.33	21.72(-2.7)	5.418	4.953(-8.6)
Medium Burnup	0.0431	0.0403(-6.5)	18.16	17.60(-3.1)	6.440	6.084(-5.5)
High Burnup	0.1188	0.114 (-4.0)	6.86	6.67(-2.8)	2.557	2.433(-4.9)

$^{240}\text{Pu}/^{241}\text{Pu}$ ratio. The gamma rays at 160 keV (^{240}Pu) and 164 keV (^{241}Pu) were employed for the evaluation of this isotopic ratio. Since the ^{240}Pu gamma-ray signature at 160 keV has to be extracted from a complex peak structure,

part of the observed bias between gamma values and actual isotopic ratios as determined by mass spectrometry may be due to the present analysis procedure.

More refined spectrum analysis methods using peak fitting with different computer codes are now being undertaken to investigate the origin of the observed biases, and to further evaluate the analysis technique.

⁺On deputation from Bhabha Atomic Research Centre, Bombay, India.

References

- (1) R. Gunnink, J.E. Evans and A.L. Prindle, Report UCRL-52139 (1976).
- (2) American National Standard, ANSI N 15.22 (1975).

6.6 Branching Intensities of ^{239}Pu Gamma Rays

H. Eberle, M.R. Iyer⁺, and H. Ottmar

The accuracy of plutonium isotopic analysis using gamma spectrometry relies on an accurate knowledge of gamma branching intensities, if the analyses are to be performed without recourse to comparison with isotopic standards. Accurate *absolute* branching intensities, or at least accurate branching intensity *ratios*, are necessary to convert the measured peak area ratios of isotopic gamma rays into atom ratios. In addition, accurate *relative* branching intensities of gamma rays from one particular isotope are required for the construction of the relative gamma detection efficiency curve for a given sample-detector combination. Gamma rays from ^{239}Pu are usually employed for this purpose.

A comprehensive compilation of absolute branching intensities for gamma rays from plutonium and americium isotopes has recently been published by Gunnink et al. (1). Other authors (2,3,4) also reported absolute branching intensities, mainly for ^{239}Pu gamma rays, which for some gamma rays deviate up to 15 % from the values reported by Gunnink. In order to examine the observed discrepancies, we made a consistency check on Gunnink's branching intensity values for ^{239}Pu gamma rays. For this purpose high-resolution gamma spectra have been accumulated from the plutonium reference materials

Table 1: Comparison of Reported Branching Intensities of Gamma Rays from ^{239}Pu

Energy (keV)	Present Analysis	Ref. /1/	Ref. /2/	Ref. /3/	Ref. /4/
129.3	6.22 E-5	6.26 E-5	6.2 E-5	6.20 E-5	6.23 E-5
144.2	2.83 E-6	2.83 E-6	3.25 E-6	2.96 E-6	2.65 E-6
161.5	1.20 E-6	1.20 E-6	1.25 E-6	1.24 E-6	1.22 E-6
171.3	1.10 E-6	1.11 E-6	1.13 E-6	1.11 E-6	1.00 E-6
179.2	6.41 E-7	6.58 E-7	6.28 E-7	6.54 E-7	
189.3	7.77 E-7	8.30 E-7	8.72 E-7	8.26 E-7	
195.7	1.07 E-6	1.06 E-6	1.07 E-6	1.09 E-6	
203.5	5.61 E-6	5.60 E-6	5.6 E-6	5.70 E-6	5.58 E-6
255.4	8.04 E-7	8.05 E-7	8.03 E-7	8.07 E-7	
297.5	5.02 E-7	5.02 E-7	5.0 E-7	5.02 E-7	
345.0	5.60 E-6	5.59 E-6	5.61 E-6	5.96 E-6	4.97 E-6
375.0	1.57 E-5	1.57 E-5	1.58 E-5	1.64 E-5	1.52 E-5
413.7	1.48 E-5	1.49 E-5	1.5 E-5	1.51 E-5	1.48 E-5

Table 2: Branching Intensity Ratios for Some Plutonium Isotope Gamma Rays Determined from Measurements of NBS-SRM 948

Ratio	1 cm ³ Gsfite	1 cm ³ Sampo	18 cm ³ Gsfite	Mean Value	Gunnink et al. /1/
$^{241}\text{Pu}(148)/^{239}\text{Pu}(144)$	0.655	0.667	0.654	0.659	0.660
$^{241}\text{Pu}(164)/^{239}\text{Pu}(161)$	0.380	0.377	0.380	0.379	0.378
$^{241}\text{Pu}(208)/^{239}\text{Pu}(203)$	0.947	0.946	0.955	0.949	0.950
$^{241}\text{Pu}(267)/^{239}\text{Pu}(255)$	0.229	0.220	0.227	0.225	0.226
$^{241}\text{Pu}(332)/^{239}\text{Pu}(345)$	0.0517	0.0493	0.0524	0.0511	0.0532
$^{241}\text{Pu}(335)/^{239}\text{Pu}(345)$	0.00426	0.00437	0.00433	0.00432	0.00428

NBS-SRM 948 and 949d. Each of the two samples has been measured with two different detector systems - a small planar diode (1 cm³) with an energy resolution of 550 eV at 122 keV and a coaxial diode (18 cm³) with a resolution of 720 eV at the same energy. The peak area analyses have been performed by the peak fitting method, using the computer codes Gsfite (5) and Sampo (6). In this way a total of six different data sets have been generated.

When plotted as a function of energy, the efficiency values $\epsilon = P/B$, i.e. the ratio of the measured peak areas P divided by the branching intensities B, should all fall on a smooth curve, provided the reported branching intensities are internally consistent. With two exceptions (179 and 189 keV gamma rays) this was indeed observed for the major ^{239}Pu gamma rays between 123 and 451 keV.

Higher order polynomials on a linear and log/log scale and functions of the form $\varepsilon(E) = aE^b \exp(cE)$ were tried for fitting the efficiencies in the various cases. We found that none of the above functions gave a satisfactory fit to the data points in the entire energy region. We therefore decided to split the fitting intervals into two regions: cubic functions were used to fit the data in the energy range from 123 to 203 or 255 keV, and in the higher energy region the data were fitted to either cubic or power functions. Table 1 compares the branching intensities for 13 of the major ^{239}Pu gamma rays in the energy range between 129 and 414 keV from the present analyses with previously reported data. The present analyses suggest that Gunning's data (1) represent a consistent set of branching intensities, with the exception of the intensities of the gamma rays at 179 and 189 keV. A more careful evaluation of the branching intensities for these 2 gamma lines is necessary.

The validity of the data in terms of absolute branching intensity ratios is best checked by evaluating isotopic ratios from gamma spectra measured on samples with accurately known isotopic composition, and comparing them with the known values. Alternative, branching intensity ratios of gamma rays important for the isotopic analysis can be determined from spectra taken from those samples. Table 2 summarizes branching intensity ratios for some important ^{239}Pu and ^{241}Pu gamma rays as obtained from the evaluation of the gamma spectra taken from the NBS 948 isotopic standard. The intensity ratios are based on the isotopic composition quoted for this standard (corrected for decay), and on the plutonium isotope half-lives quoted in (7). Again the results are in close agreement with Gunnink's data.

⁺ On deputation from Bhabha Atomic Research Centre, Bombay, India.

References

- (1) R. Gunnink, J.E. Evans, and A.L. Prindle, Report UCRL-52139 (1976).
- (2) J.L. Parker and D.T. Reilly, Report LA-5675-PR (1974) pp. 11-19.
- (3) M.F. Banham, Report AERE-R 8737 (1977).
- (4) R.J.S. Harry and J.K. Aaldijk, private communication.
- (5) V. Haase, Report KFK 730 (1968).
- (6) J.T. Routti, Report UCRL-19452 (1969).
- (7) American National Standard, ANSI N 15.22 (1975).

6.7 Determination of Heavy Element Concentrations in Solutions by K-Edge Gamma Absorptiometry

P. Matussek, I. Michel-Piper, and H. Ottmar

Work continued on the evaluation of the K-edge gamma absorptiometry tech-

nique for special nuclear material concentration measurements in solutions. The continuous photon energy distribution obtained from an X-ray generator is used for energy-dispersive gamma transmission measurements at the K-absorption edges of special nuclear materials like uranium and plutonium.

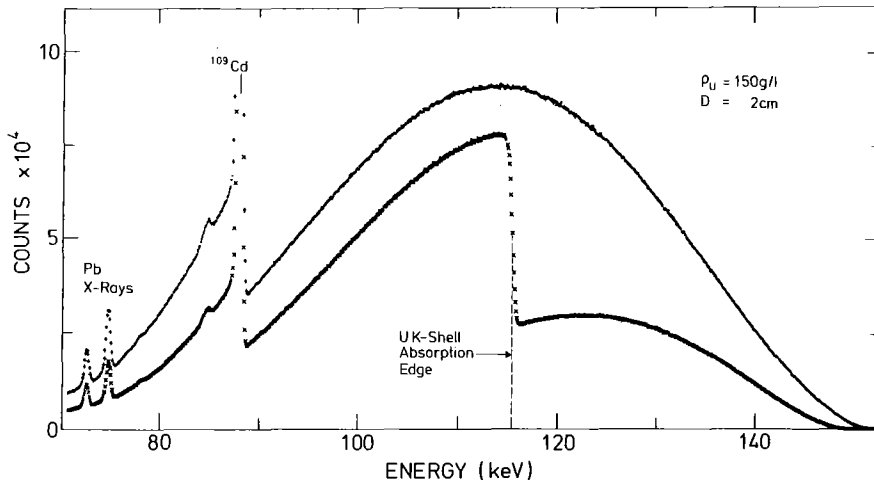


Fig. 1.
Filtered X-ray beam from an X-ray generator before and after the transmission through a 2 cm thick uranium solution ($\rho_U=150$ g/l).

Fig. 1 shows the tailored X-ray beam before and after the transmission through a uranium containing solution. The spectra are measured with a high-resolution planar Ge detector (FWHM = 550 eV at 122 keV) at a slope of approximately 70 eV/channel. The 88 keV ^{109}Cd gamma line served as reference line for digitally stabilizing the gain of the electronic chain.

The accurate concentration analysis requires an accurate determination of the ratio of the transmissions, R , below and above the absorption edge energy. The heavy element concentration, ρ_H , is determined from this ratio by the relation

$$\rho_H = \frac{\ln R}{\Delta\mu \cdot D},$$

where $\Delta\mu$ and D denote the change of the total photon cross-section at the K-absorption edge and the sample thickness, respectively. We tested several analysis procedures for determining the ratio of the transmissions at the absorption edge energy. An advantageous analysis approach which effectively utilizes most of the information provided by the continuous transmitted gamma beam has been worked out and implemented into a minicomputer-based analysis system (see also contribution 7.4.7). This approach consists of fitting,

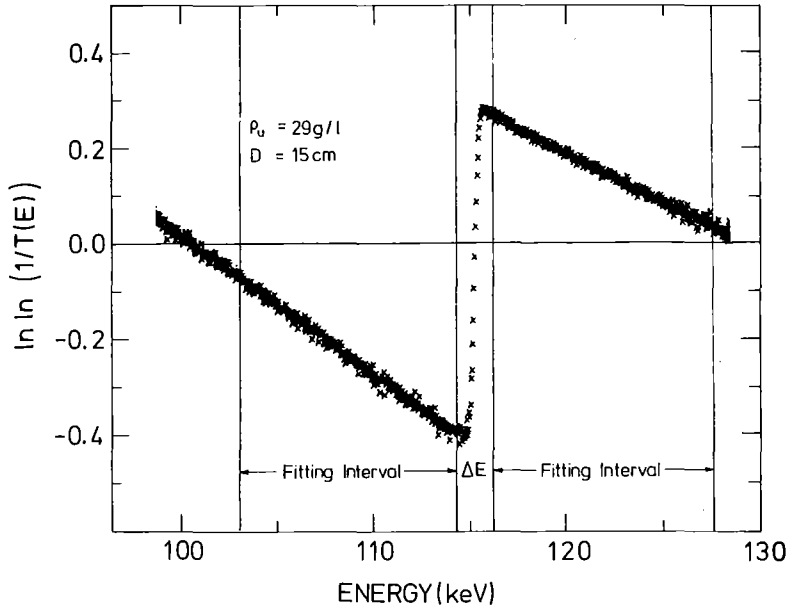


Fig. 2:
Energy dependence of the function $\ln \ln(1/T(E))$. $T(E)$ is the transmission through the heavy element bearing solution, measured with respect to the transmission spectrum through a blank nitric acid solution.

on both sides of the absorption edge, the experimentally determined transmission values, $T(E)$, to the function

$$\ln \ln (1/T(E)) = \ln (\mu(E) \cdot \rho \cdot D).$$

This function shows a nearly linear dependence upon the gamma energy E , as shown in Fig. 2. The transmission values, $T(E)$, are measured with respect to a reference spectrum which is once taken with good counting statistics through a blank nitric acid solution. This reference spectrum is permanently kept in the computer memory. The values $\ln \ln (1/T(E))$ are fitted by the least-squares method either to a linear or parabolic function on both sides of the absorption edge, using the fitting intervals as shown in Fig. 2. The transmission jump at the absorption edge energy is then calculated by extrapolating the fitted functions to the K-edge energy.

This analysis procedure has experimentally proven to be highly insensitive to matrix properties. The precision and accuracy of the special nuclear material concentration analysis attainable in a given analysis time is then largely limited by the count rate that can be tolerated in the electronics of the gamma detecting system without deteriorating appreciably the energy resolution. Fig. 3 shows the precisions attainable in different analysis times, plotted versus the product of heavy element concentration (in units of g/l)

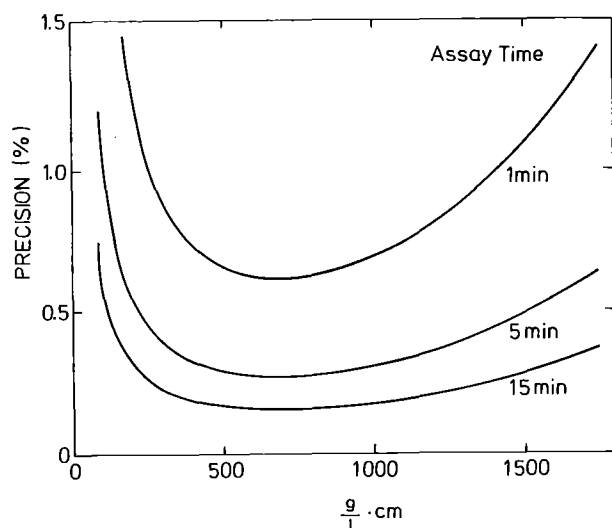


Fig. 3: Concentration assay precision attainable with K-edge absorptiometry for given analysis time intervals, plotted versus the product of concentration (g/l) times sample thickness (cm).

times the sample thickness in cm. The precision values are calculated assuming that the X-ray intensity from the X-ray generator is adjusted to give always a fixed count rate of 10 kHz, and that 50 % of this count rate is in the fitting intervals. The curves illustrate that under optimum conditions, i.e., choosing the optimum sample thickness for a given heavy element concentration, precisions of less than 0.2 % can be achieved in an assay time of 15 min. The K-absorption edge densitometry preferably applies to solutions with heavy element concentrations ranging from approximately 50 g/l upwards.

7. TECHNICAL DEVELOPMENT

7.1 CYCLOTRON

7.1.1 Operation Summary of the Karlsruhe Isochronous Cyclotron

F. Schulz and H. Schweickert

During the period of report the machine was in full operation (see Table 1). The total of available beam time of 7568 h is practically the same number compared to the last year (1), though we had a short shut-down period of 10 days. This period was used to replace several components which have proved unsatisfactory and for building in of new equipments (replacement of one of the two 10 000 l/s diffusion pumps, installation of two new cooling circuits for the internal beam isotope production, installation of new proton resonance measuring systems into the beam switching magnet and the cyclotron, installation of a cryogenic absorber system (LN) which can be plugged in automatically in the main vacuum chamber to trap especially the water from small leaks etc.). The main reason however was to prepare the main vacuum chamber of the cyclotron for the installation of the new correction coils in 1979 (see Fig. 1).

CYCLOTRON OPERATIONAL	WITH INTERNAL ION SOURCES	WITH EXTERNAL ION SOURCES	TOTAL
FOR EXPERIMENTS	5641 h 77.9 %	950 h* 74.4 %	6591 h 77.4 %
FOR BEAM DEVELOPMENT AND TESTING NEW COMPONENTS	955 h 13.2 %	22 h 1.7 %	977 h 11.5 %
TOTAL TIME OF OPERATION WITH THE BEAM ON TARGETS	6596 h 91.1 %	972 h 76.1 %	7568 h 88.9 %
SCHEDULED SHUT-DOWN FOR MAINTENANCE, REPAIR AND INSTALLATION	226 h 3.1 %	21 h 1.6 %	247 h 2.9 %
UNSCHEDULED SHUT-DOWN	415 h 5.8 %	285 h 22.3 %	700 h 8.2 %
TOTAL SHIFT TIME	7238 h 100 %	1278 h 100 %	8516 h** 100 %
* POLARIZED DEUTERONS 232 h ${}^6\text{Li}^{3+}$ -IONS (156 MeV) 718 h ** THE REAL TIME OF 8760 h IS ACHIEVED BY ADDING A 10 DAYS SHUT DOWN PERIOD FROM 22.12.77 - 5.1.78			

Table 1: Statistics of cyclotron from July 1977 to June 1978

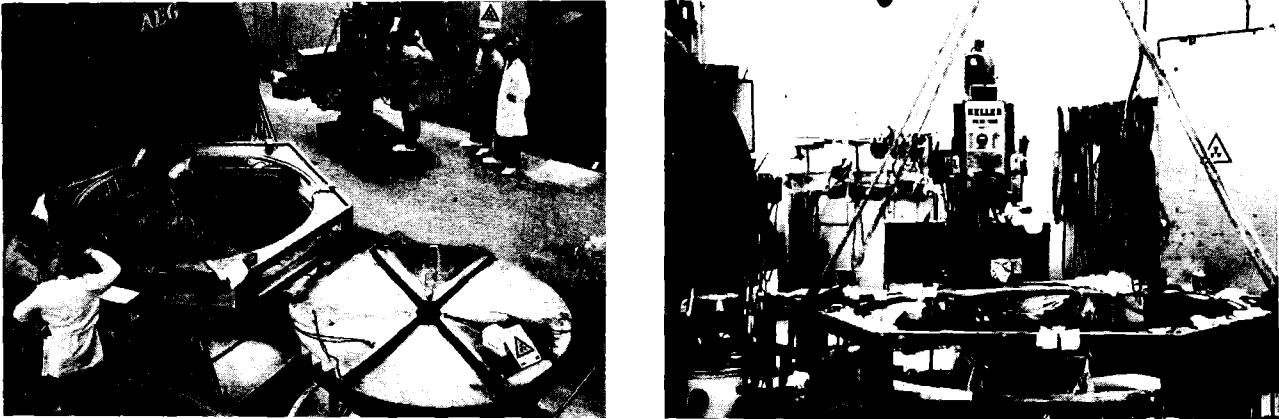


Fig. 1: Pictures taken during the first longer shut-down since 1974. For the feed-throughs of the new high power trim coils additional holes ($\phi = 100$ mm) have to be bored into the main vacuum chamber. This had to be done inside the cyclotron vault.

A considerable amount of the main unscheduled downtime of about 8 % is again due to the high burn-up of the external ${}^6\text{Li}^{3+}$ -Penning ion source. In June 1978 it turned out that, probably as a result of the steel springs found in the gliding seals of the dee tuning loops in 1972 (2), a heavy corrosion had taken place also in the watercooling vanes of the inner conductors of the dees (in 1973, the outer conductors of the dees and all the aluminium water supply tubes had to be replaced). This now led to serious water leaks in SW-dee so that the aluminium parts with the cooling vanes had to be replaced. This procedure was carried out by our operators in an extremely short time of two days. We hope that we can wait for the replacement of the two other dees up to the next longer shut-down in 1979.

The main technical developments carried out

- Extention of the computer aided operation of the cyclotron
- Production of the new correction coils
- Improvements of the pulsing systems

are described in the following contributions.

In addition there was again a considerable improvement in the available ${}^6\text{Li}^{3+}$ -currents in the scattering chamber for basic nuclear physics experiments (see Fig. 2). A number of small technical improvements at the source led to this success.

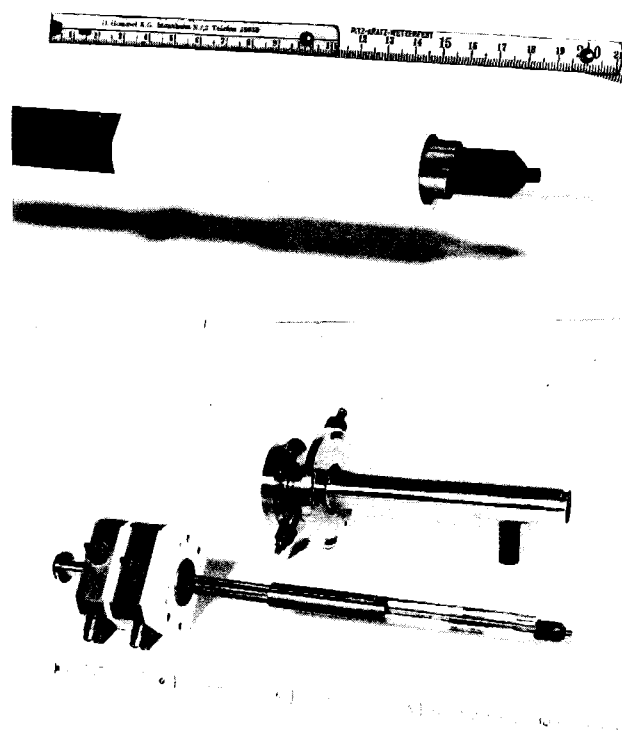
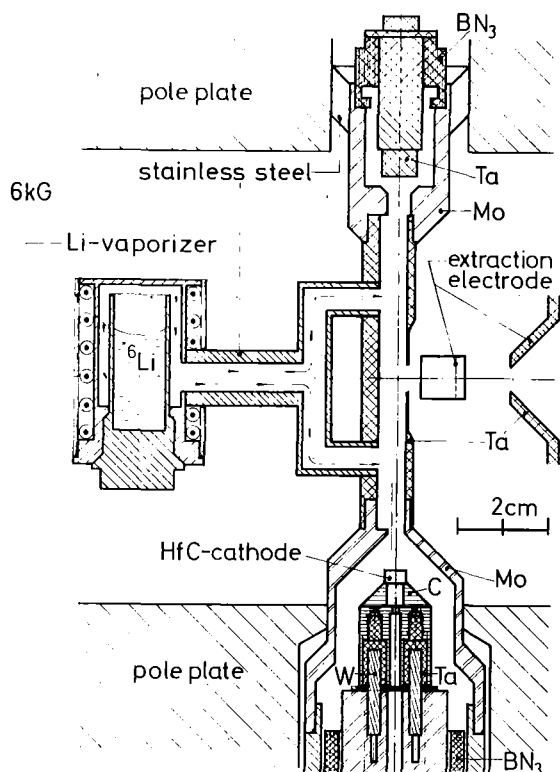


Fig. 2: Actual mechanical structure of the external ${}^6\text{Li}^{3+}$ hot filament Penning source and numbers showing the improvement from 1975 to 1978. The photographs show the HfC cathode together with the BN_3 insulators and the new arrangement of the heating supply lines.

Year	Max. electrical current in scattering chamber	total charge in scattering chamber	experimental time
1975	1 nA	50 μCb	272 h
1976	15 nA	1.2 mCb	378 h
1977	80 nA	3.8 mCb	225 h
1978 (up to July)	100 nA	16.7 mCb	394 h

In June 1978 it was decided to build up a "MAFIOS" (3) ion source for our axial injection system. This source will produce completely stripped light heavy ions (${}^{10}\text{B}^{5+}$, ${}^{12}\text{C}^{6+}$, ${}^{14}\text{N}^{7+}$, ${}^{16}\text{O}^{8+}$), which will be accelerated in our cyclotron to an energy of 26 MeV/Nucleon. This work will be done in close cooperation with the group of R. Geller in Grenoble.

KFK-KARLSRUHE USERS

INSTITUT FÜR ANGEWANDTE KERNPHYSIK	1763 h	26.8 %
LABOR FÜR ISOTOPENTECHNIK	888 h	13.5 %
INSTITUT FÜR RADIOCHEMIE	177 h	2.7 %
INSTITUT FÜR TECHNISCHE PHYSIK	90 h	1.4 %
INSTITUT FÜR KERNPHYSIK	40 h	0.6 %
PROJEKT SCHNELLER BRÜTER	11 h	0.1 %
INSTITUT FÜR HEISSE CHEMIE	6 h	0.1 %
	<u>2975 h</u>	<u>45.2 %</u>

EXTERNAL USERS

TECHNISCHE UNIVERSITÄT MÜNCHEN	1028 h	15.6 %
FREIE UNIVERSITÄT BERLIN	877 h	13.3 %
MAX-PLANCK-INSTITUT FÜR KERNPHYSIK HEIDELBERG	389 h	5.9 %
UNIVERSITÄT ERLANGEN	355 h	5.4 %
UNIVERSITÄT BOCHUM	279 h	4.2 %
KERNFORSCHUNGSANLAGE JÜLICH	146 h	2.2 %
UNIVERSITÄT BONN	124 h	1.9 %
UNIVERSITÄT ULM	75 h	1.1 %
UNIVERSITÄT HAMBURG	70 h	1.0 %
TECHNISCHE HOCHSCHULE DARMSTADT	48 h	0.7 %
DEUTSCHES KREBSFORSCHUNGSZENTRUM HEIDELBERG	47 h	0.7 %
UNIVERSITÄT SAARBRÜCKEN	31 h	0.5 %
UNIVERSITÄT MÜNSTER	26 h	0.4 %
NUKLEARMEDIZINISCHE KLINIK MÜNCHEN	23 h	0.3 %
UNIVERSITÄT KONSTANZ	12 h	0.2 %
CNRS STRASBOURG	5 h	0.1 %
UNIVERSITÄT STUTTGART	5 h	0.1 %
UNIVERSITÄT GIESSEN	3 h	0.1 %
UNIVERSITÄT GÖTTINGEN	2 h	0.1 %
	<u>3545 h</u>	<u>53.8 %</u>

COMMERCIAL IODINE-123 PRODUCTION 67 h 1.0 %

COMMERCIAL ISOTOPE PRODUCTION OTHER THAN IODINE-123 4 h 0.1 %

GRAND TOTAL 6591 h 100 %

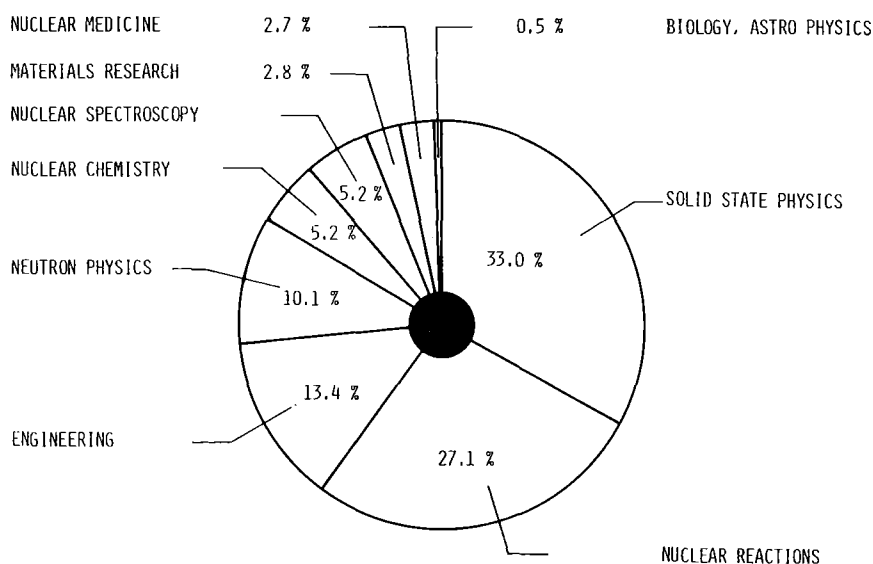


Table 2: User statistics from July 1977 to June 1978 and the distribution of the 6591 h experimental time on the different fields of activity.

On the users' side (Table 2) 53 % of our machine time was given to visitors from laboratories outside the Nuclear Research Centre Karlsruhe. Our aims are in fact to accommodate every experiment for which the facilities of this laboratory are particularly appropriate, independent of questions of institutional affiliation. The use of the cyclotron for non nuclear physics amounts to about 55 % of the total time available for experiments.

References

- (1) F. Schulz and H. Schweickert, Report KFK 2504 (1977) p. 95.
- (2) G. Schatz, F. Schulz, and H. Schweickert, Report KFK-Ext. 18/75-1.
- (3) R. Geller, IEEE Transactions on Nuclear Science, Vol. NS-23, No. 2, April 1976, p. 904

7.1.2 Status of the Routine Production of ^{123}J at the Karlsruhe Isochronous Cyclotron

K.H. Assmus, K. Jäger, R. Schütz, F. Schulz, and H. Schweickert

During the period of report the production method for iodine-123, described in the Annual Reports 1975 and 1976 (1,2), has been used routinely to prepare 140 batches with a total of 19 Ci of iodine-123 for trials at selected hospitals in the southern part of Germany. A total of more than 5000 patients were treated. During this time the production process worked with a reliability of 100 %⁺⁾ , which means that all scheduled charges to the hospitals were in time and contained the ordered activity. We must confess that this was much better than even the most optimistic people in our group expected.

In September 1977 we settled (5 years) contracts for iodine-123 delivery to three hospitals. The price amounts 12.50 DM/mCi leaving Karlsruhe. This price includes both the costs for the necessary accelerator time (DM 740,-- per hour) and for the staff required for the production process proper and its further development. The production time is now fixed between 0.00-2.00 in the night so that the transportation on the German highways is finished at 7.00 and the iodine-123 is available at the hospitals in the early morning. Since January 1978 we produce iodine-123 twice a week.

⁺⁾ One week after this report was written we had a break-down of the cyclotron for two days so that the delivery to the hospitals had to be cancelled once.

In the last year further improvements of the target technique (see Fig. 1) were achieved (3). Also the design for a fully automated extraction process inside a new hot cell was finished.

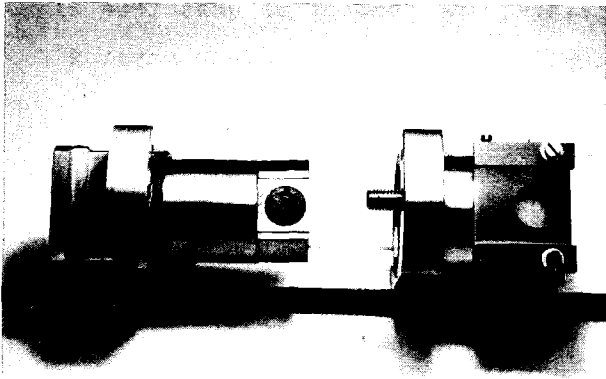


Fig. 1:
Actual iodine-123 production target. The diameter of the $^{124}\text{TeO}_2$ -sample has been enlarged to 10 mm. The homogeneity of the beam intensity over this diameter is produced by mechanical sweeping of the target.

Finally, for those who are not familiar with the iodine-123 applications, we would like to show once more (Fig. 2) the advantage of this isotope as compared to iodine-131 in one special case.

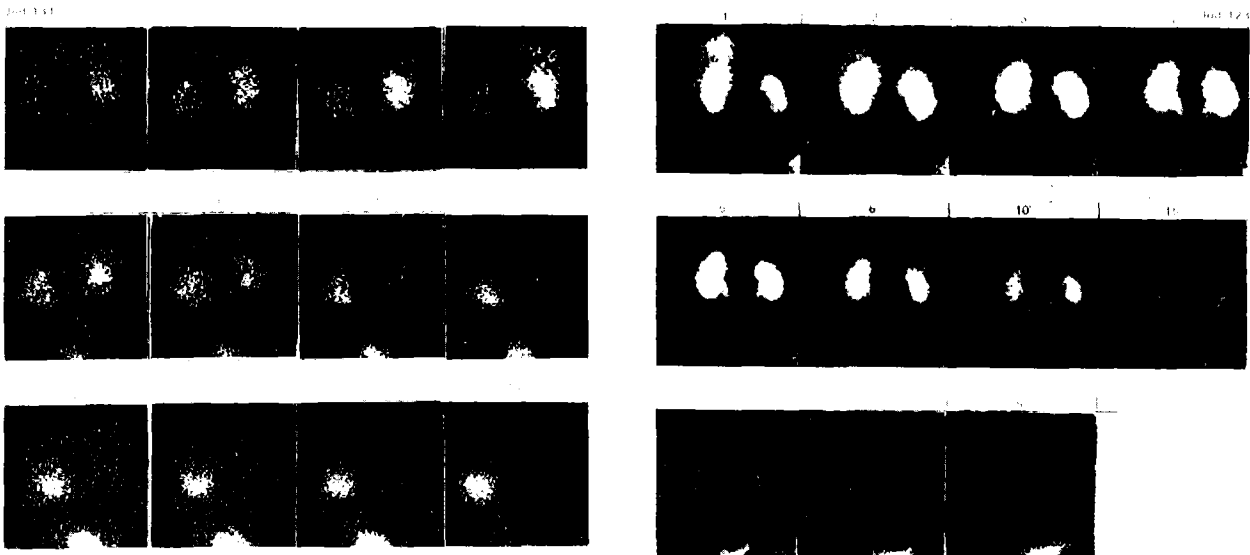


Fig. 2: Dynamic renal function study with iodine-131 (left side) and iodine-123 (right side). In addition to the clearly seen better image quality the dose to the patients is reduced by at least a factor of 50. We thank Priv. Doz. Dr. G. Buttermann from the Nuklearmed. Klinik rechts der Isar in München for these pictures.

References

- (1) K.H. Assmus, F. Michel, H. Münzel, F. Schulz, R. Schütz, and H. Schweickert, Report KFK 2378, (1976) p. 86.
- (2) K.H. Assmus, F. Michel, H. Münzel, F. Schulz, R. Schütz, and H. Schweickert, Report KFK 2504 (1976) p. 104.
- (3) F. Schulz and R. Schütz, DE-OS 2707, 390

7.1.3 Status of the Computer Diagnostic and Control for the Cyclotron

H. Heinzmann⁺, W. Kappel, W. Kneis, B. Kögel, Ch. Lehmann⁺, J. Möllenbeck, and H. Schweickert

The computer controlled diagnostic and control system (1) for the cyclotron is used intensively by the operators for machine adjustment and control. For the first quarter of 1978 this can be seen from the following statistics, showing the relations in percentages of the real time.

ready for use	38 %
phase width internal	20 %
status external beam	10 %
status cyclotron	6 %
iodine quality	3 %
3:1 pulsing	2 %
other programs	2 %
program development	16 %
service and system	
maintenance	3 %

The increasing demand to use the system for machine diagnostic and control likewise reduced the availability for program development. Therefore it was decided to build up a standby-system for program development and system security. A block diagram of the extended hardware configuration is shown in Fig. 1.

Besides tests for automatic on-line beam optimization procedures (2) the program development is concentrated on reorganization, improvement and modification of old programs. This has been necessary because the incorpora-

tion of new features into existing programs is often limited by the available user memory within the BASIC interpreter.

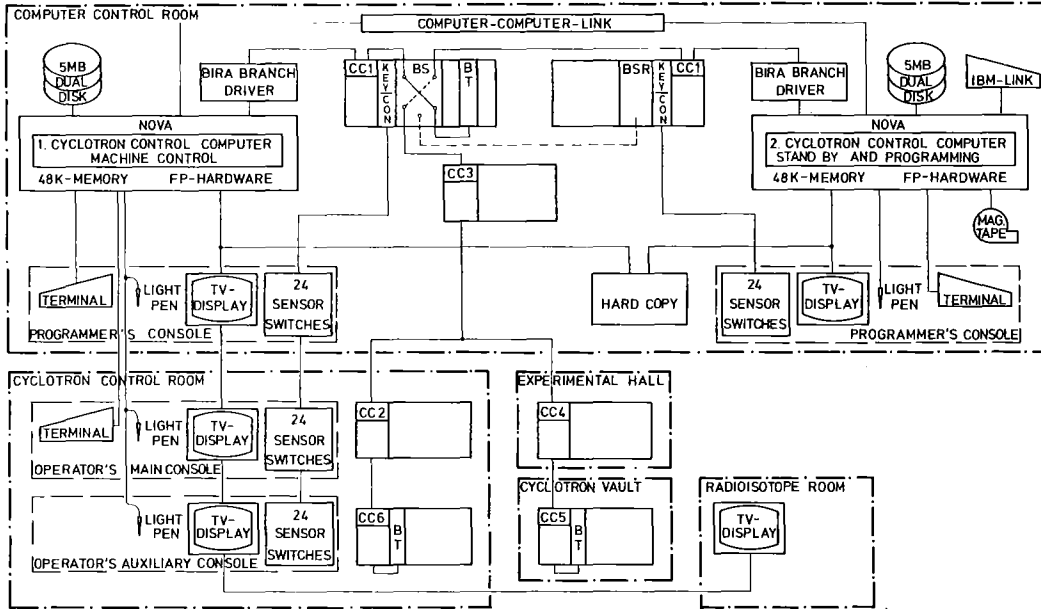


Fig. 1: New cyclotron control computer configuration showing the direct and CAMAC coupling of the dual computer system, the programming and operating consoles.

Time-of-flight measurements

All programs using time-of-flight measurements like phase-width measurement, quality test of the pulsing system and the measurement of the absolute energy have been improved by reorganization and speeded-up by using assembler subroutines for peak integration. Now e.g. the measurement of the internal phase-width only takes 10 seconds.

For the experiments with the neutron time-of-flight spectrometer a control link to the experiment computer has been established via CAMAC.

If the monitor-mode of the program "phase-width internal" is chosen this link transmits the following three signals to the on-line experiment:

- monitoring on
- phase position out of bounds
- phase width out of bounds

In case the last two conditions are true the data acquisition program reacts via interrupt either by stopping the experiment or by calling for operator attention.

A new program using the time-of-flight measurement has been established to measure the phase position as function of the radius (Fig. 2). At the moment this program needs operator intervention to position the target, but it is intended to drive the target by the computer, too.

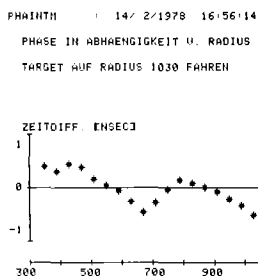


Fig. 2. Typical result of the measurement of the phase position as function of the radius with the 52 MeV deuteron beam.

Status programs

Reorganization, improvement and incorporation of new features into the status programs have been continued. This required to redesign the programs into overlay structures permanently having only the necessary main parts in core. The new features concern the "automatic adjustment" (T), and "automatic setpoint-tuning" (U) of a variety of parameters in the program status external beam. The T-mode facilitates most of the parameter settings by the exact reproduction of nominal parameter values. The U-mode only guarantees constant parameter settings within small correction limits. The purpose of the U-mode first of all is to compensate small long time drifts due e.g. to temperature effects etc.

Modular test system for CAMAC moduls

To guarantee a detailed test of most of the CAMAC hardware and to pursue the behaviour of the system a modular test system for the CAMAC interface, crate controller and the various CAMAC moduls has been developed. The system allows to run the complete test of all moduls with statistics as well as the execution of the test of one specific CAMAC modul.

⁺ Fachhochschule Karlsruhe, Germany.

References

- (1) H. Heinzmann et al. Report KFK 2504 (1976) p. 100.
- (2) W. Kneis, this report, contribution 7.1.8.

7.1.4. Status of the New Trim Coils

V. Bechtold, L. Friedrich, and L. Wiss

At the end of March 1978 the prototype coil was ready for the test bench. The voltage drop of each coil was measured as a function of current. All coils were in serial connection. The average temperature rise in the coils was 35°C at 50 A.

The temperature map at the surface of the cooling plate was measured while all coils were at 50 A. In Fig. 1 the radial temperature distribution along the mid-line of the coil is shown. The maximum temperature is about 65°C at the fringe of the coil. This value will be somewhat lowered by increasing the number of cooling canals.

The magnetic field in radial direction and along the extraction radius was determined. The field distribution along the mid-line of the coil at a distance of 3 cm from the coil is plotted in Fig. 2. For comparison the calculated data from the TCOIL-Program (1) are also shown in the figure. There is a good agreement with the experimental data especially in the inner section of the coil. The summarized data of the prototype trim coil are given in Table 1.

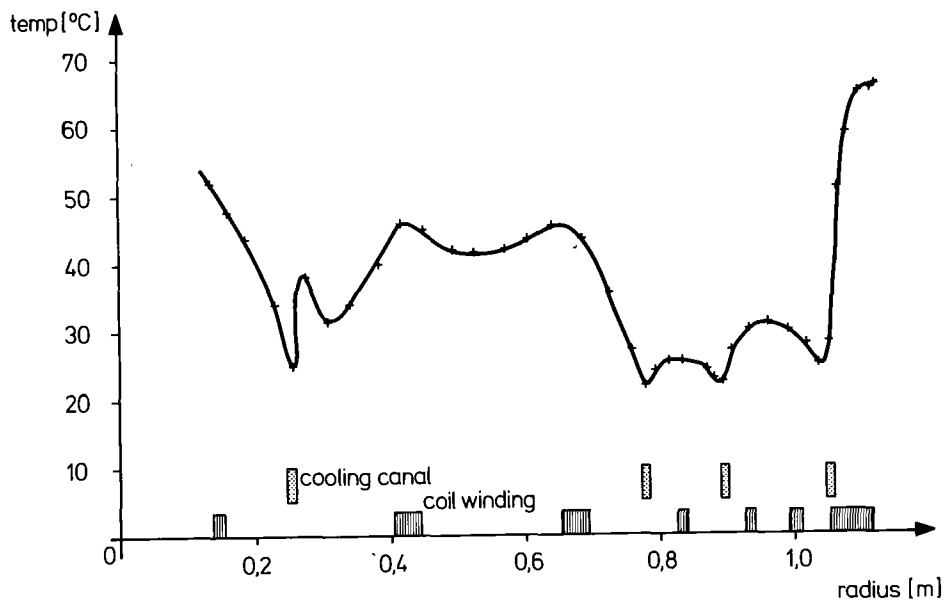


Fig. 1. The radial temperature distribution along the mid-line of the coil. The location of the cooling canals and the coils are drawn to scale in the same figure.

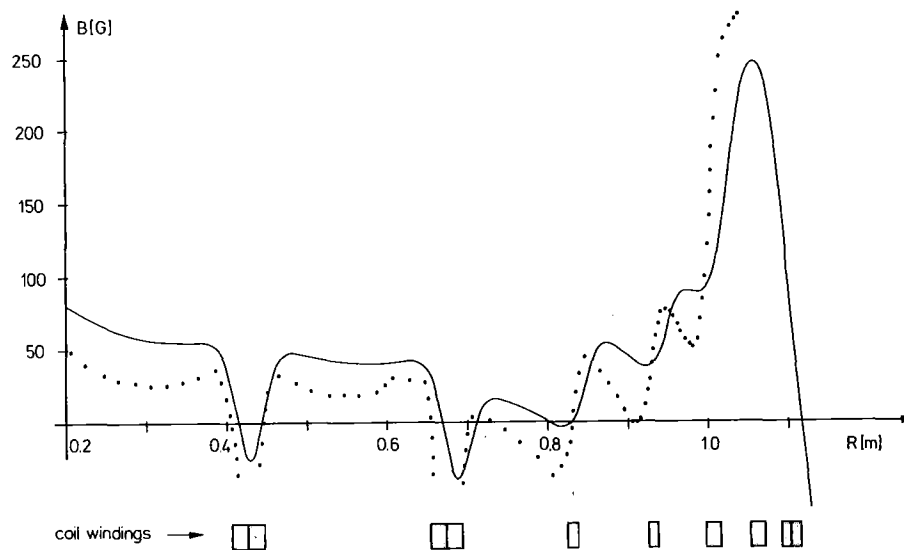


Fig. 2. The magnetic field distribution along the mid-line of the coil at a distance of 3 cm from the coil. The dotted lines are data calculated from the TCOIL-Program (1).

During the last shut-down period at the end of 1977 ten holes of 100 mm diameter were bored into the main vacuum chamber of the cyclotron for the flanges with the 12 x 50 A vacuum tight feed-throughs.

A prototype flange with the special feed-through for high currents was finished, too, and is shown in Fig. 3. This feed-through consists of hard silver plated copper bolts and copper pipes which are pasted in the epoxy flange.

Table 1: Data for the prototype trim coil plate. All six coils are in serial operation at 50 A.

Total power consumption	4 kW
Cooling water consumption	360 l/h
Resistance R_{\max}	0.32 Ω
Current density	12 A/mm ²
Heat flux density	1 W/cm ²
Average inner temperature	34°C
Weight	35 kg
Overall height	13.5 \pm 0.15 mm

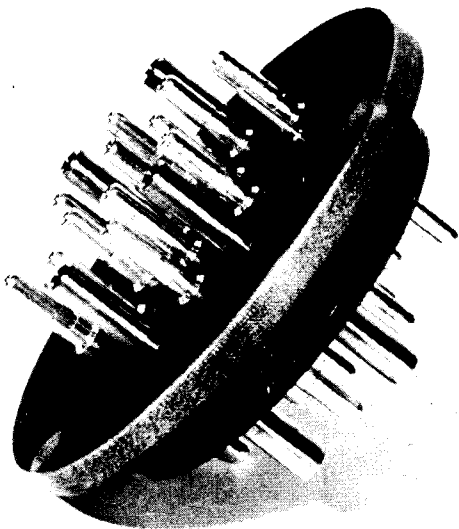


Fig. 3:

The prototype flange with the special feed-through for 12 x 50 A and for 4 water connections. Such an epoxy flange supplies one trim coil plate.

The production of the trim coils will start in the middle of this year so that in the early spring of 1979 the installation in the cyclotron can be done.

Reference

(1) H. Braun, SIN-TM-03-13 (1970).

7.1.5 Improvements of the Pulsing System for the Neutron
Time-of-Flight Spectrometer at the Karlsruhe Cyclotron
G. Schmalz, D. Erbe, and F. Schulz

In future, a regular, weekly production of ^{123}J for medical applications is planned at the Karlsruhe cyclotron by internal irradiation. This affects the operation of the pulsing system for the neutron time-of-flight spectrometer as the outer deflector plates have to be removed from the accelerating system during the time of iodine production and have to be reinserted afterwards. Because the beam time is expensive, this mode of operation required a totally new design for the deflector plates, which allows a quick and accurately reproducible movement from outside the vacuum chamber. At the same time it was aimed to improve the diagnostics of the beam position with respect to the deflector plates and to get a better overall reliability.

As a first step the cooled meandershaped stripline was replaced by a new uncooled stripline of high mechanical accuracy, which was successfully tested during a measuring period of four weeks in February and March 1978. At present a new system with moveable deflector plates is prepared for the next measuring period in October 1978. Besides remote operation the system includes a three fold entrance slit in front of the deflector plates. This allows to adjust the beam accurately to the mid plane of the system by minimizing the ion current on the outer, lower or upper part of the slit, respectively.

To improve reliability and for a more automatic operation in the future, we started to digitize the important electrical parameters of the pulsing system for undisturbed transmission to the experimental area. Some of these components will be also tested during the run in October.

7.1.6 A Pulsing System for the External Beam of the Karlsruhe Isochronous Cyclotron

M. von Hartrott⁺, G. Haushahn, K. Heidenreich, M. Luft⁺,
H. Schweickert, and E. Weihreter⁺

The ion beam of our cyclotron naturally consists of micropulses with a repetition time of 30 nsec (according to the acceleration frequency of 33 MHz) and a pulse width from 0.6 - 3 nsec. As reported earlier the time structure of the ion beam can be modified either by applying adequate voltages to a deflection system near the centre of the cyclotron (inner deflector), or to the arc voltage of the ion source (1,2). By using these techniques in principle all kinds of pulse structures can be produced in the centre of the cyclotron as shown in Fig. 1a.

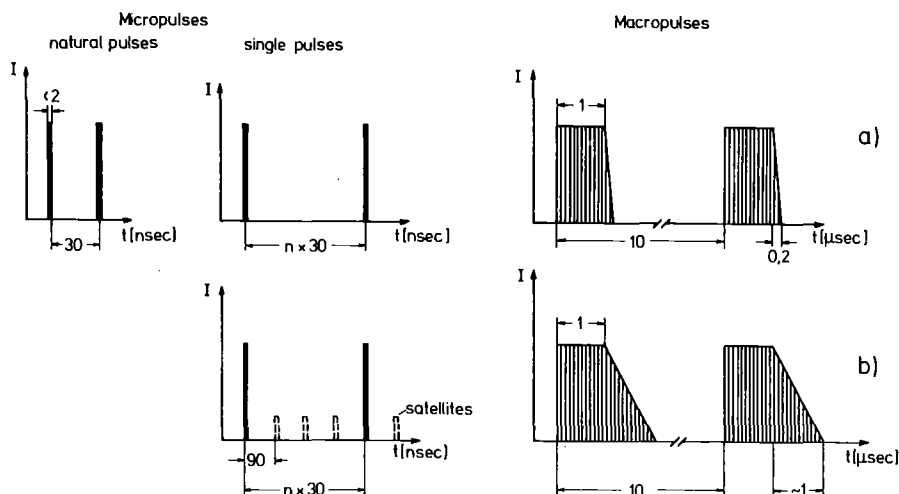


Fig. 1: Deterioration of pulse time structures in the center of the cyclotron by the acceleration and extraction processes.

a) Pulses in the centre of the cyclotron

b) Observed time structures in the external ion beam.

But the acceleration and extraction processes deteriorate the time structure of the ion beam in the following cases:

A. Microstructure pulsing (single pulses)

If a longer repetition time than 90 nsec (the revolution frequency of the ions) for the ion pulses in the external beam is desired the suppression

of the unwanted pulses is not perfect, because our cyclotron has no single turn extraction. In this case the single pulses are accompanied by satellites with the revolution frequency as shown in Fig. 1 b.

B. Macrostructure pulsing

By applying adequate pulse voltages to the inner deflector many kinds of macro ion pulses can be produced (see Fig. 1 a). The existing pulse generators (3) (6 KV , $1 \text{ kHz} < f_{\text{rep}} < 100 \text{ kHz}$, $0.5 \mu\text{sec} < \text{pulse width} < 1 \text{ msec}$) have falltimes smaller than $0.2 \mu\text{sec}$. At the inner radius ($R = 300 \text{ mm}$) the falltime of the ion beam pulses is similar to that of the pulse generator. At the outer radius ($R = 1040 \text{ mm}$) the falltime of the beam pulses is much longer ($\sim 1 \mu\text{sec}$) as shown in Fig. 1 b. This longer tail is caused by the acceleration process itself, because of the finite phase width. For example a phase width of 2.4 nsec FWHM ($\Delta\phi = 29^\circ$) yields a difference in the acceleration time of 3.5% which means that the tail of the beam pulse is about $1 \mu\text{sec}$ long.

For some experiments in the external beam, single pulses with satellites or macropulses with falltimes longer than $0.2 \mu\text{sec}$ are detrimental. Therefore to suppress the unwanted ions an additional deflection system was installed into the external beam handling system as shown in Fig.2.

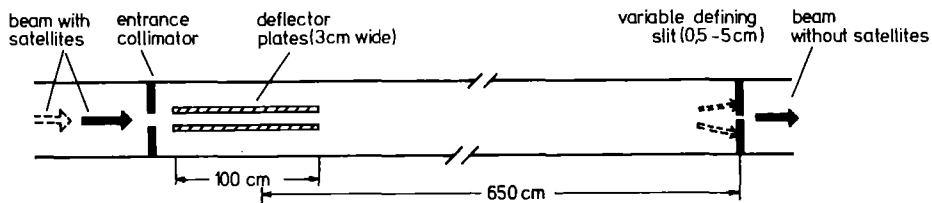


Abb. 2. Layout of the external beam pulsing system. For a 52 MeV deuteron beam which is focussed to the defining slit a voltage of 6 kV deflects the beam by about 1.5 cm.

To suppress the satellites of the single pulses a sine voltage of 2.75 MHz and $14 \text{ kV}_{\text{pp}}$ produced by a power amplifier of 1 kW is applied with adequate phase to the plate condensor. By this voltage single pulses without satellites may be produced for all repetition rates which are a multiples of 180 nsec.

To get macropulses of the ion beam with falltimes $< 0.2 \mu\text{sec}$, voltages of 6 kV with the desired repetition rates and pulse widths are applied to the plate condensor by special pulse generators (3,4).

⁺ Freie Universität Berlin, Germany

References

- (1) W. Kappel, J. Möllenbeck, and H. Schweickert, American Journal of Physics, New York, 1972, (Proc. of the 6th Cyclotron Conf. Vancouver) (July 1972) p. 358.
- (2) S. Cierjacks, B. Duelli et al., IEEE Trans. Nucl. Sci., NS-13 (4) (1966) 353.
- (3) G. Schmalz, private communication
- (4) M. Luft et al., Freie Universität Berlin, private communication.

7.1.7 Target System for the Production of ^{18}F

G. Bauer, Ch. Rämer, and A. Walter

Last year we were requested to produce fluorine-18 ($T_{1/2} = 110 \text{ min}$) for applications in nuclear medicine. For this purpose an irradiation chamber was designed and built allowing ^{18}F production at the external beam handling system.

The chosen reaction was $^{16}\text{O}(\alpha, d)^{18}\text{F}$ with an injection energy of 104 MeV (1). The target substance used was an 0.1 n NaOH solution, since ^{18}F was to be bound to sodium for medical reasons.

Fig. 1 shows the fundamental layout and a design drawing of the irradiation chamber. The activation chamber and a beam outlet flange sealing the vacuum are both connected by a bayonet joint allowing quick coupling and decoupling. The central unit of the activation chamber is a titanium flange with an activation space of 20 mm dia and 6 mm depth. The space is sealed towards the beam by a 100 μm thick tantalum foil. The rear of the flange is water cooled. The sample liquid is introduced by a syringe

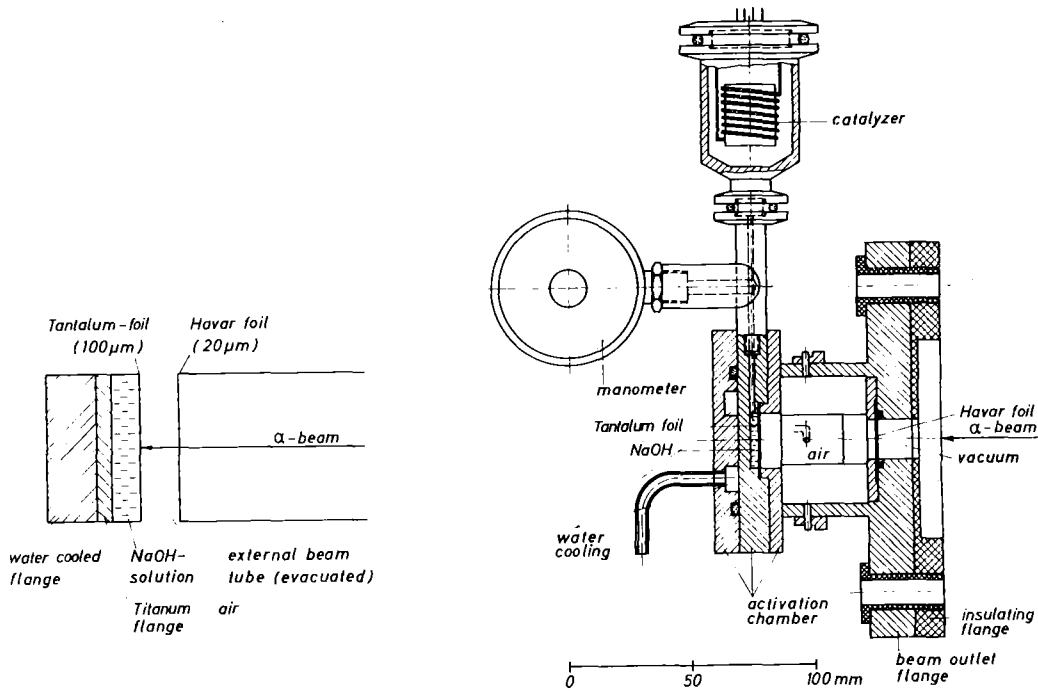


Fig. 1. Fundamental layout and design drawing of the irradiation chamber. The beam is shot through a vacuum sealing Havar foil into air and then hits the activation chamber.

into the activation space through a hole which can be closed and it is sucked off after irradiation. To avoid the possible build-up of overpressure during the irradiation, a palladium sponge catalyzer heatable up to 150°C has been provided which allows to recover the water at the activation chamber. The pressure prevailing during irradiation can be monitored by a manometer, using a television camera. For reasons of safety, the activation chamber has not been directly flanged to the vacuum system of the external beam tube. The vacuum is sealed by a 20 μm thick Havar foil. The whole irradiation chamber is flanged to a universal vacuum chamber of the external beam handling system such that it is insulated from it.

Three irradiations have so far been performed. The first two served for testing purposes and the third irradiated sample was handed over to a hospital where also pharmaceutical processing was carried out.

In all three irradiations a yield of about 10 mCi/μAh was attained measured 30 min. after the irradiation time.

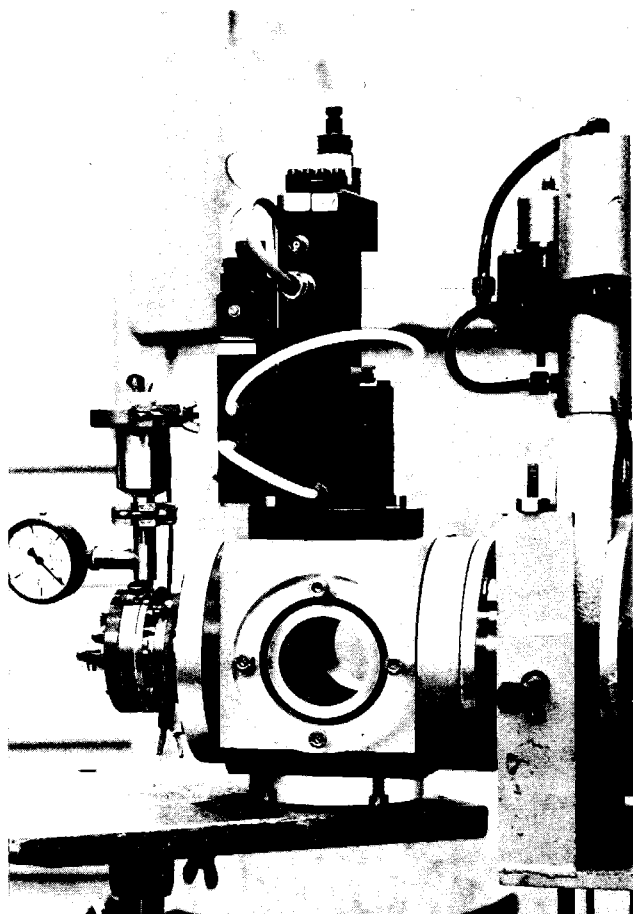


Fig. 2. Fluorine-18 irradiation chamber flanged to the universal vacuum chamber in the external beam handling system.

Reference

- (1) R. Beckmann, J. Fitschen, U. Holm, and H. Neuert, Jahresbericht des I. Instituts für Experimentalphysik der Universität Hamburg (1972) 37-41.

7.1.8. First Results of Automatic On-Line Beam Optimization Procedures

W. Kneis

Some diagnostic programs within the CICERO control system (1) require a well adjusted external beam to perform the proper measurement. One pilot example of such a program represents the measurement of the absolute energy (ENER) of the cyclotron beam. The principle of the measurement is based on the

time difference which the beam needs to reach two separate targets (Fig. 1). An explicit description of the details was already given earlier (1).

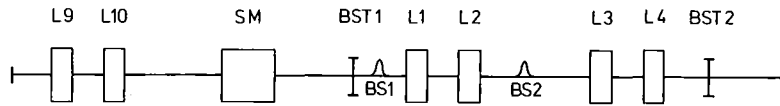


Fig. 1: Schematic view of the arrangement of switching magnet SM and quadrupole lenses L9, L10, L1, L2, L3, L4, the two beam scanners BS1, BS2 and the beam-stops BST1 and BST2 in channel 5 of the external beam handling system.

Normally if the program ENER has to be executed the operator manually has to adjust the beam in channel 5 prior to the proper measurement. As to be seen immediately a good transparency between target BST1 and target BST2 can be achieved by adjusting a flat waist at location BS2 only with the help of lens L9 and L10. The restriction to two parameters also reduces the complexity of the problem. This problem however can be solved by an iterative procedure to optimize the horizontal and vertical beam profiles and positions at the location of the beam scanner BS2.

An iterative program using least squares technique has been written to achieve automatic adjustment of the external beam for this problem. Necessary for starting the optimization program is the existence of a measurable optimizing function, CHIQU. CHIQU can be obtained as sum of the squares of the differences between nominal and actual beam profiles and beam positions. At the starting point of iteration the horizontal and vertical beam intensity distributions must not be too far from the optimum. Otherwise a computer controlled variation of the lenses would result in a discontinuous optimizing function CHIQU, because the beam transparency can vary greatly. Test results of an optimizing run can be seen in Fig. 2. As can be seen from 2a to 2e the main effect of the optimization is reached after 4 iterations. The gain

between iterations 4 and 6 is minimal. Also 10 further iterations do not minimize CHIQU any more which means that the optimum is reached. The different parameter adjustments between the 4th and 16th iteration show that there is a relatively wide "parameter-band" reaching CHIQU-values near the optimum. It may also be seen by the parameter changes (L9, L10) between the 4th and 6th iteration that the iteration procedure directly approaches the optimum. This has been solved by using method of conjugated directions of Powell (2).

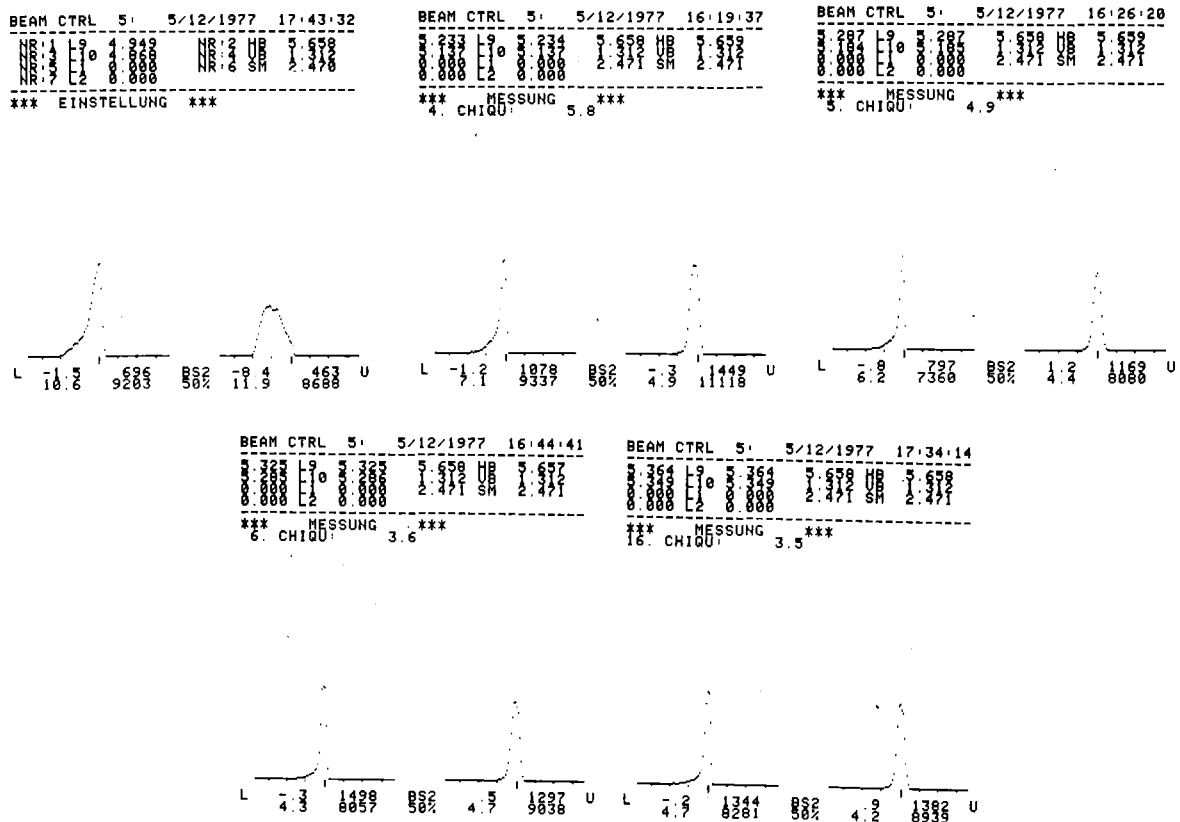


Fig. 2: On-line optimization of the 52 MeV external deuteron beam. Beam quality is measured by the beam scanner BS2, parameter variation is performed with the quadrupoles L9 and L10. In a) to e) the beam profiles are represented by the following scheme:

HORIZONTAL			VERTICAL	
POSITION	INTENSITY	BS2	POSITION	INTENSITY
FWHM	INTEGRAL	50%	FWHM	INTEGRAL

- a) showing the beam profiles at start of optimization
- b) state after 4 iterations
- c) state after 5 iterations
- d) state after 6 iterations
- e) state after 16 iterations

References

1) W. Kneis, Report KFK 2379 (1976) p. 96
 2) M.J.D. Powell, The Computer Journal, Vol. 7 (1964) p. 155 and 303

7.2. VAN DE GRAAFF ACCELERATOR

7.2.1 Operation of the 3 MV Van de Graaff Accelerator

A. Ernst, D. Roller, H. Schreiber, and J. Nadasdy

From April 1977 to March 1978 the accelerator was in operation for 5747 hours. 5058.5 hours were used by the experimenters for the different experimental programs, consisting mainly of

- 2003.5 hours neutron cross-section measurements for the fast breeder program
- 1197.0 hours for surface layer analysis techniques like Rutherford back-scattering, channelling, proton induced X-rays and specific nuclear reactions
- 1145.5 hours neutron cross-section measurements for astrophysics
- 680.5 hours experiments concerning the physics of nuclear fission
- 32.0 hours ion implantation and production of radiation damage for the fusion reactor program.

During the reported time period, the first experiment using heavy ion beams was performed at the 30 R beamline and a second experiment using heavy ions has been set up. Performance of the accelerator and of the new heavy ion analysing system (1) - intensity, stability, mass separation - have fulfilled and exceeded all our expectations.

In early summer 1977 during only a few weeks the beamline for pulsed and bunched light ion beams - used for neutron production - was replaced by a beamline system with a new switching magnet, feeding up to five different beamlines and target areas (2). Now several neutron experiments can be operative and can be prepared at the same time, thereby greatly improving accelerator utilization. One beamline is used for the proton microbeam (3), leaving four for neutron production.

Near the end of 1977, the accelerator was upgraded to a maximum terminal voltage of 3.75 MV. During all the reported period, the work was continued to get closer supervision and control of the accelerator by the associated process computer (4,5).

References

- (1) A. Ernst, KFK 2670 (1978), contribution 6.5
- (2) A. Ernst, this report (1978), contribution 7.2.3
- (3) D. Heck, this report (1978), contribution 7.2.4
- (4) A. Ernst, KFK 2670 (1978), contribution 6.6
- (5) A. Ernst, KFK 2379 (1976), contribution 6.2.2

7.2.2 Improved Synchronization of the Mobley Buncher High Frequency to the Ion Beam Pulses from the Van de Graaff Accelerator

A. Ernst

Fluctuations of the intensity of the ion beam pulses, or short periods (ranging from one pulse up to some milliseconds), during which no beam pulses are produced at all, normally are not dangerous to the quality of the experimental data acquired during a typical neutron time-of-flight experiment. Such instabilities may arise from flashovers in an aging ion source, from 800 Hz ripple due to insufficient filtering in some terminal power supply etc. However, such short term instabilities become dangerous, when, due to the lack of trigger pulses, the RF stage of the Mobley bunching system ceases oscillating. Even when the beam pulses come back, it takes some time until the buncher high frequency is back at its correct amplitude required for bunching, and during this time beam pulses with larger pulse widths can reach the target.

Therefore an electronic circuit was set up which oscillates continuously with 10 MHz and which is put into the correct phase with the beam by every single beam pulse detected. The circuit (Fig. 1) has been put together from standard NIM fast electronics modules.

Differentiated beam pulses from a capacitive beam pick-up are amplified in amplifier A1 and trigger zero crossing discriminator T1. In or-gate G1 test pulses can be inserted for adjusting the circuit without beam. Trigger T2

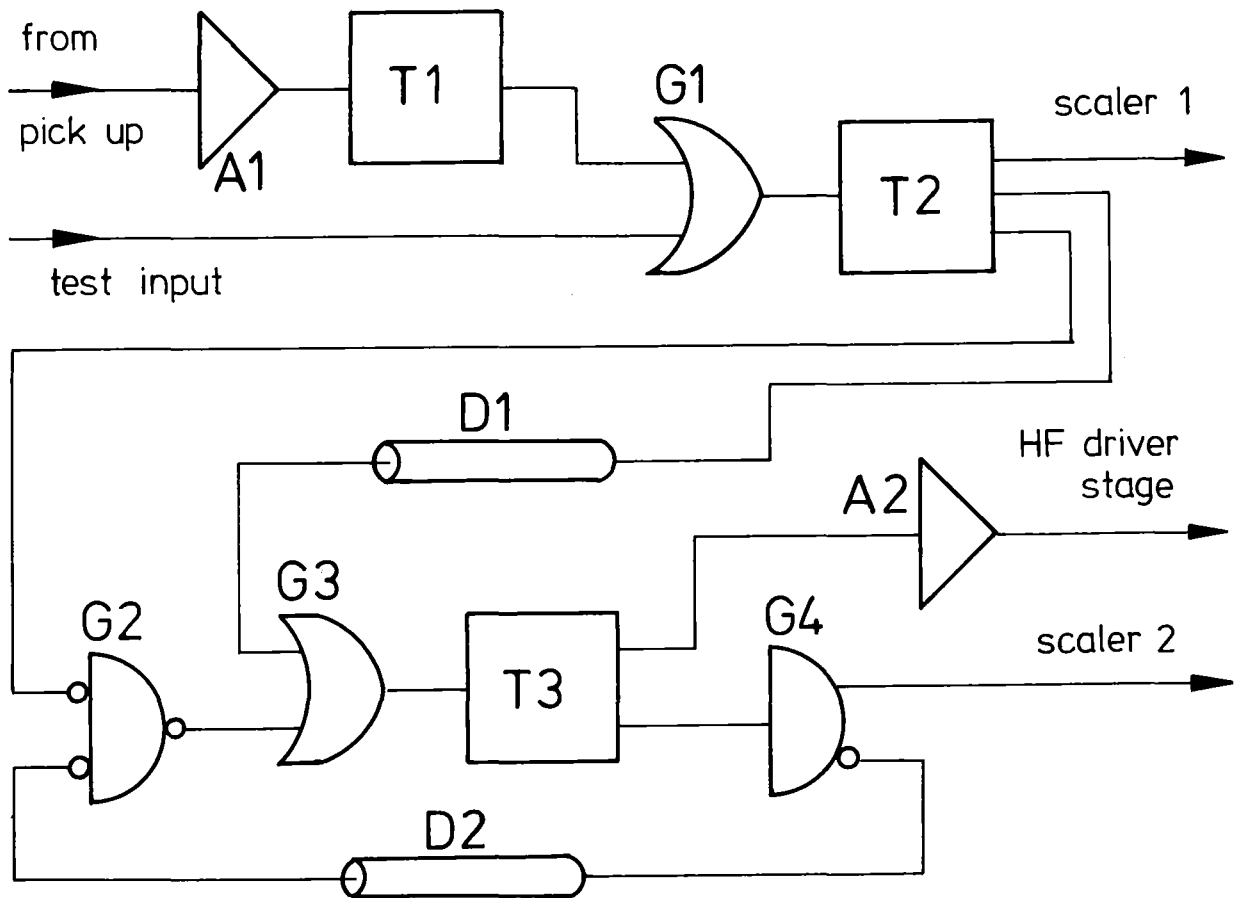


Fig. 1. Block Diagram of the circuit.

acts as shaper and its deadtime suppresses multiple triggers from a ringing signal. CAMAC scaler 1 monitors the trigger frequency of the circuit. Gates G4, G2, G3 and shaper T3 form a closed loop. Transit time around the loop is adjusted by variable delay line D2 to 100 ns. So a pulse can circle around the loop with a frequency of 10 MHz. The deadtime of T3 makes sure that not more than one pulse is circling. The 10 MHz output frequency of the circuit is monitored in CAMAC scaler 2 and - after amplification in A2 - drives the buncher RF stages. Synchronization of the output frequency to the beam is done as follows:

One output pulse from T2 inhibits the cycling pulse in gate G2 (complementary logic), and instead of the cycling pulse the clipped signal derived from the beam is inserted into the loop after delay D1 (to make sure that T3 is not busy). So a single beam pulse can bring the oscillator into the

desired phase to the beam pulses. Maximum time before the buncher runs out of phase is given by the difference between the beam frequency and the frequency of the free running oscillator loop. Fine adjustment of the oscillator frequency can be done with the trigger threshold of T3, using the trigger walk to adjust the loop transit time. Absolute adjustment of the phase is done with a CAMAC operated variable delay line inserted between this circuit and the buncher.

This circuit is in operation for over a year now and has greatly improved accelerator performance under adverse operating conditions.

7.2.3 A Beam Switching System for Pulsed and Mobley-Bunched Light Ion Beams

A. Ernst

To improve accelerator utilization by having several neutron experiments operative or in preparation at the same time, a beam switching system was designed to provide at least three target areas with pulsed and bunched light ion beams (pulse durations less than one nanosecond).

Design aims were:

- 1.) The magnet should work at relatively high magnetic field levels, in order to keep the magnet small and thus keep the flight path differences of the ions small. This is a requirement coming from the Mobley bunching system, where beam compression is achieved by different flight paths for different parts of the incoming ion pulses. Also, due to the large horizontal emittance after the bunching process, the magnet pole area and thus the magnet size would have to be increased rapidly with decreasing magnetic field for a given mass-energy-product (Fig. 1).
- 2.) The magnet should be double focussing, and the magnification for one deflection angle should be about one, thus allowing use of the beam without additional focussing. The mass-energy-product should be at least 3.3 MeV x a.m.u. for maximum deflection.
- 3.) One beamline of the switching magnet should coincide with the 30L-beamline from the heavy ion analyzing magnet (1), thus the distance between the focus of the bunching magnet and the vertex of the 35 degree deflection

angle of the switching magnet was fixed to 54.5 cm.

It was found that all these conditions could be met. The final shape of the pole piece was calculated with the inclusion of second order corrections. Due to the high field required (18 kG), a Rogowsky profile was adopted. Ion optical data together with data relevant to the bunching of the beam are given in Table 1.

For use of the straight-through port as well as for the 35-degree-ports, where the beam leaves the magnet also diverging, a focussing system using quadrupole magnets had to be designed. A three-element-configuration (Fig. 2) was chosen with the first element focussing the beam horizontally, so the remaining two quadrupoles need only moderate apertures. Finally, for experiments requiring much space and little mass in the target region, also for the 70-degree-ports a quadrupole arrangement was designed to give a secondary focus about two meters away from the switching magnet. Here existing quadrupoles having only a moderate strength and a quite small aperture had to be used, so again a three-element arrangement was found as the best solution for this problem.

Table 1.

Magnet port	Mass-energy-product	compression figure of merit &	bunching possible up to ++	horizontal magnificat. §	vertical magnificat. §
+ 70°	3.6	20.7	3.6 ⁺	1.2 ^{&&} 0.85	0.5 ^{&&} 0.55
+ 35°	12 ^{§§}	proton microbeam - no bunching used			
0°	12 ^{§§}	17.3	3.0 ⁺	0.6	0.78
- 35°	12 ^{§§}	15.5	2.7 ⁺	similar to 0°	
- 70°	3.6	13.8	2.4 ⁺	1.2 ^{&&} 0.85	0.5 ^{&&} 0.55

§ with respect to the focal point of the bunching magnet

§§ limited by analyzing and by bunching magnets

+ limited by maximum buncher RF presently attainable

++ MeV H⁺, limit higher for heavier ions

& 1 MeV H⁺ pulse width accepted for bunching (ns). Less at higher energies, more for heavier ions.

&& primary focus, without quadrupole focussing.

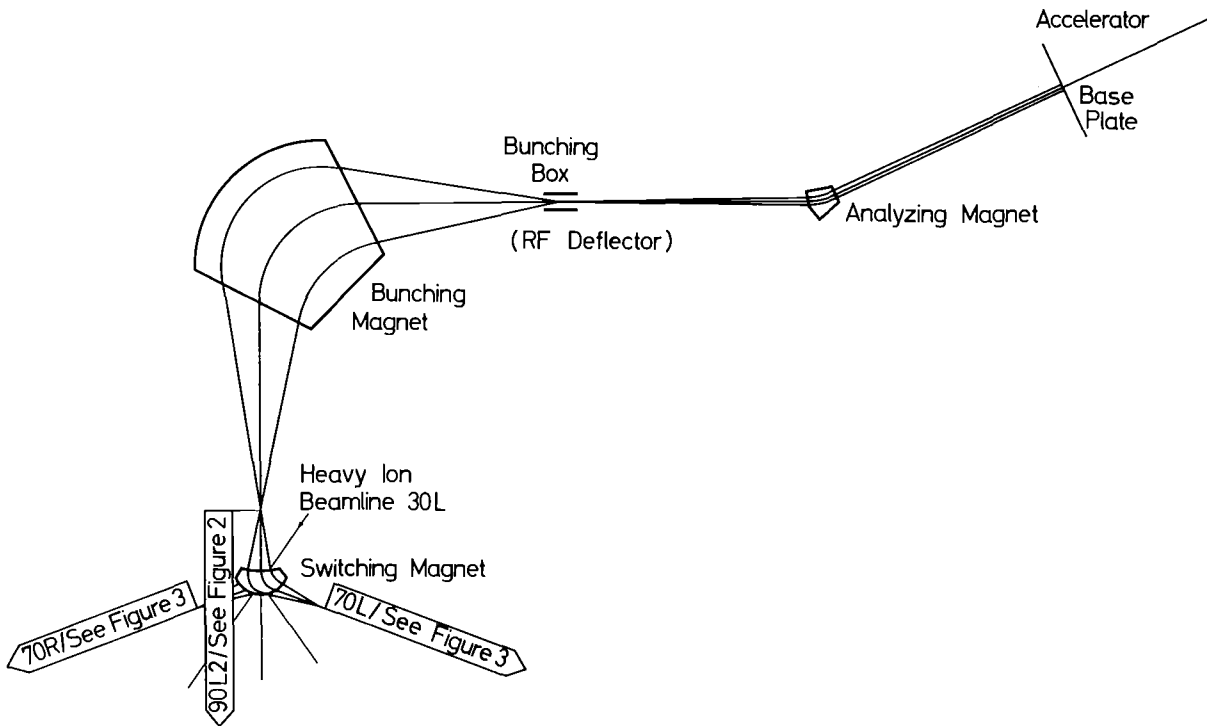


Figure 1: Switching system for Mobley bunched light ion beams

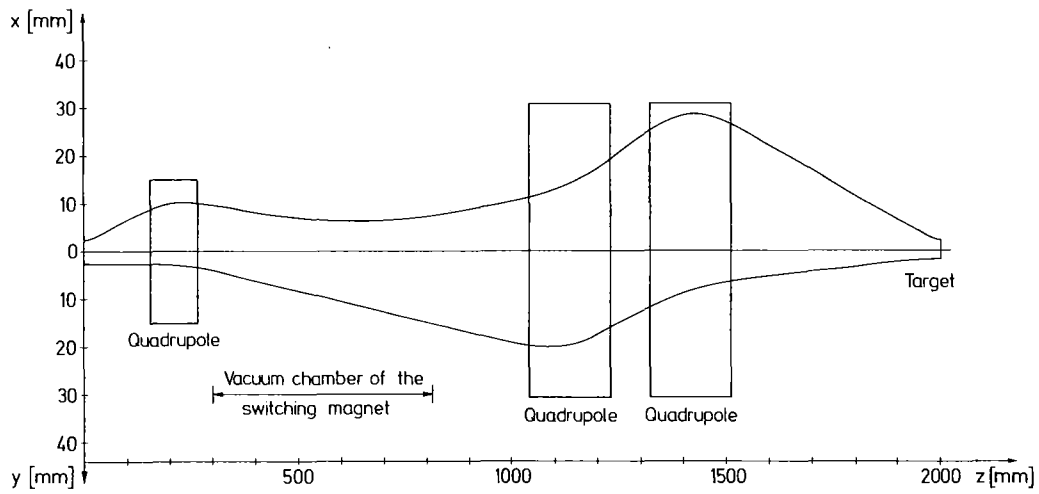


Figure 2: Beamline 90L2 (from the focal point of the bunching magnet)

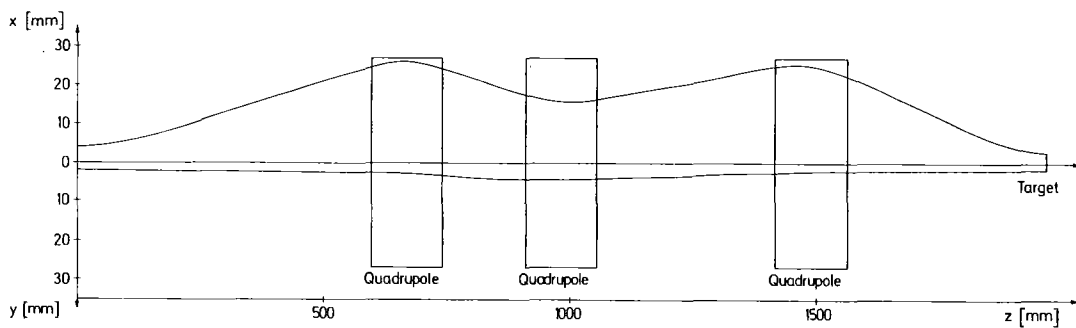


Figure 3: Beamlines 70L, 70R (from the focal point of the switching magnet)

This system has been installed in mid 1977 and the observed beam quality is as expected, especially no change of the minimum attainable pulse width was observed. The help of Dr. Heck in optimizing the quadrupole arrangements with the computer program IONBEAM (2) is gratefully acknowledged.

References

- (1) A. Ernst, KFK 2670 (1978), contribution 6.5
- (2) D. Heck, E. Kasseckert, Report KFK 2379 (1976), p. 130.

7.2.4 Realization of a Proton Microbeam with <3 Micrometer Diameter

D. Heck

During the past year the proton microbeam assembly (1) came into operation for the first time. With the experiences of the first trials the major faults were eliminated. Large efforts had to be made to get the beam diameter down to the desired value of 3 μm .

After many time-consuming tests to isolate the reason for these difficulties, it was found that magnetic ac-stray fields caused a 50 Hz modulation of the beam with an amplitude of $\sim 10 \mu\text{m}$ (at a proton energy of 2 MeV). Additional mechanical vibrations of the steel table, on which the experimental setup is mounted, caused vibrations of the beam defining components. 7 tons of sand were filled into the base of the steel table to damp the vibration amplitudes. The main resonance frequency at about 10 Hz was shifted down to 7 Hz, which is much lower than the vibration frequencies of the components.

To determine the beam diameter, two different methods were applied:

- a) The width of radiation damages, caused by the proton beam within 5 μm thick plastic scintillator foils were measured. Fig. 1 shows a microscopic view of such radiation damages. The smallest beam diameter found by this method amounts to 2.5 μm .

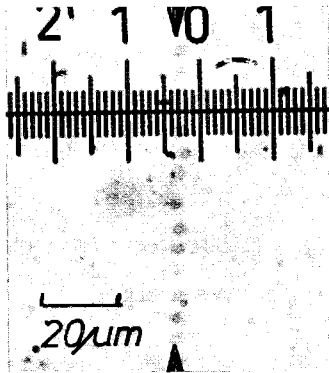


Fig. 1. Radiation damage of the proton microbeam generated within a 5 μm thick plastic scintillator foil.

- b) The proton beam was swept magnetically across the edge of a flat pressed gold wire (ϕ 25 μm) mounted onto plastic scintillator, and the gold L X-ray count rate was recorded as a function of the sweep voltage similar to (2). A minimal beam diameter of 4.5 μm was deduced, which is in fairly good agreement with method a) taking into account the hysteresis of the magnetic deflection system and the diffuseness of the edge of the gold bar.

The maximum beam current density is determined to 60 $\text{pA}/\mu\text{m}^2$, which is by far the highest value ever reported for a microbeam system. By the scattering at the collimating apertures and at the residual gas molecules some protons hit the target outside the beam spot forming a "halo". The intensity of the halo is of great importance for trace element analyses and should be as low as possible to ensure that the detected trace elements X-rays really come from the point of interest, on which the proton beam is focussed, and not from the halo region. From a measurement similar to (2) the intensity ratio of the halo to the focussed beam is deduced to be less than 1:2500.

References

- (1) D. Heck, Report KFK 2504 (1977) p. 107.
(2) R. Nobile et al., Nucl. Instr. Meth. 142 (1977) 49.

7.3 NEUTRON PRODUCTION

7.3.1 Possible Improvements in the Production of keV-Neutrons

F. Käppeler and G. Schatz

At present there are two types of accelerators in use for production of neutrons with energies between a few keV and 1 MeV. Electron linear accelerators (LINACs) exhibit very high neutron source strengths but generate broad continuous neutron energy spectra and do not allow shorter flight paths than ~ 10 m. Electrostatic accelerators can produce well defined neutron spectra and offer the possibility to measure at very short flight paths where high neutron fluxes are available so that experiments with good sensitivity can be performed. A serious drawback of electrostatic accelerators is the restricted integral source strength which is approximately three orders of magnitude less than that of the LINACs. Therefore electrostatic accelerators are not qualified for high resolution time-of-flight work although their pulse width can be significantly shorter as compared to LINACs.

For an improvement in the production of keV neutrons it would be promising if the advantageous features of electrostatic accelerators could be combined with significantly higher source strengths. With modern techniques an improvement by one or two orders of magnitude seems possible with respect to proton peak currents of $\sim 5 - 10$ mA which at present are standard for many electrostatic accelerators.

Such an improved accelerator MINI would compare very favourably with modern LINACs even for high resolution time-of-flight measurements. This is shown by a comparison with the Oak Ridge Linac ORELA and with the LAMPF II neutron facility at Los Alamos. For a given neutron energy resolution of 10^{-2} the neutron fluxes available at the respective minimum flight path are plotted in Fig. 1. The values for ORELA and LAMPF II were taken from the literature (1,2) whereas for MINI a pulsed proton beam of 1 MHz repetition rate, 500 psec pulse length and 1 mA average current was assumed to fall on a thick metallic Lithium target.

Due to the higher repetition rate of 1 MHz the background situation will be worse for MINI but this is compensated for at least below 100 keV

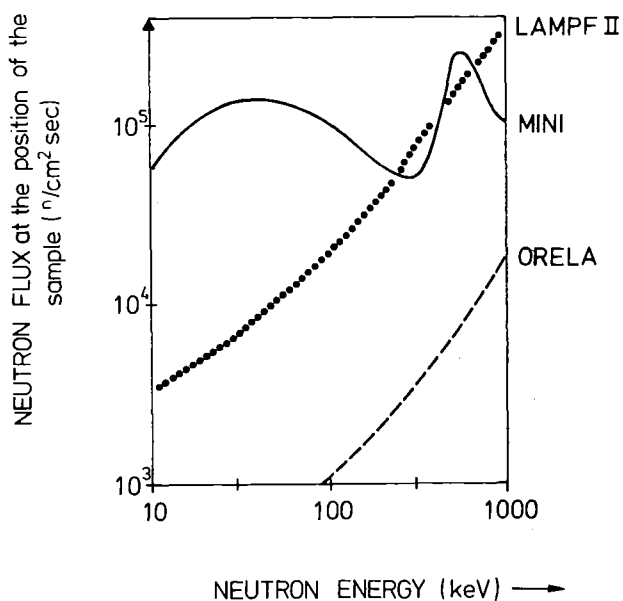


Fig. 1. Comparison of neutron fluxes for ORELA, LAMPF II and MINI. The curves were calculated for an energy resolution of 10^{-2} .

by the high flux.

While Fig. 1 demonstrates the suitability of MINI for high resolution measurements being comparable to large moderated neutron sources, this accelerator would be superior to existing machines with respect to measurements with moderate energy resolution. The possibility to use short flight paths and intense neutron fluxes would open a new field of very sensitive experiments.

At present several possibilities for the design of a high current fast pulsed proton accelerator are in discussion. In any case the costs are considerably less than are required for intense moderated neutron sources.

References

- (1) E.R. Rae and W.M. Good in "Experimental Neutron Resonance Spectroscopy", J.E. Harvey ed., Academic Press, New York (1970), p. 62.
- (2) J.E. Lynn, Proc. International Conference on the Interactions of Neutrons with Nuclei, Lowell (1976), Vol. II, p. 827.

7.3.2 Development of the KARIN High Intensity Neutron Generator

K.A. Schmidt and H. Dohrmann

Since 1970, a high intensity generator of 14 MeV neutrons has been developed (1). It is of the sealed tube type and operates at 200 kV and an ion current of 150 mA. The neutron source strength is $5 \times 10^{12} \text{ sec}^{-1}$. The main fields of application of the KARIN generator will be cancer therapy, activation analysis, and materials research.

Neutron generator systems making use of the KARIN tube are manufactured by E. Haefely & Cie., Basel, Switzerland, under a licensing agreement. One system for cancer therapy was installed at the German Cancer Research Centre, Heidelberg, and is in routine use since summer 1977. A second similar system is being installed in a hospital at Zürich, Switzerland.

The main activity of the last year was to transfer the know-how for producing the generator tubes to the licensee. A small prototype series of 10 tubes was fabricated by a joint Haefely-KfK team in the institute. In the production of these tubes a number of technical improvements were incorporated.

A KARIN system for use in activation analysis, biomedical and materials research is being built up at the Karlsruhe Research Centre. The shielded building is ready, but delivery of the high voltage power supply is considerably delayed.

References

- (1) K.A. Schmidt and H. Dohrmann, Atomkernenergie 27 (1976) 159.
K.A. Schmidt and H. Dohrmann, KFK 2379 (1976) p. 89-92.

7.4 COMPUTERS

7.4.1 Further Developments on Data Acquisition and On-Line Analysis for the Experiment Computer Nova-2 at the Cyclotron

J. Bialy, B. Kögel, W. Kneis, and W. Segnitz

BASIC Programs

The data acquisition and analysis program (1) was expanded and reorganized. Some off-line routines were added and the file handling for saving experiment data records can be selected on tape or disk. In case the disk is used as storage medium the user can request the free disc space at run time. Furthermore the program contains routines for live display of an two-dimensional spectrum (Fig. 1). The TV display can be used for map display with 4 different base lines (Fig. 2).

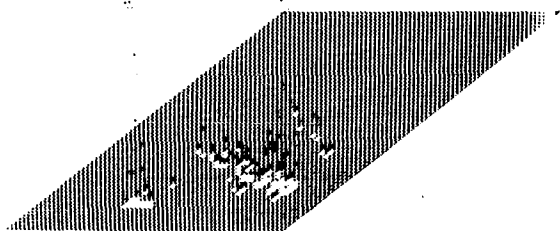


Fig. 1. Live-display of the two-dimensional spectra.

HOEHENSCHNITTE: 1 2 4 16
ROUTER-NR.: 1



Fig. 2. Map display with the 4 base lines.

The incorporation of the new routines into the existing program has been possible only by dividing it into several overlays.

FORTRAN programs

For the time-of-flight experiments an analysis program has been written in FORTRAN IV multitasking. Via the Silent-Keyboard the experimentalist communicates with the program to perform the 18 parts of the program.

Fortran data acquisition program (1)

When using higher beam currents for the experiments the BASIC program is too slow to perform data acquisition for higher data rates. Therefore an alternative program in FORTRAN IV multitasking has been written. The keyboard communication will be released using instead a 24-bit sensor board and a light pen.

Reference

(1) W. Karbstein, W. Kneis, and W. Segnitz, Report KFK 2504 (1977) p. 115

7.4.2 Standards and Proposals of Industrial Real Time FORTRAN*

G. Heller⁺, W. Kneis, U. Rembold⁺⁺, and G. Wiesner⁺⁺⁺

The paper deals with real-time languages which remain strictly within the syntactical frame of FORTRAN, i.e. all operations necessary for industrial real-time applications in addition to FORTRAN are realized by FORTRAN procedures. Firstly the main features of the American papers ISA S. 61. 1-3, standards and proposals for industrial real-time FORTRAN from 1972 up to now are described. Secondly comments are given on the German paper, VDI/VDE Guidelines 3556, Prozess-FORTRAN 75 which has been developed in 1974 and 1975. Thirdly the recent European paper, Industrial Real-Time FORTRAN, PE TC1-1/78, of the Technical Committee 1 (FORTRAN) of Purdue Europe is explained. (Purdue Europe is the European branch of the International Purdue Workshop on Industrial Computer Systems).

* Proc. of the IFAC/IFIP Workshop on Real-Time Programming, Marienhamn/Åland, Finland, June 19-21, 1978

+ Fachhochschule Mannheim, Germany

++ Universität Karlsruhe, Germany

+++ Hahn-Meitner-Institut für Kernforschung, Berlin, Germany

7.4.3 Hardware Improvements for the NOVA-2 Computer at the Cyclotron

J. Bialy and B. Kögel

Our effort in the last year was to improve the given hardware concept and to make more comfortable the use of the NOVA-2 computer for the experimentalists (1).

that images the light spot into the photosensor. Furthermore it has a finder beam. This is a circle of light projected through the lens system. This finder beam image on the screen exactly defines the acceptance area. A further feature is an actuator which activates the light pen.

This light pen in connection with a modification of the TV board gives a very good sensitivity and resolution. Two neighbouring points on the screen which can be separated optically are also distinguished by the light pen.

3. Memory switch

The memory switch was changed in such a way that the experimental data in the "external" memory of the computer can be written directly on magnetic tape. This leads to a "high speed" list mode because a larger data buffer can be transferred on magnetic tape at once.

The speed of the list mode could not be tested till now because the modification of some software calls is not yet finished.

References

- (1) G. Ehret, H. Hanak, Report KFK 2183 (1975) p. 99.
W. Karbstein, B. Kögel, Report KFK 2461, (1977) p. 26.

7.4.4 Connection of the Large Neutron Spectrometer to the NOVA-2 Computer at the Cyclotron

J. Bialy and B. Kögel

In the last year the large neutron spectrometer was connected to the NOVA-2 computer for nuclear physics experiments (1). The experimentalists specified the following requirements on the hardware and software configuration for transmission experiments.

Hardware

- a) A large memory for data acquisition
- b) Measurement of several one parametric spectra (one time-of-flight spectrum, at least two monitoring spectra)
- c) A high speed of data acquisition.

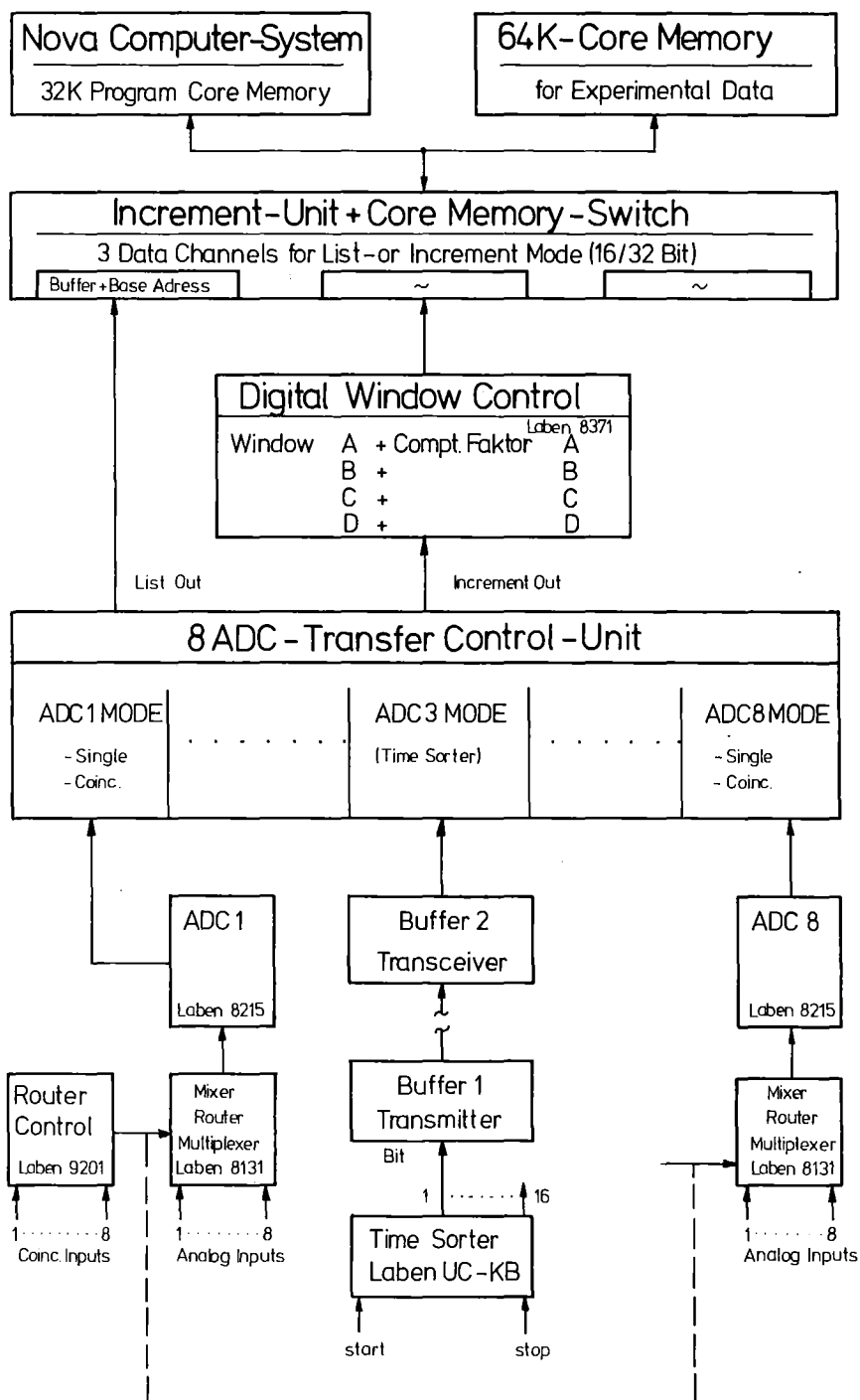


Fig. 1. The hardware configuration of the data channel

Software

- a) Automatic control sequence including the change of the target
- b) Monitoring the beam quality of the cyclotron (phase width and phase position)
- c) Representation of all measured data on the data display.

The hardware configuration of the data channel is shown in Fig. 1. The neutron time-of-flight spectrum is measured with the Time Sorter type Laben 4C-KB (2). The fixed time resolution of this device is 250 psec independent of the measured time interval. The practicable length of spectrum goes up to 19 bits.

The Time Sorter is connected to the ADC-Interface of the NOVA-2 computer via an eightfold buffer. This configuration allows to measure one time-of-flight spectrum and up to 16 monitor spectra. The multiparametric ADC interface type Laben is connected to the computer in the DMI mode. So we have accumulated data with a rate of more than 60 kHz in the incremental mode.

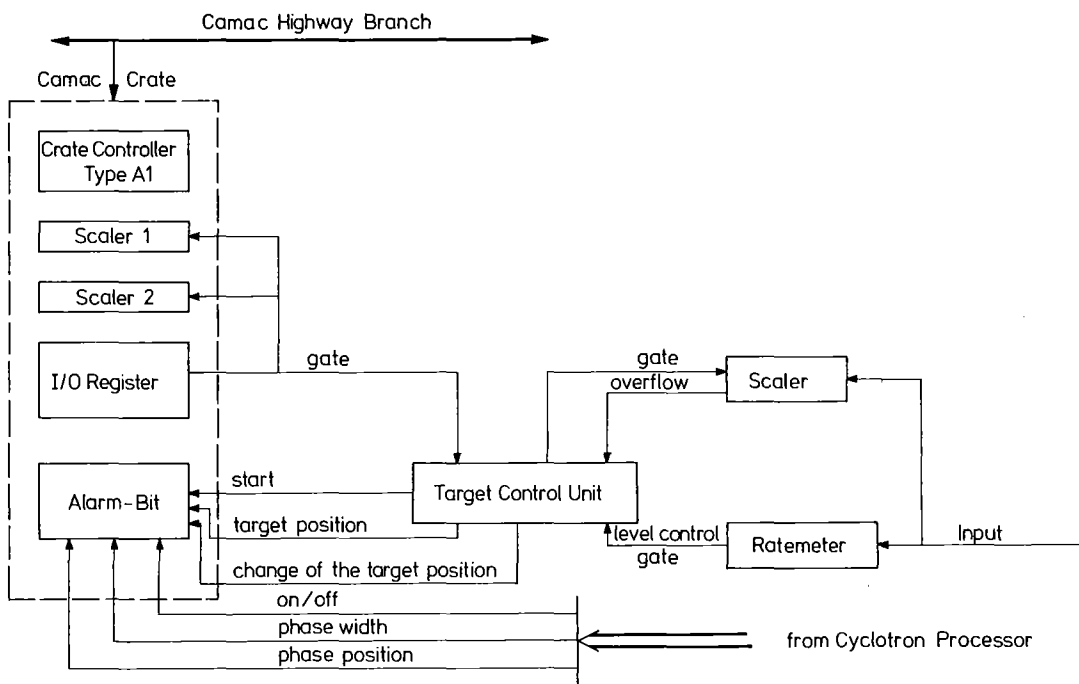


Fig. 2. The connection of the interrupt and control signals to the CAMAC branch.

The logic connection of the interrupt and control signals to the CAMAC branch of the NOVA-2 computer is shown in Fig. 2. A gate signal given by a program command enables the Target Control Unit to work.

The interrupt signals and the bit configurations given by the Target Control Unit are initiating corresponding program steps (3). If the phase width and the phase position of the cyclotron beam are changing, the cyclotron processor gives interrupt signals which activate program steps.

References

- (1) W. Karbstein and B. Kögel, Report KFK 2461 (1977) 26.
- (2) Laben Division Montedel: Manual Time Sorter Mod. UC-KB.
- (3) J. Bialy, B. Kögel, W. Kneis, W. Segnitz, this Report contribution 7.4.1

7.4.5 Status of a BASIC Compiler for a NOVA-2 Computer

G. Ehret and W. Kneis

In our institute BASIC is well-known and often used for data acquisition and process control. Since users like interactive programming they estimate the way to write and test BASIC programs. This is especially true during the development phase. But once program development stagnates and usage of programs increases the users want faster program execution. Without rewriting the whole program this can only be achieved by a BASIC compiler. Therefore the 'Institut für Angewandte Informatik und formale Beschreibungsverfahren' was initiated by us to implement a BASIC compiler for NOVA-2 Computers (1).

For simplification the following restrictions are taken into account.

- Use of "sub-BASIC"-software, like operating system, macro-assembler, relocatable loader.
- Use of existing interpreter subroutines for arithmetics and functions, e.g. the hardware multiply/divide and floating point package.
- Since translation times are of minor importance the compiler itself is written in BASIC. This ensures the readability of the compiler.
- Only programs completely checked by the interpreter are supposed to be translated by the compiler. Therefore no syntax checking is necessary.

Up to now the BASIC compiler is able to translate the so-called "Minimal-BASIC" which is a subset of Data General's Extended BASIC (2). The statements not yet implemented are: CALL/CHAIN/ENTER/MAT/NEW/PRINT USING/READ, WRITE FILE/SAVE/LOAD. This will be done in a second step.

Compilation and execution of a tested BASIC program can be performed according to the scheme shown in Fig. 1. The BASIC program "BEISPIEL" has been produced previously by the BASIC "LIST"-command.

References

- (1) J. Dornheim, BACOMP - Ein Compiler für ausgetestete BASIC Programme, Diplom-Arbeit, Universität Karlsruhe (1978).
- (2) Data General, Extended BASIC Reference Manual, No. 093-000 065-05.

7.4.6 Concept of an Integrated Mega-Channel-Kicksorter

G. Ehret, H. Hanak, and H. Sobiesiak

On-line totalization of spectra is superior to recording each event first on magnetic tape during the experiment and totalizing them off-line, provided the unstabilities of the experimental source and/or analysing electronics are small compared to the experimental resolution. Small and medium scale array experiments (typically less than 64 - 128 K channels) may also eliminate time dependencies by dumping periodically the add-one storage on magnetic tape or disk units. Using the same technique on larger arrays is prohibitive because the relation between the time for data collection and data dumping is too bad on those devices operating at Karlsruhe as mega channel kicksorters: moving head discs (1)(2) and fixed head discs (3) with special controllers.

In order to replace such rotating storage both using also a computer for presorting the data to be totalized, a review of the market has been done, which resulted in a new concept of an Integrated Mega-Channel-Kicksorter (IMCK):

1. Mega byte storage units suitable for a mega-channel-kicksorter are

commercially available in core and semiconductor technology (access time $> 1 \mu\text{s}$, $< 0.5 \mu\text{s}$ respectively).

2. Access time times price is nearly a constant
3. Because the lower access time is tolerable for a kicksorter, core storage may be chosen. Core is also preferred because its contents is nonviolable in the case of a power shut-down.
4. Manufacturers of core storage also offer an interface to the computer. These interfaces have a form which is supported by the RDOS (Real-Time-Disk. Operating System): They simulate the storage as a fixed-head-disk with zero rotation time and highest data transfer rate.

Two interfaces may be connected to one storage unit. With this computer interface, data handling of the totalized spectra is done using standard commands of the RDOS. Especially one can simply type on the console

```
CCONT name 2000
```

in order to request a storage block for 512 K channels. In this command CCONT (Create a CONTiguous file) is the command key word name is the arbitrary file name in the storage unit and 2000 is the number of channels requested in units of disk blocks (≈ 256 words).

If the second port of the storage unit (item 4) is not used by a second real computer but by a small logic which does the "add-one" job including boundary surveillance we have Integrated Mega Channel Kicksorter.

Communication between the main and the auxiliary computer may be done via digital interfaces or via disc files. Typical data to be passed are boundaries of the contiguous ("add one") disc file and the mode of operations. The IMCK is a very flexible device. Because it is supported by the Real Time Disc Operating System RDOS all hardware test programs are operational. Therefore special testing hardware for the storage unit is not necessary. Additionally, if the RDOS and the programs used are located in IMCK rather than on a moving head disc gain factors up to 10 in program run time have been measured for the Fortran Analyser Software System (4) and for most RDOS utility programs like Fortran compiler, assembler, and loader.

References

- (1) S. Cierjacks, KFK Report 982 (1969)
- (2) R. Töpke, KFK Report 2122 (1974)
- (3) G. Ehret, KFK Report 2538, (1977) p. 138.
- (4) H. Sobiesiak, this report, contribution 7.4.9

7.4.7 A Computerized System for On-Line Data Acquisition
and Evaluation

P. Matussek

A versatile computerized analysis system for on-line data acquisition and evaluation has been assembled and programmed. The system consists of a NOVA-2 computer with 32 K of core memory, a CAMAC crate with controller, a teletype, and a magnetic tape drive. The numerous commercially available CAMAC modules provide a great flexibility of the system for various applications. Experimental control functions like stepping motor drives, relay switching or line voltage supervision are easily performed with the help of these modules. In connection with an analog-to-digital converter the system can also be used as a multichannel analyzer.

BASIC has been chosen as the programming language because it allows the user to change easily program statements or data even at runtime. This will be helpful for the development and testing of new programs. Since the BASIC interpreter is inherently slow, the fast data transfer required for spectrum accumulation or live display of data cannot be performed under BASIC. For this reason an interrupt module and a number of BASIC calls have been written in ASSEMBLER language, which allow fast data transfer between the CAMAC controller and the computer. In particular, the interrupt module can be activated by special BASIC subroutine calls for each ADC separately. Once initiated, the data transfer will proceed under interrupt control, independently from the BASIC program. Parameters and flags can also be transferred to the interrupt handler, and status information can be transmitted to BASIC via BASIC calls.

The 32 K of core memory are subdivided into 3 regions: 14 K are dedicated to the SOS operating system, BASIC interpreter, BASIC calls, interrupt module, and to the status arrays, while 12 K are available for spectra accumulation and 6 K are left for user programs.

In the present hardware configuration up to 7 ADCs can be connected to the system. The 7 ADCs have to share the 6 K channels available in the core memory. The word length of each channel is 32 bits or 4 billion counts/channel. The number of ADCs may be increased within the limits of available CAMAC-crate positions and core memory space. Each ADC may be connected to a CAMAC timer to allow live-time or real-time measurements.

The magtape will be used both for data recording and as a program overlay buffer for large user programs which exceed the 6 K program memory. The system is now continuously in use since the end of 1977. It has been mainly used for the development of data evaluation routines for gamma-spectrometric ²³⁵U enrichment measurements and heavy element concentration measurements using the K-edge gamma absorptiometry technique (see contribution 6.8).

7.4.8 Final Status of "Analyser"

A.A. Naqvi and H. Sobiesiak

The primary organization of "Analyser", the multiparameter data acquisition program for NOVA-2 computers, has been described earlier (1). This report provides the final status of "Analyser" and its complementary programs.

"Analyser" was designed to acquire 4-parameter data simultaneously in "list" as well as in "increment" mode. In "list" mode the respective addresses of the four words can vary from 1024 to 8192 channels. In the increment mode two spectra of 8192 channels and two others of 1024 channels can be accumulated.

"Analyser" offers the following features for on-line data control:

1. Data Input/Output-Control

- a) Acquire (ON/OFF)
- b) Data Transfer (4 modes. XN DISK, DISK XN, XN TAP, TAPXN for transfer between the external memory and magnetic disk as well as magnetic tape)
- c) Acquisition Mode Selection (List, Increment).

2. Data Display

- a) Group Change
- b) Counts full scale variation
- c) Two markers
- d) Spectrum expand
- e) Display from buffer region
- f) Isomeric display of two-dimensional spectra.

3. Data Handling

- a) Spectrum erase
- b) Spectrum integration
- c) Spectrum print-out
- d) Spectrum storage in selectable groups of the external memory.

The experimental requirements demand also various additional on-line procedures, but the limited computer memory has forced us to write the remaining part of "Analyser" essentially as an off-line program, containing two parts:

- 1. Enalyser
- 2. Calplot

The main features of "Enalyser" are

a) List-acquire

Analogous to "Analyser", this subroutine generates off-line the same control spectra from the list-data stored on magnetic tape or disk.

b) Spect. Comp.

This subroutine compresses data blocks of variable length, which are written on magnetic tape into disk files of a fixed block length of 256 words.

c) Spect. Add

With this subroutine two spectra can be added channel by channel.

d) File Display

By this subroutine, the content of a file is displayed on the TV screen .

e) File Transfer

With this subroutine disk files containing list data are appended to magnetic tape files.

The second complimentary program "Calplot" offers different modes of spectrum plotting, like for instance, linear or isometric plots. In Fig. 1 an example for an isometric plot is given.

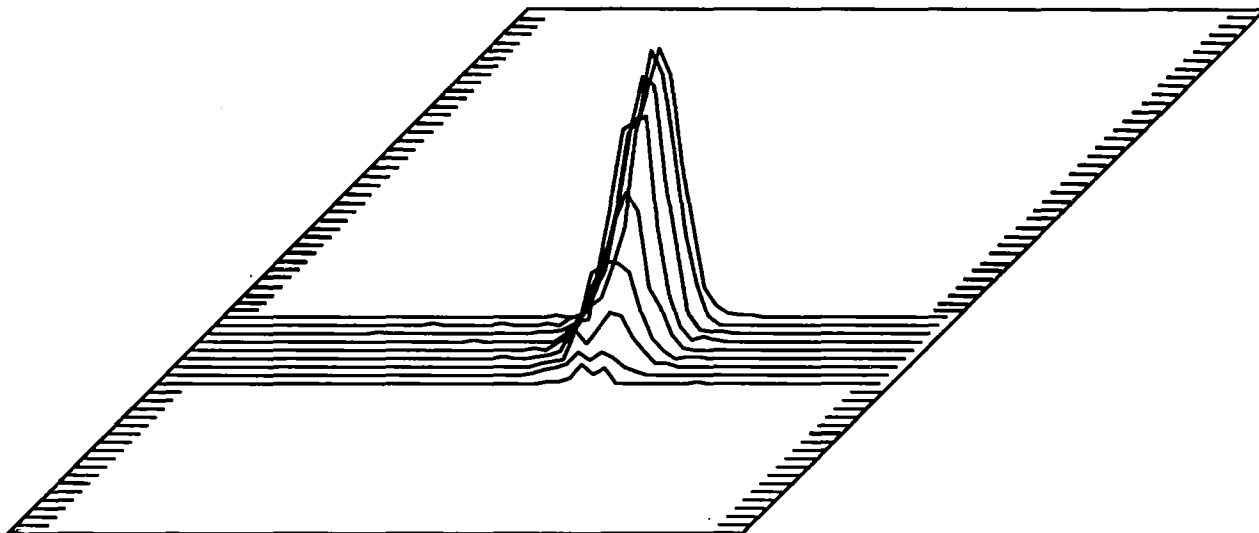


Fig. 1: Fission fragment yields as a function of light fragment kinetic energy and heavy fragment velocity, an example for the capability of the plot routine "Calplot"

Reference

(1) A.A. Naqvi, H. Sobiesiak, Report KFK 2504 (1977) p. 122

7.4.9 FASS (FORTRAN ANALYSER SOFTWARE SYSTEM) - an Approach to a Universal Multichannel Analyser Program

H. Sobiesiak

Based on the experiences with multichannel analyser programs written in Extended BASIC (1) it was the aim of this work to create a software system for MCA usage that provides both of the following two features:

1. fast reaction to user decisions as well as fast data manipulation
2. easy to expand and to tailor according to specific user applications.

For these two reasons FORTRAN IV was chosen as the basic programming language for such a system. Although a poor assembler based system would still be faster in response and execution, matching point 2 seemed to be possible only by the use of a programming language familiar to most of the users. The FASS program, which is so far only partially developed, consists of three FORTRAN TASKS: one to service device interrupts, one (not yet implemented) to do high priority calculations (like on-line evaluation of list mode data) or background supervisor functions (e.g. monitoring peak locations and peak widths), and a last one to do display-functions, data evaluation, input/output operation etc. This third task contains an expandable command interpreter which is structured similarly to the BASIC language. Current commands range from simple desk calculator mode e.g.

```
PRINT 4 * 4 ↓
```

16

to file arithmetic commands like

```
FILE DATA1 = (DATA2 * 2 + DATA3 * 100)/10 ↓
```

where DATA 1,2,3 are the names of Diskfiles or of parts of the kicksorter memory-region.

and evaluation commands like

```
PEAKLAGE DATA1, 10,20,100,110
```

which will determine the location of a peak between channels 20 and 100 of all data groups in the file DATA1.

All commands can be linked together to form a "command program" if it is necessary to perform a set of operations for more than one time. For this purpose there are 26 numeric "variables" and 26 text "variables" available to the user. Thus the second example above may be done in the following way, too:

```
1 LET A$ = DATA1 ↓
```

```
2 LET B$ = DATA2 ↓
```

```
3 LET C$ = DATA3 ↓
```

```
4 FILE A$ = (B$ x 2 + C$ x 100)/10 ↓
```

```
RUN ↓
```

Such "command programs" can be saved on disk by the command

SAVE Name

and can be restored with the commands

LOAD Name

or RUN Name

The routines that execute these commands are all written in FOTRAN IV. Thus the user can easily add his own commands to the FASS system.

As the system is permanently doing display operations the user has to request attention by pressing the "ESC" key on the keyboard before he can enter any of the commands mentioned above. Besides this there are two other ways to influence the system performance.

1. Display related functions like changing counts-full-scale or marker-positions are done by the use of a lightpen.
2. Functions related to the MCA memory are initiated via a special interrupt board (acquisition on/off, Erase)

Furthermore the selection of the actual data set that is to be displayed is done via this interrupt board.

The MCA memory region (currently up to 60 K - 16 bit words) can be divided into 4 parts referenced by the names \$EX1, \$EX2, \$EX3, \$EX4 which are treated like diskfiles in all filehandling commands. Files \$EX1-3 correspond to the 3 independent DMA-channels of the increment-one interface, while \$EX4 is used for software evaluations. Generally FASS datafiles are organized in two subunits: a file is partitioned into variable length SPECTRA which themselves can be divided into equalsized GROUPS. Three different data formats are available (16, 32 bit integer, 32 bit real). Currently the maximum group size is 4 K channels (16 bit) or 2 K (32 bit) whereas the maximum size for a SPECTRUM is 60 K channels for all data types.

For each SPECTRUM there is a block of 256 (16 bit) words available for storing additional information like energy calibration, marker position, text etc. The current revision (0.0) of FASS needs about 21.5 K of computer memory and uses an overlay file of about 100 disk blocks (à 256 words).

Reference

- (1) K. Wisshak, H. Sobiesiak, KFK 2379 (1976) p. 124.

7.4.10 A Load-On-Call Overlap-Manager for DGC Fortran IV

H. Sobiesiak

DGC's Real Time Disk Operating System (RDOS) allows the user to divide large programs into memory and disk-resident parts. The disk-resident parts of a program (overlays) have to be loaded into reserved memory areas before execution.

Although DGC FORTRAN IV provides a full interface to this technique use of these calls will result in clumsy program codes. For example the call to a subroutine SUB1 in an overlap OSUB1 in a multitasking environment has to be done with the following code:

```
CALL FOVLD (IFN,OSUB1,0,IER)
CALL SUB1 (...)
CALL FOVRL (OSUB1,IER)
```

An alternative way is provided by DGC only for the FORTRAN 5 environment (1). There overlay names, callable subroutine mnemonics and subroutine entries are linked via a special table specified at load time such that the F5 linkage routines do the overlay load and release functions by themselves.

An extended version of such a load-on-call overlay manager has been implemented for FIV. The link table and the manager routines are built by the use of the Macro Assembler with four different Macro calls:

1. O.LOCA A,B specifies the environment A = 0 is for single-task systems, A = 1 for multitask. Parameter B is valid only for multitask-systems and specifies the number of overlay areas.
2. N.LOCO called name, subroutine entry, overlap name creates an entry in the link table. For the example mentioned above, program code would be:

Main Progr.	Table	called subroutine
.	N.LOCA SUB1, XSUB1,OSUB1	OVERLAY OSUB1
.		SUBROUTINE XSUB1
.		

CALL SUB1(...)

Thus the names of the entries in the subroutines cannot be the same as the name in the call.

3. U.LOCO called name, subroutine entry, overlay name creates an entry in the link table for overlays in a special overlay area. Out of these there cannot be another overlay load request.
4. Z.LOCO entry, overlay name creates an entry for page zero calls

Both in single and multitasking environments it is possible to call routines that request a load into the same overlay area the caller currently occupies. The advantage of such a load on call-overlay-manager is obvious for programs like FASS (see contribution 7.4.9), where the total size of overlay modules is about three times the size of the core-resident part of the program.

Reference

- (1) Data General: FORTRAN 5 User's Manual 093-000085-03
Release Letter 5.21 078-000004-00.

7.4.11 How to Avoid Complicated IF Clause Structure in FORTRAN Real-Time Programming*

H. Sobiesiak and W. Kneis

The paper deals with an extension to an existing FORTRAN implementation to incorporate the following features:
The first set of calls enables the user to alter the program flow in one activity from outside. Up to now this feature was used in the following two cases. Normally in multitasking the whole stack area is divided into equal sized portions of task stacks. Otherwise the user has to specify the task stack area for each of his user tasks. Therefore it is necessary to keep the number of tasks as small as possible. To overcome this difficulty an activity is created and put in the running state doing one of a set of computations of some lower priority. Then the computations actually performed can be influenced from outside without programming in complicated conditional branching. The proper releasing of resources in aborting tasks is a severe problem. Normally only the target task has access to information concerning specific

actions that have to be performed before releasing the resources. The possibility is provided to direct the task that is to be aborted to a computation which will shut down the resources in a controlled way.

The second set of calls is an approach to implement the concept of the conditional critical regions and is currently used to assure that only one activity has access to user devices such as CAMAC, Display etc. at the same time.

This could be achieved without modifying the general scheme of the existing task scheduler.

* Proc. of the IFAC/IFIP Workshop on Real-Time Programming,
Mariehamn/Åland, Finland, June 19-21, 1978.

7.4.12 Data Analysis on the Experiment Computer NOVA-2 at the Cyclotron

S. Zagromski, J. Buschmann, and H.J. Gils

In addition to the pure on-line use of the experiment computer NOVA-2 at the cyclotron a preselection and sorting of data is very effectively performed at the same computer in interactive off-line mode. For this purpose several FORTRAN-IV programs have been developed. Part of them shall be included into the final on-line version of the measuring programs for scattering experiments.

In this contribution several programs are described for handling pairs of list-mode data provided by ΔE -E solid state detector telescopes. The evaluation of data essentially consists of the following steps:

- a) Presorting of the list mode data
- b) Energy calibration of the converted pulse-heights
- c) Particle identification and evaluation of the total energy

$$E_{\text{tot}} = \Delta E + E$$

Presorting

Data of up to 8 detector telescopes at different scattering angles can be acquired simultaneously. Presorting with respect to the angle parameter is advantageous for the further treatment of the data. Each of the presorted data blocks gets an identification head which contains all important experimental parameters. The presorted list mode data are stored on magnetic tape.

Energy calibration

The energy calibration of the spectra is performed in the following way. Deviations of the amplification system from linearity are determined by pulse generator peaks distributed over the whole spectrum. The energy calibration uses the peaks of elastically scattered particles in the projected spectra from the ΔE - and E-detector. For particles lighter than ${}^6\text{Li}$ the energy-loss ΔE is determined from the primar energy E_{tot} and the detector-thickness, using range tables.

For ${}^6\text{Li}$ -particles, however, range tables are only available up to 72 MeV and therefore have to be extrapolated into the energy region of interest (about 150 MeV). As this does not seem to be very reliable it is necessary to use a method of energy calibration without the need of range tables. This can be performed by providing two energy calibration points by prominent scattering peaks of well-known energy. It is convenient to use elastic scattering from the light target nucleus ${}^{12}\text{C}$ where - due to the cinematic shift - it is possible to adjust the elastic scattering peak inside a large range of energy.

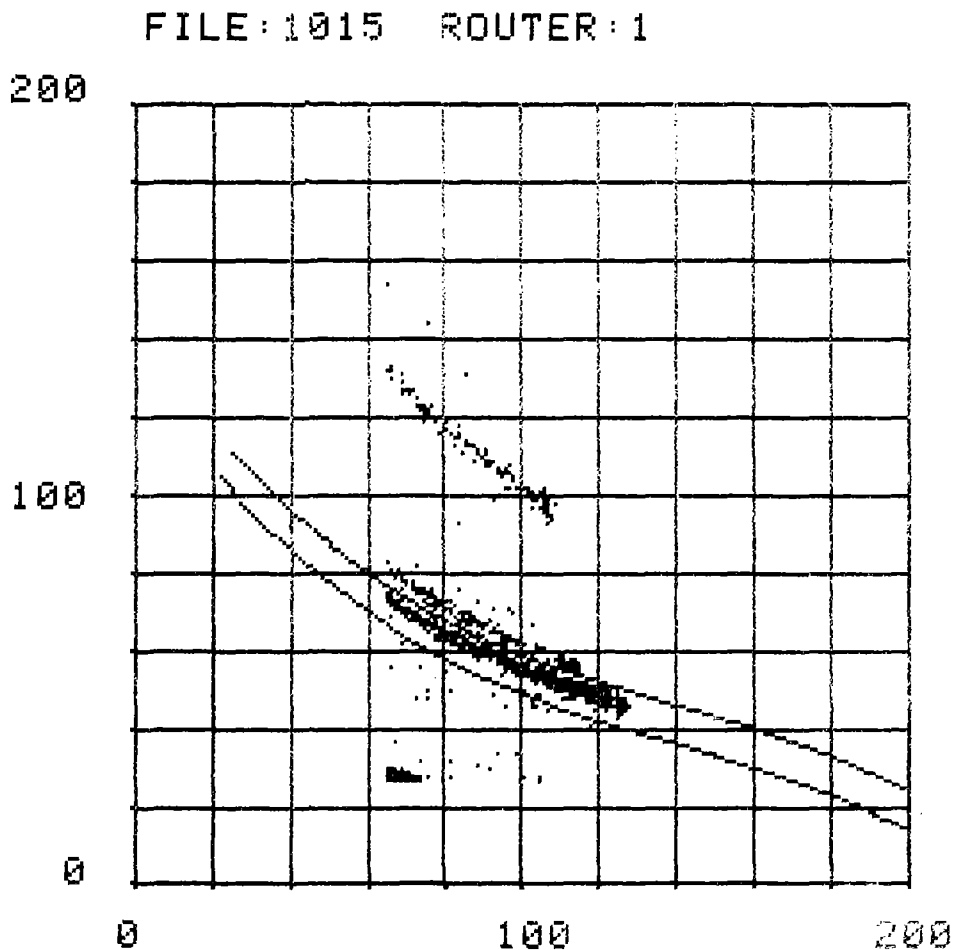


Fig. 1: Two-dimensional ΔE -E-spectrum for scattered particles induced by ${}^6\text{Li}$ -particles of 156 MeV. Particles with $Z < 3$ were cut off by a discriminator. The solid lines indicate the region of ${}^6\text{Li}$ events.

The energy calibrations for ${}^6\text{Li}$ -scattering with and without the use of extrapolated range tables show no considerable deviations ($< 5 \cdot 10^{-4}$) so that in future the simpler method using extrapolated range tables can be applied.

Particle identification:

By selection of certain regions corresponding to a specific charge and mass in the two-dimensional ΔE - E -spectrum and by addition of the energy losses in the front- and back-detector one calculates the spectra of specific particles. These are stored on disc as 2K-spectra and can be plotted on a CALCOMP plotter and displayed on TV.

Fig. 1 shows a two-dimensional ΔE - E -spectrum, taken from the computer display. Events for ${}^6\text{Li}$ -particles ($Z = 3$, $A = 6$) are enclosed between the solid lines.

7.4.13 A European Proposal for Industrial Real-Time FORTRAN

W. Kneis

Though originally an IBM development in 1955, the FORTRAN language has become the most important high level language for scientific applications. It was finally standardized internationally in 1972. First of all the wide use of FORTRAN led to its application in industrial real-time systems. Additionally to the scope of the language in these systems a variety of special operations as real-time operations, bit-string manipulations and facilities for file and process I/O are needed. One way to offer these capabilities is to include them into FORTRAN via subroutine or function calls. Within the frame of the "Workshop on Standardization of Industrial Computer Languages" which has been founded in 1970 at the Purdue University a "FORTRAN Committee" worked on the extension of FORTRAN for real-time systems. Two years later their first national standard extension for real-time FORTRAN has been approved by the Instrument Society of America (ISA). Since 1973, the workshop is named "International Purdue Workshop of Industrial Computer Systems" (IPW) as European counter parts of the American groups were founded. Among them in 1976 the European FORTRAN committee "Purdue Europe Technical Committee I" (PE TC1) has been founded.

Since cooperation with the respective American groups mainly takes place by exchange of papers PE TC1 decided to work out a complete proposal for industrial real-time FORTRAN. In March 1978 the complete proposal of "Industrial Real-Time FORTRAN" (IRTF) of PE TC1 (1) was finished. It

Multiprogramming

DATIM	- obtain date and time
CLOCK	- obtain clock counts
CREATE	- create a new activity
START	- start an activity immediately or after a specified time delay
STRTAT	- start an activity at a specified absolute time
CYCLE	- start an activity in periodic execution (START)
CYCLAT	- start an activity in periodic execution (STRTAT)
CON	- connect a program to an event
DECON	- eliminate an event connection
CANCEL	- eliminate previous schedules
KILL	- eliminate an activity from the real-time system
STOP	- normal termination of execution
AWAIT	- waiting for an event
WAIT	- delay continuation of an activity
SIGNAL	- release of semaphore
WAITS	- wait on semaphore
PRESEM	- initialization of semaphore
RDSEM	- read a semaphore value

Binary-pattern and bit processing

IOR	- inclusive OR
IAND	- logical AND
NOT	- logical complement
IEOR	- exclusive OR
ISHL	- logical shift
ISHA	- arithmetic shift
ISHC	- circular shift
BTEST	- bit testing
BSET	- set bit
BCLR	- clear bit
BCHNG	- change bit

Process input/output

AISQW	- sequential analog data input
AIRDW	- analog data input in random sequence
AOW	- analog data output
DIW	- digital input
DOMW	- digital pulse output
DOLW	- latched digital output

File Handling

CRFILW	- create random file
CSFILW	- create sequential file
RENAMW	- change filename
OPENW	- open file
MODAMW	- modification of access mode
CLOSEW	- close file
DFILW	- delete file
RDRW	- read random access file
WRTRW	- write random access file

Fig. 1. Table of subroutines of Industrial Real-Time FORTRAN

contains sections on multiprogramming and real-time features, binary-pattern and bit processing, process input/output and file handling (Fig. 1). The most difficult and controversial part of IRTF in relation to ISA- and other proposals (cited in (1)) is in the section multiprogramming. This paper therefore opens a broad discussion between the American and European groups. But nevertheless an outcoming standard of Industrial Real-Time FORTRAN will need to be adapted in the future from time to time to allow the progress of FORTRAN and also the progress of real-time operating systems. Thus additions, supplements, and changes must be expected.

Reference

- (1) Purdue Europe Technical Committee 1, Industrial Real-Time FORTRAN, March 1978 (draft proposal).

7.5 ION SOURCES AND DETECTORS

7.5.1 Recent Improvements of the Karlsruhe Polarized Ion Source C-LASKA

V. Bechtold and L. Friedrich

Since 1974 the Lambshift-source C-LASKA is in operation at the cyclotron without any considerable failures. Whereas the same polarization could be obtained every time very well some difficulties arose in reproducing the maximum intensity together. Sometimes the intensity was only one half of the maximum. In all these cases we observed that the canal of the extraction electrode burned out in one direction inclined to the axis of the source and we supposed getting a slanting beam from the rf ion source. Indeed we could regain a major part of the lost beam by fixing a small permanent magnet between the rf ion source and the cesium cell (1). But it is rather tedious to adjust this magnet, because the source has to be operated on high voltage potential. Therefore we replaced this permanent magnet by a small stator magnet (1). Its transverse magnetic field can be changed from 0 to 15 Oe and turned around the axis of the source. This stator magnet can be operated on high potential and therefore the beam of the rf ion source can be adjusted properly for maximum output of the cyclotron. Furthermore to find out the iodine pressure for maximum $I \cdot P^2$ (I = intensity, P = polarization) we measured the intensity of the accelerated polarized ion beam as a function of this pressure (Fig. 1).

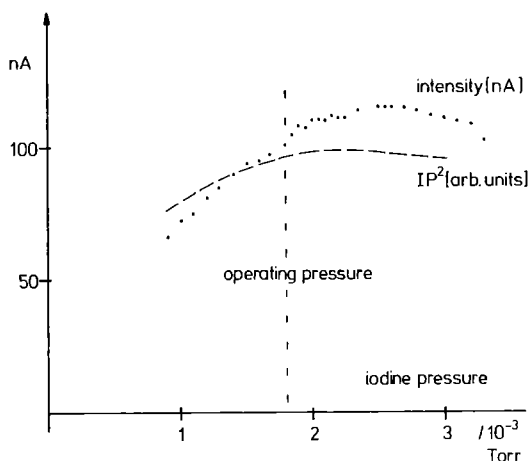


Fig. 1. The intensity of the accelerated polarized deuteron beam as a function of the iodine pressure. The dashed curve gives the figure of merit $I P^2 = (\text{intensity} \times \text{polarization}^2)$ and is taken from (2).

Now we get the intensity shown in Fig. 2.

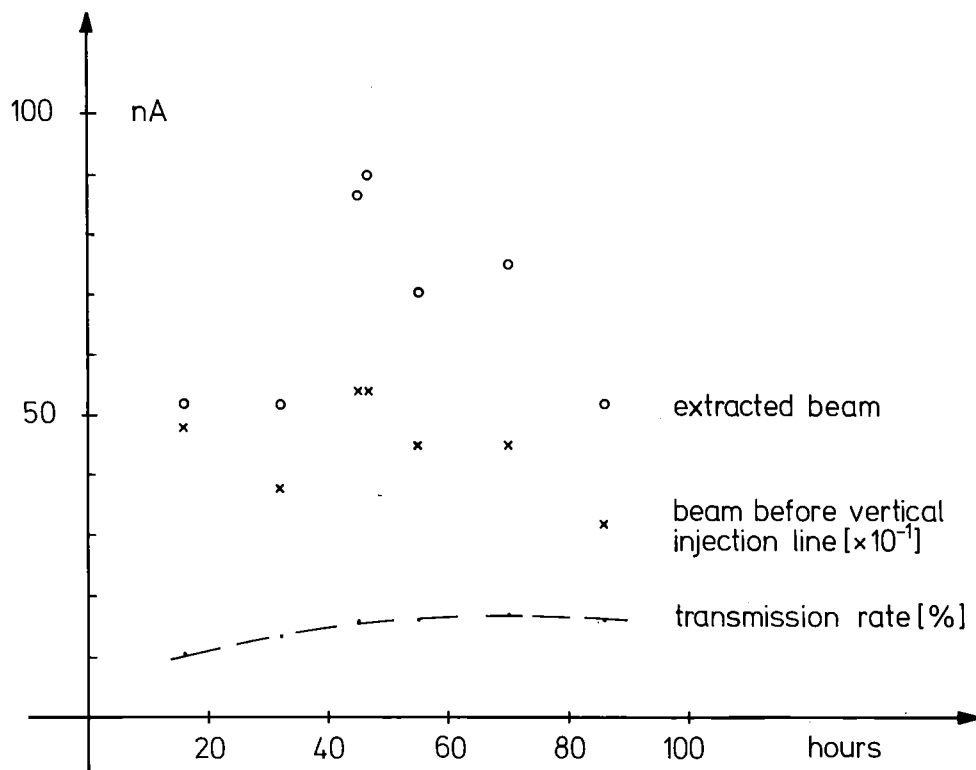


Fig. 2. Extracted and injected intensity of the polarized beam as a function of time during the last beam period. The transmission rate increases with better vacuum in the injection line.

With a transmission rate of more than 15 % we can now extract typically 70 to 80 nA vectorpolarized deuterons from the cyclotron, 100 nA have been observed. So it might be worthwhile to use this beam by O^0 -stripping as a source for polarized neutrons (3).

References

- (1) V. Bechtold, L. Friedrich, P. Ziegler, R. Aniol, G. Latzel, and H. Schieck, Nucl. Instr. Meth. 150 (1978) 407.
- (2) H. Brückmann, D. Finken, and L. Friedrich, Nucl. Instr. Meth. 87 (1970) 155.
- (3) R.L. Walter, Proc. Fourth Int. Symp. on Polarized Phenomena in Nuclear Reactions, Zürich (1975) p. 390.

7.5.2 The Lambshift Polarized Ion Source at the FN Tandem
Van de Graaff Accelerator of the University of Cologne*

V. Bechtold, L. Friedrich, P. Ziegler, R. Aniol⁺, G. Latzel⁺,
and H. Paetz gen. Schieck⁺

The design and performance of a Lambshift polarized ion source at the Cologne FN tandem accelerator is described with special emphasis on optimum phase space matching to the accelerator. Proton currents on target of 200 nA with a polarization of 0.63 have been obtained.

* Nucl. Instr. Meth. 150 (1978) 407-416.

⁺ Universität zu Köln, Institut für Kernphysik, 5000 Köln, Germany.

7.5.3 Monte Carlo Calculation for the Pulse Height Weighting
Function of a C_6D_6 Scintillation Detector

F. Hensley

For detection of neutron capture events by the associated prompt gamma-rays a detector with an efficiency that grows linearly with gamma-ray energy is desirable. Maier-Leibnitz suggested to achieve this property for almost any detector by multiplying its pulse height spectra $P(I, E_\gamma)$ with an appropriate weighting function $W(I)$ such that

$$P(I, E_\gamma) \cdot W(I) \sim E_\gamma$$

To calculate $W(I)$ one must know the response of the detector for gamma-rays over the entire energy region to be measured which can be up to 10 MeV in neutron capture. As monoenergetic gamma-ray sources are not available for these energies, one must gain the spectra from calculations.

For a total energy detector consisting of two cylindrical C_6D_6 liquid scintillators a pulse height weighting function was calculated with a modification of a code by C. LeRigoleur (1). Pulse height spectra were simulated with a Monte-Carlo code taking account for photo absorption, Compton scattering

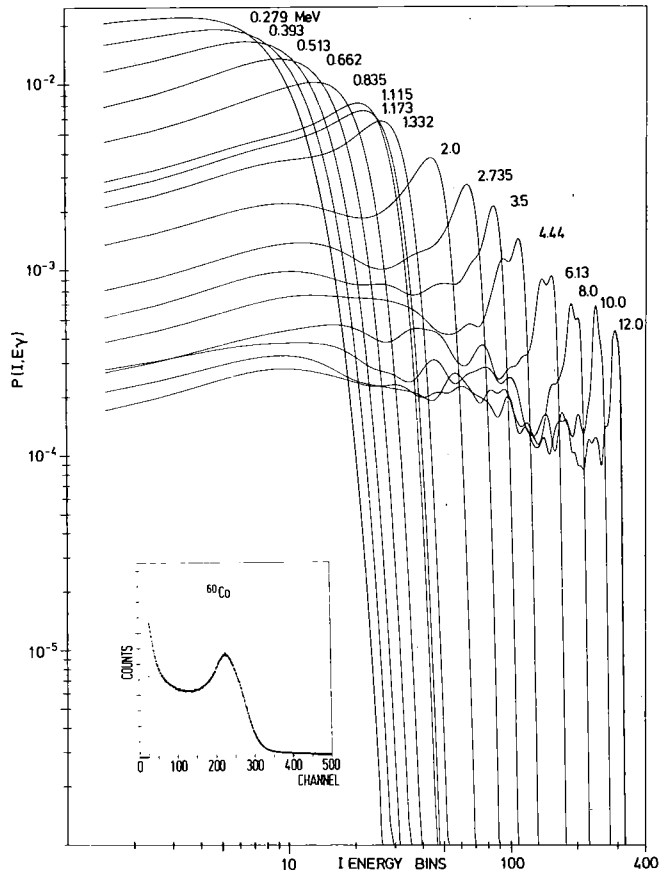


Fig. 1: Calculated pulse-height spectra for various γ -ray energies.
 For comparison the inset shows an experimental ^{60}Co spectrum.

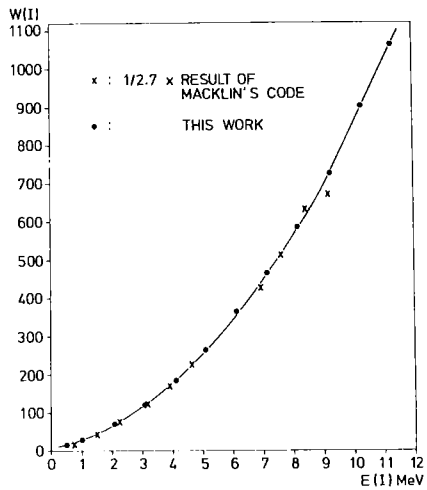


Fig. 2: Pulse-height weighting function
 calculated with spectra shown in
 Fig. 1 and results of a code by
 Macklin.

and pair production of gamma-rays in a geometry consisting of two detectors with aluminium/glass canning and lead shielding positioned symmetrically to an isotropic gamma-ray source.

Fig. 1 shows a set of simulated spectra and for comparison an experimental spectrum taken with a ^{60}Co source is given. The resulting weighting function is shown in Fig. 2. Its energy dependence was found to be

$$W(I) = 2.2846 \times I + 0.060009 \times I^2 + 0.64912 \times 10^{-6} \times I^3$$

for an energy bin width of $(I+1) - I = 0.2 \text{ m}_e c^2$.

Fig. 2 are also included the results of a calculation with a code by R.L. Macklin (2) which takes no account for the lead shielding of the detector, and which uses various approximations concerning the absorption processes and integration of the spectra. The results of the two calculations differ by a factor of 2.7, which is mainly due to different solid angles entering the calculations, but has no effect when the weighting method is used in relative measurements.

References

- (1) C. LeRigoleur, unpublished
- (2) R.L. Macklin, J.H. Gibbons, Phys. Rev. 159 (1967) 1007

8. SEMINARS

- 6.7.77 D.H. Stacey, Oxford University
Optical Isotope Shift Studies of Nuclei - an Appraisal
- 13.9.77 J.A. Cookson, AERE Harwell
Analysis with Ion Beams of a Few MeV Energy
- 28.9.77 M.F. Finlan, Radiochemical Centre, Amersham
Commercial Isotope Production in the Amersham Cyclotron
- 19.10.77 M.R. Geller, CEN Grenoble
Production of Highly Stripped Ions for Injection into
a Cyclotron
- 21.10.77 H. Vonach, Universität Wien
Gamma-Zerfall ungebundener Zustände
- 26.10.77 C. Ekström, CERN, Genf
Nuclear Spins and Moments Determined by Atomic-Beam
Magnetic Resonance Techniques
- 2.11.77 H. Hühnermann, Universität Marburg
Bestimmung von Kerneigenschaften mit optisch-
spektroskopischen Methoden
- 12.12.77 A.B. Smith, Argonne National Laboratory
The ANL Nuclear Data Program for Fast Breeder Reactor
and Fusion Energy Systems
- 14.12.77 G. Wagner, MPI für Kernphysik, Heidelberg
Riesenresonanzen in leichten Kernen
- 1.2.78 S.G. Rohozinsky, Universität Warschau
Dynamical Effects in the Collective Motion of the
Even-Even Xe and Ba Isotopes
- 14.2.78 T. von Egidy, ILL Grenoble
Kernphysikalische Experimente am ILL
- 15.2.78 T.D. Reilly, Los Alamos Scientific Laboratory
Developments in Nondestructive Assay of Nuclear Material
at Los Alamos Scientific Laboratory

- 21.2.78 O. Schult, KFA Jülich
Verstehen wir die K-Röntgenenergien?
- 22.2.78 M.S. Moore, Los Alamos Scientific Laboratory
Fission Experiments with Polarized Neutrons
- 27.2.78 R.C. Haight, Lawrence Livermore Laboratory
(n, charged particle) Measurements and Applications
- 1.3.78 M. Schumacher, Universität Göttingen
Messung der Vakuumpolarisation mit elastischer
Photon-Streuung
- 12.4.1978 E. Friedman, Hebrew University, Jerusalem
Recent Results on Pionic Atoms Studies
- 19.4.78 C. Jacquot, CEN, Grénoble
New Electron Cyclotron Resonance Ion Source for
High Intensity Proton Beams
- 26.4.78 G. Schütte, Universität Heidelberg
Dynamik der Kernspaltung
- 2.5.78 R. Nöbling, Universität Heidelberg
Arbeiten an der Heidelberger Protonenmikrosonde
- 17.5.78 U. Schryber, SIN, Villigen
Der neue Injektor für die SIN-Beschleunigeranlage
- 2.6.78 Y. Patin, Centre d'Etudes de Bruyères-le-Châtel
Fission Fragment Energy-Velocity Correlation Measurement
of the $^{233}\text{U}(d,pf)$ Reaction
- 7.6.78 M. Arnould, TH Darmstadt
Isotope Anomalies in Meteorites and Their Possible
Astrophysical Implications
- 13.6.78 H.J. Kluge, Universität Mainz
Optische Atomspektroskopie an kurzlebigen Isotopen
- 21.6.78 J. Speth, KFA Jülich
Die neuen Riesenresonanzen in den Atomkernen
- 27.6.78 S. Penselin, Universität Bonn
Laserspektroskopie metastabiler Atomzustände

9. PUBLICATIONS AND CONFERENCE CONTRIBUTIONS

9.1 PUBLICATIONS

Eyrich, W., Hofmann, A., Scheib, U., Schneider, S., Vogler, F., Rebel, H.

Alpha-Gamma Angular Correlations in the Reaction $^{24}\text{Mg}(\alpha, \alpha\gamma)$ at $E_\alpha = 104$ MeV. Nuclear Physics A, 287 (1977) S. 119-36.

Gils, H.J., Rebel, H., Buschmann, J., Klewe-Nebenius, H.

Giant Resonance Excitation by 156 MeV ^6Li Scattering. Physics Letters, 68B (1977) S. 427-28.

Nowicki, G., Bekk, K., Göring S., Hanser, A., Rebel, H., Schatz, G.

Nuclear Radii and Magnetic Moments of $^{128,131}\text{Ba}$ from High-Resolution Laser Spectroscopy. Physical Review Letters, 39 (1977) S. 332-34.

Schulz, F., Schweickert, H. (Editors)

Operation of the Karlsruhe Isochronous Cyclotron in 1976. KFK-2461 (August 1977).

Schouky, I.

Untersuchung der Niveaustuktur von ^{17}O und ^{29}Si im Bereich zwischen Neutronenbindungsenergie und 12 MeV Anregungsenergie. Dissertation, Univ. Karlsruhe, 1977; KFK-2503 (August 1977).

Bechtold, V., Ottmar, H. (Editors)

Annual Report, Teilinstitut Kernphysik (July 1, 1976 - June 30, 1977); KFK-2504 (Oktober 1977).

Baumung, K., Böhnel, K., Eyrich, W., Iyer, M.R., Matussek, P., Michel-Piper, I., Ottmar, H.

Zerstörungsfreie Methoden. In: Projekt Spaltstoffflußkontrolle. Jahresbericht 1976. KFK-2465 (Juli 1977) S. 2/1-2/18.

Heck, D.

Ion Beam Optics of Misaligned Beam Transport Elements. Nuclear Instruments and Methods, 143 (1977) S. 423-27.

Hanser, A., Faust, H., Klewe-Nebenius, H., Rebel, H., Buschmann, J., Gils, H.J.

Experimental Studies of Hexadecapole Motion in Spherical Nuclei. KFK-2470 (November 1977).

Felix, W., Wilcke, W., Elze, Th.W., Rebel, H., Huizenga, J.R., Thompson, R.C. Dreizler, R.M.

Study of Nuclear-Coulomb Interference Effects in Inelastic Deuteron Scattering on ^{238}U . Physics Letters, 69B (1977) S. 407.

Bechtold, V., Friedrich, L., Abdel-Wahab, M.S., Bialy, J., Junge, M., Schmidt, F.K.

Vector Analysing Power in d-p and d-d Elastic Scattering at 52 MeV. Nuclear Physics A 288 (1977) S. 189-91.

Vetter, J.E., Bauer, W., Böhme, G., Borgstedt, U., Citron, A., Ehrlich, K., Eyrich, W., Grimm, L., Kaletta, D., Käppeler, F., Kapulla, H., Küchle, M., Mittag, K., Moritz, J., Müller A., Pepler, W., Piosczyk, B., Reichardt, W., Rusch, D., Schatz, G., Schmidt, F.K., Schneider, J., Vetter, J.E., Vogg, H., Zieher, K.W.

Vorstudie für eine intensive Neutronenquelle. KFK-2542 (Dezember 1977).

Cierjacks, S. (Editor)

Progress Report on Nuclear Data Research in the Federal Republic of Germany for the Period January 1, 1976 to March 31, 1977. NEANDC(E)-182 U Vol. 5 (April 77) INDC (Ger)-19/L + Special.

Lange, J., Tamm, U., Borcharding, K., Döbele, R., Eberle, H., Erbacher, I., Hauschild, J., Hübener, J., Lange, J., Müller, G., Rapp, W., Rathjen, E., Rusch, K.D., Schaef, A., Tamm, U.

Manganknollen-Analysensystem - MANKA. (Abschlußbericht) KFK-2537 (Dezember 1977).

Bechtold, V., Friedrich, L., Doll, P., Knöpfle, K.T., Mairle, G., Wagner, G.J.

Spins of Proton Hole States from Analyzing Power of (d,t) Reactions at 52 MeV. Physics Letters, 72B (1977) S. 169-72.

Käppeler, F., Beer, H.

Neutron Interlab Seminar 1977. KFK-Nachrichten, 9 (1977) Nr. 3/4, S. 72.

Bechtold, V., Friedrich, L., Ziegler, P., Aniol, R., Latzel, G., Paetz, H., gen. Schieck.

The Lambshift Polarized Ion Source at the FN Tandem Van de Graaff Accelerator of the University of Cologne. Nuclear Instruments and Methods, 150 (1978) S. 407-16.

Faust, H., Hanser, A., Klewe-Nebenius, H., Rebel, H., Buschmann, J., Gils, H.J.

Experimental Studies of Hexadecapole Motion in Spherical Nuclei.

Journal of Physics G: Nuclear Physics, 4 (1978) S. 247-60.

Schweickert, H.

Produktion of Jod-123 für die Nuklearmedizin am Karlsruher Isochronzyklotron.

KFK-Nachrichten, 10 (1978) Nr. 1, S. 19-24.

Wisshak, K., Käppeler, F.

Neutron Capture Cross-Section Ratios of ^{240}Pu , ^{242}Pu , ^{238}U and ^{197}Au in the Energy Range from 10 to 90 keV. Nuclear Science and Engineering, 66 (1978) S. 363-77.

Phuoc, D.H., Chery, R., Börner, H.G., Davidson, W.F., Pinston, J.A., Roussille, R., Schreckenbach, K., Koch, H.R., Seyfarth, H., Heck, D.

Study of the Level Structures of ^{80}Br and ^{82}Br Using the Thermal Neutron Capture Reaction.

Zeitschrift für Physik A 286 (1978) S. 107-199.

Börner, H.G., Koch, H.R., Seyfarth, H., Egidy, T. von, Mampe, W., Pinston, J.A., Schreckenbach, K., Heck, D.

Study of the Level Structure of ^{239}U Using the Thermal Neutron Capture Reaction.

Zeitschrift für Physik A 286 (1978) S. 31-43.

Majka, Z.

$N-\alpha$ and $N-^6\text{Li}$ Microscopic Potentials.

Physics Letters 76B (1978) S. 161-164.

Beer, H., Spencer, R.R., Käppeler, F.

Measurement of Partial Radiation Widths of High Energy Transitions from keV Capture Resonances in ^{56}Fe and $^{58,60}\text{Ni}$.

Zeitschrift für Physik A 284 (1978) S. 173-181.

Cierjacks, S., Gupta, S.K., Schouky, I.

Isobaric Analog Impurity from Total and Differential Neutron Scattering Cross Sections of Silicon.

Physical Review C17 (1978) S. 12-16.

9.2 CONFERENCE CONTRIBUTIONS

9. ANNUAL CONFERENCE ON ATOMIC SPECTROSCOPY, EGAS

CRACOW, POLAND, JULY 12-15, 1977.

Nowicki, G., Bekk, K., Göring, S., Hanser, A.,
Rebel, H., Schatz, G.

High Resolution Laser Spectroscopy of Radioactive
Light Barium Isotopes.

INTERNATIONAL CONFERENCE ON NUCLEAR STRUCTURE, TOKYO, SEPTEMBER 5-10, 1977

Do Huu, P., Chery, R., Charvet, A., Duffait, R.,
Börner, H., Davidson, W.F., Pinston, J.A.,
Roussille, R., Schreckenbach, K., Koch, H.R.,
Seyfarth, H., Heck, D.

Levels in ^{80}Br and ^{82}Br Observed in (n, γ) and (p,n γ)
Reactions.

Eyrich, W., Hofmann, A., Scheib, U., Schneider, S.,
Vogler, F., Rebel, H.

($\alpha,\alpha'\gamma$) Angular Correlation Measurements on ^{28}Si at
 $E_{\alpha} = 104$ MeV.

Börner, H., Koch, H.R., Seyfarth, H., Schult, O.W.B.,
Heck, D., Mampe, W., Schreckenbach, K., Pinston, J.A.,
Jeuch, P.

Collective States in ^{239}U .

Nowicki, G., Bekk, K., Göring, S., Hanser, A.,
Rebel, H., Schatz, G.

High Resolution Laser Spectroscopy of Radioactive
Light Barium Isotopes.

Gils, H.J., Rebel, H., Buschmann, J., Klewe-Nebenius,
H.

Giant Resonance Excitation by Scattering of ^6Li Ions
at $E_{\text{Li}} = 156$ MeV.

41. PHYSIKERTAGUNG 1977, KARLSRUHE, 20.-23. SEPTEMBER 1977

Cierjacks, S.

Moderne kernphysikalische Experimentiertechniken und
Meßmethoden in der Kerntechnik.

NEUTRON INTERLAB SEMINAR, KARLSRUHE, 14.-16. SEPTEMBER 1977

Schmalz, G., Erbe, D., Haushahn, G., Heidenreich, K.,
Schulz, F.

A Time-of-Flight Device for Ultra-High-Resolution
Transmission Measurements.

Hensley, F., Käppeler, F., Leugers, B.

A Method for Capture Cross-Section Measurements on
Noble Gases.

Kazerouni, M.A., Käppeler, F.

A Fast Spherical Avalanche Fission Detector with
Good Alpha-Discrimination.

Müller, R., Naqvi, A., Käppeler, F.

Prompt Fragment Mass Yields from Fast Neutron
Induced Fission of ^{235}U .

Cierjacks, S., Gupta, S.K., Schouky, I.

Isobaric Analogue Impurity from Total and Differen-
tial Neutron Scattering Cross Sections of Silicon.

Cierjacks, S., Erbe, D., Leugers, B., Schmalz, G.

Ultra-High Precision Measurements of Neutron Resonance
Energies of Carbon and Oxygen Between 3 and 15 MeV.

Voss, F.

Measurement of (n,n' γ)-Cross-Sections on ^{238}U .

Schouky, I., Cierjacks, S.

Measurement of the Differential Elastic Neutron Scattering Cross-Section of O and Si between 0.5 and 6 MeV

Hage, W., Hettlinger, H., Käppeler, F., Kumpf, S., Wisshak, K.

Measurement of the Fission Cross-Section of ^{241}Am .

Wisshak, K.

A Method to Determine the Neutron Capture Cross-Sections to the ^{242}Am Ground and Isomeric State in the keV Energy Range.

Beer, H., Käppeler, F.

A Measurement of the Capture to Fission Cross-Section Ratio, α , of ^{235}U in the Energy Range 10 to 500 keV.

Kari, K., Cierjacks, S., Erbe, D., Leugers, B., Schmalz, G.

Absolute Fast Neutron Fission Cross-Section of ^{239}Pu and ^{240}Pu .

Wisshak, K., Käppeler, F.

Neutron Capture Cross Sections of $^{240,242}\text{Pu}$ and the Subthreshold Fission Cross Section of ^{240}Pu in the Energy Range from 10 to 200 keV.

SPECIALISTS MEETING ON NEUTRON DATA OF STRUCTURAL MATERIALS FOR THE FAST REACTORS

GEEL, DECEMBER 5-8, 1977

Hong, L.D., Beer, H., Käppeler, F.

Capture and Total Cross-Section Measurements on ^{58}Fe below 325 keV.

Cierjacks, S., Schouky, I.

Investigation of s-Wave Resonances and a Possible Doorway State in Fe Below 850 keV.

16. NUCLEAR PHYSICS MEETING, BORMIO, JANUARY 16-21, 1978

Gils, H.J., Rebel, H., Majka, Z.

Folding Model Studies of $^{40,48}\text{Ca}$ (α, α) and $^{40}\text{Ca}-^{48}\text{Ca}$ rms Radii Differences.

Rebel, H., Gils, H.J., Knüpfer, W.

Hexadecapole Motion in Spherical Nuclei.

FRÜHJAHRSTAGUNG DPG, ATOMPHYSIK.

MÜNCHEN, 6.-10. MÄRZ 1978

Bekk, K., Nowicki, G., Göring, S., Hanser, A., Rebel, H., Schatz, G.

Bestimmung der Isotopieverschiebung und Hyperfeinstruktur leichter Barium-Isotope mittels Laserspektroskopie.

FRÜHJAHRSTAGUNG DPG, KERNPHYSIK, HEIDELBERG, 13.-17. MÄRZ 1978

Bechtold, V., Bialy, J., Friedrich, L., Abdel-Wahab, M.S., Schmidt, F.K.

Die Winkelverteilung der Vektorpolarisation T_{11} in der Aufbruchsreaktion $p(d \text{ pol. pp}) n$.

Bechtold, V., Friedrich, L., Breuer, H., Doll, P., Knöpfle, K.T., Mairle, G., Riedesel, H., Schindler, K., Wagner, G.J.

Untersuchung der Schalenstruktur der Kerne mit $A=17$ und 21 durch Pick-up Reaktionen mit polarisierten Deuteronen.

Beer, H.

Resonanzneutroneneinfang in der Massengegend $40 < A < 70$ und die Gültigkeit des Valenzmodells.

Buschmann, J., Gils, H.J., Rebel, H., Zagromski, S., Bechtold, G., Klewe-Nebenius, H., Faust, H., Neumann, B.

Streuung von 156 MeV ^6Li -Teilchen an ^{12}C , ^{40}Ca , ^{90}Zr und ^{208}Pb .

Cierjacks, S., Schmalz, G., Erbe, D., Leugers, B., Hinterberger, F., Rossen, P. von

Untersuchung energiescharfer $T=3/2$ Resonanzen in ^{17}O .

Cierjacks, S., Schouky, I.

Elastische Neutronenstreuung an ^{56}Fe .

Cierjacks, S., Kari, K.

Messung des absoluten Spaltquerschnitts von ^{239}Pu und ^{240}Pu zwischen 1-20 MeV.

Dickmann, F.

Kerndeformation und -deformationsgeschwindigkeit im Schalenmodell.

Eyrich, W., Hofmann, A., Rost, H., Scheib, U., Schneider, S., Vogler, F., Rebel, H.

Untersuchung der isoskalaren Riesenresonanzen in ^{208}Pb mit Hilfe von Teilchen-Gamma-Winkelkorrelationen.

Gils, H.J., Rebel, H., Buschmann, J., Zagromski, S.

Untersuchung der Kernradien von $^{40,48}\text{Ca}$ und der Proton-Neutron-Radiusdifferenz von ^{48}Ca durch elastische Streuung von 104 MeV Alpha-Teilchen.

Heck, D.

Ionenoptik des Karlsruher Protonenmikrostrahls.

Hensley, F.

Messung der Neutroneneinfangquerschnitte von natürlichem Krypton und ^{84}Kr .

Hong, L.D., Beer, H., Käppeler, F.

Messung des Neutroneneinfangquerschnitts von ^{58}Fe und seine Bedeutung für die Elemententstehung.

Käppeler, F., Schatz, G.

Erzeugung von Neutronen im keV-Bereich.

Knüpfer, W., Gils, H.J., Rebel, H.

Konsistente Beschreibung der Anregungsspektren in ^{90}Zr .

Latz, R., Buschmann, J., Gils, H.J., Rebel, H.

Alpha-Teilchen induzierte Mehrnukleonen-Transfer-Reaktionen an ^{12}C .

Latzel, G., Paetz, H., gen. Schieck, Bechtold, V., Friedrich, L.

Streuung polarisierter Protonen an ^{207}Pb im Bereich stark überlappender Analogresonanzen.

Majka, Z., Gils, H.J., Rebel, H.

Exchange and Density Dependence Effects in Folding Models of Alpha-Particle and ^6Li -Scattering.

Nowicki, G., Bekk, K., Göring, S., Hanser, A., Rebel, H., Schatz, G.

Isotopieverschiebung und Hyperfeinstruktur neutronenarmer Barium-Isotope.

TECHNIQUES OF CAPTURE CROSS SECTION MEASUREMENTS, OAK RIDGE, TENN., APRIL 3-7, 1978

Beer, H., Hensley, F., Hong, L.D., Käppeler, F., Leugers, B., Wisshak, K.

Recent Capture Cross-Section Measurements at Karlsruhe.

15. EUROPEAN CYCLOTRON PROGRESS MEETING, BERLIN, APRIL 4-7, 1978

Bechtold, V., Friedrich, L., Wiss, L.

New Trim Coils for the Karlsruhe Cyclotron.

Schulz, F., Schweickert, H.

Status Report on the Karlsruhe Isochronous Cyclotron.

Kappel, W., Kneis, W., Kögel, B., Möllenbeck, J., Schweickert, H.

Computer Diagnostics and External Beam Optimization.

CONFERENCE ON NUCLEAR PHYSICS, EDINBURGH, APRIL 5-7, 1978

Friedman, E., Gils, H.J., Rebel, H., Majka, Z.

Nuclear Matter Radii of $^{40,48}\text{Ca}$ and Proton-Neutron Radii Difference of ^{48}Ca Determined by 104 MeV Alpha-Particle Scattering.

EUROPHYSICS STUDY CONFERENCE ON THE STRUCTURE OF LIGHTER NUCLEI,

HVAR, JUGOSLAVIA, MAY 8-13, 1978

Eyrich, W., Hofmann, A., Scheib, U., Schneider, S., Vogler, F., Rebel, H.

The Deformation of ^{26}Mg from Particle-Gamma Angular Correlations.

2. LOUVAIN-KRAKOW SEMINAR ON ALPHA-NUCLEUS INTERACTION

LOUVAIN-LA-NEUVE, BELGIUM JUNE, 5-7, 1978

Majka, Z., Gils, H.J., Rebel, H.

104 MeV Alpha-Particle Scattering and 156 MeV ${}^6\text{Li}$ -Scattering and the Validity of Refined Folding Model Approaches for Light Complex Projectile Scattering.

Rebel, H., Gils, H.J., Friedman, E.

Nuclear Matter Radii Difference in ${}^{48-40}\text{Ca}$ from Elastic Alpha-Particle Scattering at $E_\alpha = 104$ MeV.

DISCUSSION MEETING ON CHARACTERIZATION AND QUALITY CONTROL OF NUCLEAR FUELS

KARLSRUHE, JUNE 13-15, 1978

Eberle, H., Matussek, P., Michel-Piper, I., Ottmar, H., Alex, H.

Elemental and Isotopic Concentration Analyses on Nuclear Fuels Using Nondestructive Assay Techniques.

IFAC/IFIP WORKSHOP ON REAL-TIME-PROGRAMMING, MARIENHAMN/ALAND, FINLAND, JUNE 19-21, 1978

Heller, G., Rembold, U., Wiesner, G., Kneis, W.

Standards and Proposals of Industrial Real-Time FORTRAN.

Sobiesiak, H., Kneis, W.

How to Avoid Complicated If Clause Structure in FORTRAN Real-Time Programming.

3. INTERN. CONFERENCE ON CLUSTERING ASPECTS OF NUCLEAR STRUCTURE AND NUCLEAR REACTIONS

WINNIPEG, MANITOBA, CANADA, JUNE 19-23, 1978

Dickmann, F.

Finite Velocity of Deformation in Nuclear Fission

Majka, Z., Rebel, H., Gils, H.J.

Importance of the Density Dependence of the Nucleon-Nucleon Interaction for Elastic Scattering of Light Complex Projectiles.

INTERNAT. ASTROPHYSICAL SYMPOSIUM, LIÈGE, BELGIUM, JUNE 20-22, 1978

Hong, L.D., Beer, H., Käppeler, F.

A Capture Cross-Section Measurement on ${}^{58}\text{Fe}$ and its Implication for the s-Process near the Iron Seed.

9.3 LECTURES AND SEMINARS

Rebel, H.

Alpha-Teilchen-Streuung als Informationsquelle über Größe und Gestalt der Atomkerne.
Kolloquiumsvortrag an der Universität Göttingen,
21. November 1978

Nowicki, G.

Messung von Isotopieverschiebung und Hyperfeinstruktur neutronenarmer Barium-Isotope mittels Laserspektroskopie.
Gesellschaft für Schwerionenforschung, Darmstadt,
13. Januar 1978.

Schatz, G.

Hochauflösende Laserspektroskopie an radioaktiven Barium-Isotopen.
Institut für Experimentalphysik, Universität Hamburg,
23. Januar 1978.

Cierjacks, S.

Untersuchung energiescharfer $T = 3/2$ Resonanzen von leichten $T_2 = 3/2$ Kernen mit dem Karlsruher Neutronenspektrometer.
Service de Physique Nucléaire, CEA-Paris,
21. April 1978.

Schatz, G.

Untersuchung der Hyperfeinstruktur an radioaktiven Bariumisotopen.
Institut für Atom- und Festkörperphysik, FU Berlin,
27. April 1978.

Rebel, H.

Ist die Kernoberfläche neutronenreich?
Universität Heidelberg, Physikalisches Kolloquium,
5. Mai 1978.

Nowicki, G.

Isotope Shifts of Neutron Deficient Ba-Isotopes.
Clarendon Laboratory, Seminar, Oxford, U.K., May 11,
1978.

Schatz, G.

Spectroscopy of Minute Samples or How to Look with Lasers at Nuclei.
Institut Max von Laue - Paul Langevin, Kolloquium,
Grenoble, 11. Mai 1978.

Cierjacks, S.

Messungen der Neutronenstreuung an leichten Kernen.
Physikalisch-Technische Bundesanstalt, Kolloquium,
Braunschweig, 15. Juni 1978.

Rebel, H.

Laserspektroskopie an instabilen Barium-Isotopen.
Justus-Liebig-Universität Gießen, Kolloquium,
29. Juni 1978.

10. PERSONNEL

Head of the Teilinstitut Kernphysik: Prof. Dr. G. Schatz

Scientific and technical staff:

Bechtold, G., Mrs.	Feurer, B.	Michel-Piper, I., Mrs., Ing.
Beck, R., Dr.	Gils, H.J., Dr.	Nowicki, G., Dr.
Beer, H., Dr.	Göring, S., Dipl.-Phys.	Ottmar, H., Dr.
Buschmann, J., Dr.	Hanser, A., Dr.	Rebel, H.G., Prof. Dr.
Cierjacks, S., Dr.	Heck, D., Dr.	Rupp, G.
Dickmann, F., Dr.	Hong, L.D., Dipl.-Phys.	Schmalz, G., Dipl.-Ing.
Dohrmann, H., Ing.	Käppeler, F., Dr.	Schmidt, K.A., Dipl.-Phys.
Eberle, H., Ing.	Leugers, B. Dipl.-Phys.	Wisshak, K., Dr.
Erbe, D.	Matussek, P., Dipl.-Phys.	Zagromski, S., Ing.

Guests and research students:

Andl, A., Dipl.-Phys.	Kari, K., Dipl.-Ing.	Neumann, B., Dipl.-Phys.
Bekk, K., Dipl.-Phys.	Kazerouni, M.A., Dipl.-Phys.	Schouky, I., Dipl.-Phys.
Hensley, F., Dipl.-Phys.	Naqvi, S.A.A., Dipl.-Phys.	

Secretarial staff: Mrs. H.M. Friederich, Mrs. E. Maaß

Head of the Cyclotron Laboratory: Dr. H. Schweickert

Scientific and technical staff of the Cyclotron Laboratory:

Assmus, K.H.	Friedrich, L., Dr.	Kneis, W., Dipl.-Phys.
Bauer, G.	Günther, O.	Kögel, B.
Bechtold, V., Dr.	Haushahn, G., Dipl.-Phys.	Kuhn, H.
Bialy, J., Dipl.-Phys.	Heidenreich, K.	Mangold, D.
Biber, J.	Hirth, W.	Möllenbeck, J., Ing.
Depta, A.	Jäger, K., Miss	Radtke, G., Ing.
Ehret, H.-P.	Kappel, W.-R., Ing.	Rämer, Ch., Miss, Ing.
Erdel, E.	Kauther, P.	Röhr1, E.
Franz, J.	Kessel, M.	

Schimpf, P.
Schulz, F., Ing.
Segnitz, W.

Seidel, H.
Seitz, J.
Seufert, H.

Walter, A., Miss
Wiss, L.

Workshops of the Cyclotron Laboratory:

Bleier, W.
Ernst, R.
Hauer, W.
Klinger, G.

Maier, W.
Möck, W.
Ripp, H.
Schlenker, G.

Schönstein, E.
Schütz, R.
Würges, J.

Secretarial staff: Mrs. E. Kirste